REPORT DOCUMENTATION PAGE

AFOSR-TR-97

0304

1. AGENCY USE ONLY *(Leave blank)*	2. REPORT DATE	3. REPORT T	...COVERED
	December, 1996	Aug. 1, 1994 – Aug. 30, 1996	

4. TITLE AND SUBTITLE Implementation and Application of 3-D Numerical and Analytical (Modal) Modeling Methods for the Prediction and Analysis of Discriminatory Seismic Signals

5. FUNDING NUMBERS

F49620-94-1-0124

6. AUTHOR(S)

Dr. Charles Archambeau

7. PERFORMING ORGANIZATION NAME(S) AND ADDRESS(ES)

University of Colorado
Campus Box 19
Boulder, CO 80309-0019

8. PERFORMING ORGANIZATION REPORT NUMBER

9. SPONSORING / MONITORING AGENCY NAME(S) AND ADDRESS(ES)

AFOSR/PKA
110 Duncan Avenue
Room B115
Bolling Air Force Base, D.C. 20332-8080

10. SPONSORING / MONITORING AGENCY REPORT NUMBER

11. SUPPLEMENTARY NOTES

12a. DISTRIBUTION / AVAILABILITY STATEMENT

unlimited

DISTRIBUTION STATEMENT A
Approved for public release
Distribution Unlimited

12b. DISTRIBUTION CODE

13. ABSTRACT *(Maximum 200 words)*

   The generalization of the Fourier pseudospectral method developed in this study involved supplementing a Fourier trigonometric basis set with discontinuity functions and using the weak Galerkin form of weighted residuals to approximate the governing equations for momentum conservation for wave propagation in heterogeneous media. Using the sawtooth and quadratic discontinuity functions, accurate simulations were obtained for problems with a traction-free surface and general 3-D velocity variations. It is shown how a general coordinate transformation can be used to incorporate surface topography and irregular material interfaces into models of strongly heterogeneous earth structure and to improve the resolution of small scale wavefield features. Comparisons of modeling results with analytic and other numerical solutions for both elastic and anelastic media with discontinuities shows an exceptional level of accuracy without significantly increasing the computational requirements compared to the standard Fourier method.

   An analytical approach, using modes defined on subregions of the medium, was also developed to model seismic wave propagation in media with vertically and horizontally variable elastic and anelastic properties. The restriction on the medium variability is that it can be represented by step function variations in its properties in both the vertical and horizontal directions. The theory is exact when the lateral variations are actually discontinuous step changes in properties. Consequently, when the actual changes can be well approximated as a sequence of steps, the method should be superior in computational accuracy and speed to numerical methods.

14. SUBJECT TERMS			15. NUMBER OF PAGES
	DTIC QUALITY INSPECTED 2		16. PRICE CODE

17. SECURITY CLASSIFICATION OF REPORT	18. SECURITY CLASSIFICATION OF THIS PAGE	19. SECURITY CLASSIFICATION OF ABSTRACT	20. LIMITATION OF ABSTRACT

Table of Contents

Part I

Complete Seismic Wavefield Synthesis with a Pseudospectral Method: The Generalized Fourier Method

J. L. Orrey[1], C. B. Archambeau[2] and G. A. Frazier

[1]Technology and Resource Assessment Corporation - North America, 3800 Arapahoe Ave., Suite 225, Boulder, CO 80303

[2]Department of Physics, Theoretical and Applied Geophysics Group, University of Colorado, Boulder, CO 80309-0583

short title: The Generalized Fourier Method

key words: synthetic seismograms, numerical modeling, pseudospectral,

Fourier method, Galerkin, finite element.

Summary

This study involves the development and testing of a new method for numerically modeling seismic wavefields in arbitrarily heterogeneous media. The method is a generalization of the Fourier pseudospectral method. In the standard Fourier method, a wavefield 's spatial dependence is approximated by a truncated series of harmonic functions and the expansion coefficients are integrated in time using finite differencing. In the new method, the expansion set is supplemented by a finite set of functions, called discontinuity functions, which are not infinitely differentiable with continuous derivatives like the harmonic functions. With the discontinuity function set included, the generalized Fourier method is capable of accurately representing high frequency wavefields in two- or three-dimensional media with surfaces of discontinuity. The discontinuity functions synthesize the discontinuous or rapidly varying portion of the wavefield's spatial dependence, leaving a smooth, continuous remainder for which the Fourier series representation is rapidly convergent. The method is formally expressed as a weighted residuals statement of momentum conservation with boundary conditions at discontinuities included. It is shown how a general coordinate transformation can be used to incorporate surface topography and irregular material interfaces into models of strongly heterogeneous earth structure and to improve the resolution of small-scale wavefield features. Using a particular set of discontinuity functions, a traction-free boundary is incorporated into the generalized method. Comparisons of modeling results with analytic and other numerical solutions for both elastic and anelastic media with discontinuities shows an exceptional level of accuracy without significantly increasing the computational requirements compared to the standard Fourier method.

1 Introduction

Methods of full-wavefield simulation such as finite difference and finite element methods are appropriate for elastodynamic modeling in arbitrarily inhomogeneous, anelastic and anisotropic media, but the use of wavefield simulation in seismology is limited to relatively low-frequency wave propagation and to short propagation paths. Machine storage and computation time requirements of wavefield methods render broad-band simulations unfeasible. As a result, most applications presently are limited to two-dimensions, as three-dimensional modeling is impractical for propagation distances greater than several wavelengths.

Storage considerations alone favor high-order or global (pseudospectral) methods over lower-order finite difference or finite element methods, especially for 3-D simulations. For simulations with a fixed bandwidth, a doubling of the wavefield sampling requires eight times as many nodes in a 3-D grid. Similarly, for a fixed sampling of the wavefield, doubling the bandwidth of a 3-D simulation requires eight times as many nodes. Because doubling the grid density used with a typical numerical method also requires a reduction of the time step by a factor of two in order to maintain the same low level of numerical dispersion, twice as many iterations are required with the denser grid than with the finer grid to perform computations over a fixed interval in time. Therefore, the overall computational effort of a 3-D method increases by roughly an order of magnitude with a doubling of sampling or bandwidth. For a fixed level of numerical dispersion, however, the time step size that can be used with low-order finite difference methods is somewhat larger than that which can be used with the Fourier pseudospectral method (Daudt et al. 1989). As a result, a fourth-order in space, second-order in time finite difference method is somewhat faster than the Fourier pseudospectral method in terms of required computation time for 2-D simulations, but it requires about twice the amount of storage for comparable accuracy (Vidale 1990). We are not aware of any published comparisons for 3-D computations, but we expect that the lower storage requirements of the Fourier method, compared to the fourth-order finite difference method, will lead to computation times that are roughly equal to or shorter than those of the finite difference method.

The focus of this study has been to increase the tractable bandwidth of seismic wavefield simulations through the development of a more computationally efficient and accurate simulation method. We use efficiency to refer to a measure of both a method's storage requirements and

computation time for a given problem and chosen level of accuracy. A method's efficiency for a particular simulation is therefore roughly proportional to the total required number of discrete points in space and time. Typically, accuracy is measured in terms of solution error, such as the percentage error in phase velocity determined from a simulation. In this study, particular emphasis is placed on the accuracy of boundary condition approximations.

The treatment of boundary conditions is a very limiting aspect of pseudospectral methods for seismic applications. With the Chebyshev polynomial-based pseudospectral method of Kosloff *et al.* (1990), a fourth-order Runge-Kutta time-stepping scheme is required for stability (Canuto *et al.* 1988). Compared to a simple leap-frog time-stepping scheme, the fourth-order scheme results in much more computation and storage. In addition, the time-step size is limited by the necessarily small grid spacings in the vicinity of the interval endpoints of the set of Chebyshev polynomials (Kosloff and Tal-Ezer 1993).

In the Fourier pseudospectral method, the spatial approximations of the field variables are truncated Fourier series, and the spatial sampling of the method is optimal, for homogeneous media. That is, the smallest wavelength computed with the Fourier series approximation corresponds to the length of two grid point spacings. However, pseudospectral methods used for simulations in heterogeneous media do not achieve accurate reflection and transmission at material interfaces unless the sampling is greater than or equal to about four nodes per minimum wavelength (Witte 1989). Such oversampling, and the corresponding reduction in computational efficiency, is required because discontinuities in the media and wavefields are approximated with continuous, periodic functions. Because the method's basis functions are periodic, boundary conditions at grid edges also must be periodic. On the other hand, if the boundary conditions of a given modeling problem are different at opposite edges of the problem space, the field variables will, in general, have different values at one edge than at the other edge. If such a problem is modeled using the Fourier method, this mismatch behaves like a discontinuity. It causes rapid oscillations in the Fourier approximation due to poor convergence.

The central contribution of this work is to incorporate into the Fourier method boundary conditions at material discontinuities. This is achieved by combining the trigonometric functions of the Fourier method with additional functions which are not, like the trigonometric functions, infinitely differentiable with continuous derivatives. The additional functions, referred to as *discontinuity functions*, approximate the spatial discontinuities of the field variables, leaving a continuous re-

3

mainder to be synthesized by the trigonometric functions. We refer to the resulting method as the generalized Fourier method (GFM).

Consider such a scheme to simulate wavefields in a realistic model of earth structure which contains free surface topography, dipping layers, and random variations in material properties. It would be impossible to account for all material discontinuities in such a model by explicitly incorporating boundary conditions at all interfaces. However, most discontinuities in the Earth can be approximated as continuous but rapid changes in material properties with position. Using the generalized Fourier method, these structural features can be treated with the (continuous) trigonometric functions. Other structural features may be sufficiently abrupt, for the wavelengths of interest, that they must be treated as actual discontinuities. Figure 1 schematically illustrates an earth structure with both continuous and discontinuous variations in material properties. Discontinuities are indicated by thin black lines, and continuous variations are indicated by thicker gray lines. Using the generalized Fourier method for simulations in the structure of Figure 1 requires the use of discontinuity functions for those interfaces that are treated as actual discontinuities (as opposed to being approximated with continuous functions) and the use of a coordinate transformation to map the space with irregular interfaces, the *physical* space, into the Cartesian *computational* space. In the nth domain of the multi-domain computational space, the sets of trigonometric functions of the Fourier method are denoted $e^n_{(1)}$ and $e^n_{(3)}$, in the x_1 and x_3 coordinate directions, respectively. The periodicity of the Fourier method is eliminated within the nth domain by using the sets of discontinuity functions $d^n_{(1)}$ and $d^n_{(3)}$. The discontinuity functions account for discontinuities at the interfaces connecting neighboring domains and at the bounding surfaces of the entire problem space. They effectively decouple the coordinate endpoints of each domain, since the boundary conditions on the surfaces of each domain are no longer periodic when the discontinuity functions are included. The resulting independent problem spaces are coupled together with boundary conditions, while the material properties within each domain remain spatially continuous.

In some cases it may be advantageous, in view of the oversampling required of the Fourier method for accurate representations of heterogeneous media, to model only the most abrupt changes in material properties with position, treating all of them as surfaces of discontinuity between domains of very smooth and continuous variations in material properties. In such cases, boundary conditions would be applied explicitly on all interfaces, and the grid-point-per-minimum-wavelength sampling of the resulting multi-domain method would be optimal: It would require a sampling of

4

only two nodes per minimum wavelength.

In this study, we introduce discontinuity functions in only the vertical coordinate direction, as illustrated in Figure 2. This is sufficient for applying a traction-free boundary condition at the top of the model and a radiation condition at the base of the model. The computational space remains periodic in the horizontal coordinates. We present results of wavefield modeling only for single-domain problems, but the analytical formulation that is presented accounts for multi-domain methods as well.

In section 2, the elastodynamic problem is posed in terms of an integral statement of momentum conservation for a volume of material containing surfaces of discontinuity. Then an approximation to the governing equations is presented in terms of the method of weighted residuals. In section 3, the pseudospectral approximation of field variables and their derivatives is introduced, using an arbitrary set of global basis functions. The approximation is applied to the weighted residuals statement of momentum conservation to obtain a general formulation of pseudospectral methods for elastodynamics. Choosing trigonometric basis functions, we obtain the Fourier pseudospectral method and demonstrate the method's inherent periodicity. In section 4, a generalization of the Fourier method which handles discontinuities is derived by choosing a particular set of discontinuity functions to supplement the trigonometric basis set of the standard Fourier method. The derivation is presented in Cartesian coordinates and then extended to a curvilinear system. In section 5, the accuracy of the generalized Fourier method is tested for wave propagation problems involving a traction-free boundary condition.

2 Analytical Formulation

2.1 Equations of Momentum Conservation

The governing equations for the wavefields in a continuum are obtained from an integral statement of momentum conservation with surfaces of discontinuity present. In the following derivation, Greek subscripts denote spatial coordinate directions, and a comma before a subscript indicates a derivative with respect to the coordinate whose label follows the comma. The Einstein summation convention is assumed unless otherwise indicated.

Consider the Lagrangian description of momentum conservation in a volume V bounded by a surface of discontinuity S. Let the bounding surface S have an outward normal unit vector $\mathbf{n}$.

5

Then a jump in a quantity Q across S is defined as $[Q]_S = Q^+ - Q^-$ where Q^+ and Q^- are the values of Q immediately near S on the positive and negative sides of n, respectively. (From now on we neglect the subscript S on double brackets, understanding that all jump conditions are taken across surfaces of discontinuity.) When the boundary S moves with the particle velocities, then the equation of momentum conservation for the volume V bounded by S is

$$\int_{V\Theta(V\cap S)} [\rho \ddot{u}_\alpha - t_{\alpha\beta,\beta} - f_\alpha] dV - \oint_S [t_{\alpha\beta} n_\beta] dS = 0 \tag{2.1.1}$$

(Archambeau and Minster, 1978) where $\ddot{u}_\alpha$ and f_α are the components of particle acceleration and body force density, respectively, in the α coordinate direction and $t_{\alpha\beta}$ is the stress tensor. The symbols Θ and $\cap$ denote the set theoretic difference and intersection, respectively. (In the following, $V - S$ is used to abbreviate $V\Theta(V \cap S)$.) Since V is arbitrary and therefore could be chosen to exclude S, the integrals in (2.1.1) are zero separately. While the first integral provides the differential equation of momentum equation in the continuum, the second integral provides the boundary conditions: Across S the traction jump condition is $[t_{\alpha\beta} n_\beta] = 0$. From an analogous treatment of mass conservation, the jump condition for the particle velocity is $[\dot{u}_\alpha n_\beta] = 0$. Consequently, the relevant boundary conditions and equations of motion for the medium are the following:

$$\rho\, \partial_t^2 u_\alpha \quad - \quad t_{\alpha\beta,\beta} - f_\alpha = 0$$

$$[t_{\alpha\beta}\, n_\beta] \quad = \quad 0$$

$$[\dot{u}_\alpha\, n_\beta] \quad = \quad 0 \tag{2.1.2}$$

A comma before a subscript indicates a derivative with respect to the coordinate whose label follows the comma. Here it should be pointed out that the boundary conditions apply at every material discontinuity, so that the surface S represents both internal and external boundaries. To be explicit,

$$S = S_1 \oplus S_2 \oplus \ldots \oplus S_N$$

where S_k denotes the external boundaries of the volume V_k $(k = 1, \ldots, N)$ in which the material properties are continuous. Therefore, $S_1, S_2, \ldots, S_N$ account for internal boundaries as well as the external boundary of the medium, so that S is the set of all surfaces of discontinuity. When internal boundaries of material discontinuity occur, the equations of motion, expressed by the first equation in (2.1.2), apply in each zone in which the medium properties are continuous, while the boundary conditions in (2.1.2) apply at the boundaries of each zone of continuity to connect the wavefields

6

across medium discontinuities separating the zones V_k. That is,

$$[t_{\alpha\beta} n_\beta]_1 = [t_{\alpha\beta} n_\beta]_1 = \ldots = 0$$

and similarly for $[\dot{u}_\alpha n_\beta]$. In a solid medium, it is usual to consider all internal boundaries to be "welded", that is, to be non-slip boundaries such that not only is the normal component of the particle velocity continuous, but the tangential components are as well. In this case, for solid-solid interface boundaries, the final boundary condition in (2.1.2) is replaced by the displacement continuity condition

$$[\dot{u}_\alpha] = 0$$

with the other conditions in (2.1.2) unmodified. For solid-fluid or fluid-fluid boundaries, slip (*i.e.* discontinuities of tangential velocities) can of course occur, so in these cases the entire set in (2.1.2) applies as is.

2.2 Weighted Residuals Approximation

Approximate solutions to the equations of motion and boundary conditions are obtained by expressing the spatial dependence of the displacement components $u_\alpha(\mathbf{x}, t)$ and the material parameters in terms of finite expansions with time-dependent expansion coefficients. The displacement coefficients are obtained at discrete instants in time by minimizing approximation error, using the method of weighted residuals. With the spatial dependence of the field variables in (2.1.2) approximated by a finite expansion, the momentum of the approximate system is not the same as the momentum of the continuous system. In other words, the lack of completeness in the expansions produces an error, or residual, in momentum. Therefore, the expansion coefficients of the field variables are chosen to satisfy momentum in a sufficiently accurate approximate sense, by making the momentum residual orthogonal to a specified set of weighting functions. Such an approximation method is termed a method of weighted residuals (MWR) (Finlayson 1972).

For the weighted residuals formulation in this section, we introduce a general set of basis functions that could correspond to the set in any numerical method of MWR type. Finite difference methods are equivalent to weighted residuals formulations whose basis functions are nonzero only at a set of collocation points. Finite element methods are equivalent to weighted residuals formulations whose basis functions are typically piecewise-continuous polynomials. With finite difference and finite element methods, the expansion coefficients are typically values of nodal displacement.

With pseudospectral methods, the basis functions are spatially global, and the coefficients are wave vector coefficients. However, the pseudospectral expansion coefficients are related to nodal displacement values, as shown in section 3.

Let $b(\mathbf{x}, \mathbf{k})$ denote a general basis function for the particle displacement expansion in a 3-D orthogonal coordinate system with directional unit vectors $\mathbf{i}_\alpha$, $\alpha = 1, 2, 3$ along coordinate axes. The vector $\mathbf{k} = k_\alpha \mathbf{i}_\alpha$ labels the basis functions in terms of the set of indices $k_\alpha = (k_1, k_2, k_3)$. Although we will use Cartesian coordinates for particular choices of basis functions, the weighted residuals method is applicable in any coordinate system. Each component of displacement is approximated as

$$u_\gamma^{(b)}(\mathbf{x}, t) = \sum_{\mathbf{k}} \hat{u}_\gamma(\mathbf{k}, t)\, b(\mathbf{x}, \mathbf{k}) \qquad (2.2.1)$$

where the superscript on $u_\gamma^{(b)}(\mathbf{x}, t)$ distinguishes this field from the exact field $u_\gamma(\mathbf{x}, t)$. All quantities that are approximated by a finite expansion will be labeled with such a superscript, and the letter used in the superscript will identify the basis functions used for the expansion. With this convention, we will be able to distinguish between the expansion coefficients of different basis functions when using more than one type of basis set.

Since numerical methods, in general, can be formulated as series of matrix operations, it is useful to adopt matrix notation for our formulation. Let lowercase boldface type denote column vectors and uppercase boldface type denote matrices with components in the space of the vector $\mathbf{k}$. We denote the displacement approximation of equation (2.2.1) as

$$u_\gamma^{(b)} = \hat{\mathbf{u}}_\gamma^\top\, \mathbf{b} \qquad (2.2.2)$$

where the superscript $^\top$ denotes a matrix transpose. The column vectors have a component for each possible value of the discrete vector $\mathbf{k}$, and each component of $\mathbf{k}$, in general, has different limits.

For the following analysis we consider a linear constitutive relation $t_{\alpha\beta} = c_{\alpha\beta\gamma\delta}\, \epsilon_{\gamma\delta}$ with strain $\epsilon_{\gamma\delta} = \frac{1}{2}\left(u_{\gamma,\delta} + u_{\delta,\gamma}\right)$. In general, $c_{\alpha\beta\gamma\delta}$ can be an integral operator incorporating relaxation and viscous terms as well as elastic moduli. We denote the strain approximation obtained by using the finite expansion of (2.2.1) with the superscript (b):

$$\epsilon_{\gamma\delta}^{(b)} = \frac{1}{2}\left(\hat{\mathbf{u}}_\gamma^\top\, \mathbf{b}_{,\delta} + \hat{\mathbf{u}}_\delta^\top\, \mathbf{b}_{,\gamma}\right) \qquad (2.2.3)$$

where $\hat{\mathbf{u}}_\gamma$ is a (time-dependent) expansion coefficient. The elastic modulus tensor $c_{\alpha\beta\gamma\delta}(\mathbf{x})$ and the mass density $\rho(\mathbf{x})$, which fundamentally give rise to the complications in the wavefield, are

likewise expanded using a finite basis set $\mathbf{b}'$ and expressed as

$$c^{(b')}_{\alpha\beta\gamma\lambda} = \hat{\mathbf{c}}^{\mathsf{T}}_{\alpha\beta\gamma\lambda}\, \mathbf{b}' \quad \text{and} \quad \rho^{(b')} = \hat{\rho}^{\mathsf{T}}\, \mathbf{b}' \tag{2.2.4}$$

The material basis set $\mathbf{b}'$ can, in general, be different from the set $\mathbf{b}$ used for the displacement and strain fields. However, for efficient evaluation of the equations of the weighted residuals formulation, it is necessary that the material basis set $\mathbf{b}'$ be orthogonal to the displacement basis set $\mathbf{b}$. This necessitates choosing the set $\mathbf{b}'$ to be either the complete set $\mathbf{b}$ or a subset of $\mathbf{b}$. Both cases will be discussed below. The corresponding stress approximation is therefore

$$t^{(b)}_{\alpha\beta} = c^{(b')}_{\alpha\beta\gamma\delta}\, \epsilon^{(b)}_{\gamma\delta} \tag{2.2.5}$$

The displacement expansion of (2.2.1) and the stress tensor expansion of (2.2.5) are used in the equations of motion and boundary conditions of (2.1.3). In general, the body force density f_α can also be approximated with a corresponding expansion, although for relatively simple sources the body force density can be applied exactly. For generality at this point, however, we assume an expansion for the body force density of the form

$$f^{(b)}_\alpha = \hat{\mathbf{f}}^{\mathsf{T}}\, \mathbf{b} \tag{2.2.6}$$

2.3 Galerkin's Method

The time-dependent expansion coefficients $\hat{\mathbf{u}}_\gamma$ are determined by minimizing the solution error within the volume and on the (bounding) surface of the problem space. Therefore, the MWR formulation incorporates a residual of both the solution to the differential equations of momentum conservation and the boundary conditions. Of course the relative accuracy of the numerical solution within the volume V to the accuracy on the surface S depends not only on the basis functions, but also on the weight functions used in the volume and surface norms. In general, the weighting functions of the weighted residuals method must be chosen so that the system of algebraic equations that results can be evaluated efficiently for the expansion coefficients. We adopt the approximation referred to as Galerkin's method by choosing the set of weighting functions to be the same as the field variable expansion set. In this case, the error is made orthogonal to the expansion set. For the set of orthogonal basis functions $\mathbf{b}$, the Galerkin weighted residuals statement of momentum conservation is

$$\int_{V-S} \mathbf{b}^* \left[\rho^{(b')}\partial_t^2 u^{(b)}_\alpha - t^{(b)}_{\alpha\beta,\beta} - f^{(b)}_\alpha \right] dV = 0$$

9

$$\oint_S \mathbf{b}^* [\, t_{\alpha\beta}^{(b)} n_\beta \,] \, dS = 0 \quad \text{and} \quad \oint_S \mathbf{b}^* [\, u_\alpha^{(b)} \,] \, dS = 0 \tag{2.3.1}$$

for all $\alpha = 1, 2, 3$. In cases involving fluid boundaries, the integrand term $[u_\alpha]$ in the final boundary constraint integral is replaced by $[\dot{u}_\alpha n_\alpha]$, so that only the normal particle velocity component need be continuous.

In (2.3.1) we have used "condensed" representations, in that these relations apply piecewise in a discontinuous material volume. That is, the global representation in explicit form is

$$\int_{V_1 - S_1} \mathbf{b}^* \left[\rho^{(b')} \partial_t^2 u_\alpha^{(b)} - t_{\alpha\beta,\beta}^{(b)} - f_\alpha^{(b)} \right] dV = \int_{V_2 - S_2} \mathbf{b}^* \left[\rho^{(b')} \partial_t^2 u_\alpha^{(b)} - t_{\alpha\beta,\beta}^{(b)} - f_\alpha^{(b)} \right] dV$$

$$= \ldots = \int_{V_N - S_N} \mathbf{b}^* \left[\rho^{(b')} \partial_t^2 u_\alpha^{(b)} - t_{\alpha\beta,\beta}^{(b)} - f_\alpha^{(b)} \right] dV = 0$$

$$\oint_{S_1} \mathbf{b}^* [\, t_{\alpha\beta}^{(b)} n_\beta \,] \, dS = \oint_{S_2} \mathbf{b}^* [\, t_{\alpha\beta}^{(b)} n_\beta \,] \, dS = \ldots = \oint_{S_N} \mathbf{b}^* [\, t_{\alpha\beta}^{(b)} n_\beta \,] \, dS = 0 \tag{2.3.2}$$

and

$$\oint_{S_1} \mathbf{b}^* [\, u_\alpha^{(b)} \,] \, dS = \oint_{S_2} \mathbf{b}^* [\, u_\alpha^{(b)} \,] \, dS = \ldots = \oint_{S_N} \mathbf{b}^* [\, u_\alpha^{(b)} \,] \, dS = 0$$

where S_1, S_2, etc. are defined to mean the surfaces bounding the sub-regions V_1, V_2, etc. within which the material properties are continuous. Therefore, relations like those in (2.3.1) are to be interpreted as applying in any of the sub-regions V_k. The boundary conditions serve to connect fields between the regions since, for example,

$$[\, t_{\alpha\beta}^{(b)} n_\beta \,] = \left[t_{\alpha\beta}^{(b)}(S_k^+) - t_{\alpha\beta}^{(b)}(S_k^-) \right] n_\beta = 0 \tag{2.3.3}$$

constrains the traction fields in adjacent sub-regions to be equal at their common boundary.

If the medium can be represented adequately by a basis set that is continuous throughout the entire model volume, then there are no internal discontinuities in the material properties. In this case, traction, displacement and velocity fields are also continuous and the boundary condition integrals in (2.3.1) and (2.3.2) for internal boundaries are absent (they are automatically satisfied). Then the explicit form of (2.3.1) can be expressed as

$$\int_{V - S_0} \mathbf{b}^* \left[\rho^{(b')} \partial_t^2 u_\alpha^{(b)} - t_{\alpha\beta,\beta}^{(b)} - f_\alpha^{(b)} \right] dV = 0$$

$$\oint_{S_0} \mathbf{b}^* [\, t_{\alpha\beta}^{(b)} n_\beta \,] \, dS = 0 \quad ; \quad \oint_{S_0} \mathbf{b}^* [\, u_\alpha^{(b)} \,] \, dS = 0 \tag{2.3.4}$$

10

where S_0 denotes (only) the external boundary of the medium considered. Clearly the equations in (2.3.4) have the same form as in (2.3.1). That is, if we interpret S in (2.3.1) to be the external boundary of a region in which the material properties can be represented by a continuous basis set, then the equations of (2.3.1) are equivalent to those in (2.3.4). In general, however, the set in (2.3.1) represents the set (2.3.2), which allows for the existence of many zones of continuous material variations separated by discontinuities in material properties and, therefore, discontinuities in wavefield variables. The equations in (2.3.2) show how the separate wave fields given by (2.3.4) for continuous domains must be connected through boundary conditions at the domain boundaries. Thus, the equations in (2.3.2) describe the multi-domain equation set while the equations in (2.3.4) describe a single continuous domain set, while the set (2.3.1), with the conventions adopted for S and V, represents either.

The situation for most geophysical applications is that material property variations in the continuum approximation are well represented by continuous variations in parameter values. Therefore, a self consistent approximation for wave propagation in composite solid and fluid media, like that composing planetary bodies, are the equations in (2.3.4), *provided* a basis set is used that can accurately represent rapid changes in material properties and field variables over rather small distance intervals. In order to model very rapid spatial variations in material properties which cannot easily be represented by a convenient finite set of basis functions, it is important to include material discontinuities in the medium description. We therefore treat the general case here, given in (2.3.1) and (2.3.2), to obtain a formulation that can be used in a multi-domain representation. However, since (2.3.1) and (2.3.4) are essentially interchangeble in terms of formalism, we are able to simulataneously develop a formalism that is appropriate for the single domain case of (2.3.4). Since, as we will demonstrate, the set in (2.3.4) is sufficient for modeling many problems of interest, in this study we concentrate on examples involving the use of the set in (2.3.4).

2.4 The Weak Form of Galerkin's Method

A significant advantage of using Galerkin's method in a pseudospectral approximation for elastodynamics is that it can be formulated so that the resulting algebraic equations are expressed in terms of self-adjoint, *i.e.* normal, matrices. Normal matrices have a complete, orthogonal set of eigenvectors, and the well-known von Neumann stability analysis can be applied to numerical methods with normal matrices. Most importantly, the computational requirements for time-stepping an initial

11

value problem with a method whose algebraic equations can be put in a normal matrix form typically are less than for a method with a non-normal matrix (Trefethen 1988; Richtmyer and Morton 1967, Chapter 4). In particular, leapfrog time-stepping can be used for numerical methods with normal matrices (Orrey 1995), whereas methods with non-normal matrices require time-stepping schemes which stably iterate matrix equations with complex eigenvalues, and particular schemes are stable over particular regions of a complex space of eigenvalues. Canuto *et al.* (1988) describe many time-stepping schemes for pseudospectral methods and indicate their regions of stability.

In order to express the equations of (2.3.1) as an algebraic system of equations with normal matrices, the so-called weak Galerkin formulation is obtained by applying Gauss' theorem to the second term in the volume integral:

$$
\int_{V-S} \mathbf{b}^* \, t_{\alpha\beta,\beta}^{(b)} \, dV = \oint_{S^+} \mathbf{b}^* \, t_{\alpha\beta}^{(b)} \, n_\beta \, dS - \int_{V-S} \mathbf{b}_{,\beta}^* \, t_{\alpha\beta}^{(b)} \, dV
\tag{2.4.1}
$$

where S^+ is used to denote the surface approached from inside V. Now the first integral expression in (2.3.1) can be written as

$$
\int_{V-S} \left[\mathbf{b}^* \, \rho^{(b')} \, \partial_t^2 u_\alpha^{(b)} + \int_V \mathbf{b}_{,\beta}^* \, t_{\alpha\beta}^{(b)} - \int_V \mathbf{b}^* f_\alpha^{(b)} \right] dV = \oint_{S^+} \mathbf{b}^* \, t_{\alpha\beta} n_\beta \, dS
\tag{2.4.2}
$$

Equation (2.4.2) and the boundary conditions

$$
\oint_{S^+} \mathbf{b}^* \, t_{\alpha\beta} n_\beta \, dS = \oint_{S^-} \mathbf{b}^* \, t_{\alpha\beta} n_\beta \, dS
$$

$$
\oint_{S^+} \mathbf{b}^* \, u_\alpha^{(b)} \, dS = \oint_{S^-} \mathbf{b}^* \, u_\alpha^{(b)} \, dS
\tag{2.4.3}
$$

constitute integral equations to be used in the numerical approximations. In this approach, the first boundary relation in (2.4.3) is used to connect the fields across boundaries S since it may be used in (2.4.2) to link the tractions on S^+ to those in a neighboring domain, expressed on S^-.

In the case of a single domain, where (2.3.4) applies and material properties are represented by a continuous basis function expansion, the formalism simplifies because only the external boundary S_0 appears. In this case the set (2.4.2) plus (2.4.3) reduces to

$$
\int_{V-S_0} \left[\mathbf{b}^* \, \rho^{(b')} \, \partial_t^2 u_\alpha^{(b)} + \mathbf{b}_{,\beta}^* \, t_{\alpha\beta}^{(b)} - \mathbf{b}^* f_\alpha^{(b)} \right] dV = \oint_{S_0^-} \mathbf{b}^* \, \bar{t}_{\alpha\beta}^{(b)} n_\beta \, dS
$$

$$
\oint_{S_0^+} \mathbf{b}^* \, t_{\alpha\beta}^{(b)} n_\beta \, dS = \oint_{S_0^-} \mathbf{b}^* \, \bar{t}_{\alpha\beta}^{(b)} n_\beta \, dS
\tag{2.4.4}
$$

where $\bar{t}_{\alpha\beta}^{(b)}$ are the (assumed specified) applied stresses on the surface S_0. If the external boundary is a free surface, then the displacements are unconstrained at this surface and the tractions on S_0 must vanish. In this case the governing equations are

$$\int_{V-S_0} \left[\mathbf{b}^* \rho^{(b)} \partial_t^2 u_\alpha^{(b)} + \mathbf{b}_{,\beta}^* t_{\alpha\beta}^{(b)} - \mathbf{b}^* f_\alpha^{(b)} \right] dV = 0$$

$$\oint_{S_0^+} \mathbf{b}^* t_{\alpha\beta}^{(b)} n_\beta \, dS = 0 \tag{2.4.5}$$

It is important to note that the first equation in either (2.4.4) or (2.4.5) is true only if the boundary integral involving the tractions over S_0 is satisfied explicitly by the numerical approximation. That is, satisfying the first equation is not sufficient to result in a field representation that satisfies the boundary condition on S_0, so the boundary condition must be applied explicitly to the tractions.

The effect of energy sources can be represented in the field equations in a number of possible ways, all of which must of course be equivalent. A simple and direct way is to use the external body force density f_α to represent both the actual external forces, in particular gravity in the case of seismic and acoustic wavefields, and the applied sources, such as an explosion or an earthquake. In this case the body force density is approximated with the basis set $\mathbf{b}$, and the volume integral over the external forces may be written in two parts:

$$\int_{V-S_0} \mathbf{b}^* f_\alpha^{(b)} dV = \int_{V-S_0} \mathbf{b}^* g_\alpha^{(b)} dV + \int_{V-S_0} \mathbf{b}^* s_\alpha^{(b)} dV \tag{2.4.6}$$

Here $g_\alpha^{(b)}$ represents a body force field, like gravity, and $s_\alpha^{(b)}$ represents the (spatially confined) forces on the medium produced by the source. Because the force fields g_α and s_α are represented as expansions (of the form in (2.2.6)) with the global basis set $\mathbf{b}$, the field representations $g_\alpha^{(b)}$ and $s_\alpha^{(b)}$ have value over the entire domain $V - S$. However, s_α can typically be made zero outside some relatively small source volume V_S. Therefore, rather than expanding s_α in the basis set $\mathbf{b}$ to generate the series representation $s_\alpha^{(b)}$, it is often simpler to use the known (specified) source function s_α directly in the integral. In this case, with s_α having value only inside the source volume V_S, we have

$$\int_{V-S} \mathbf{b}^* s_\alpha^{(b)} dV = \int_{V_S} \mathbf{b}^* s_\alpha \, dV \tag{2.4.7}$$

A similar simplification can be used for the field g_α and for the applied surface tractions $\bar{t}_{\alpha\beta} n_\beta$.

13

In terms of these source fields, the equations in (2.4.4) can be written as

$$\int_{V-S_0} \left[\mathbf{b}^* \rho^{(b')} \partial_t^2 u_\alpha^{(b)} + \mathbf{b}^*_{,\beta} t_{\alpha\beta}^{(b)} - \mathbf{b}^* g_\alpha \right] dV = \oint_{S_0^-} \mathbf{b}^* \bar{t}_{\alpha\beta}^{(b)} n_\beta \, dS + \int_{V_S} \mathbf{b}^* s_\alpha dV$$

$$\oint_{S_0^+} \mathbf{b}^* t_{\alpha\beta}^{(b)} n_\beta \, dS = \oint_{S_0^-} \mathbf{b}^* \bar{t}_{\alpha\beta} n_\beta \, dS \tag{2.4.8}$$

Of course the form corresponding to (2.4.5), where no surface stresses are applied on the external boundary S_0, is obtained by simply setting $\bar{t}_{\alpha\beta} = 0$.

In the multi-domain case, where V is partitioned into sub-regions V_k with surfaces S_k, $k = 1, 2, \ldots, N$, the relations take the form

$$\int_{V_k - S_k} \left[\mathbf{b}^* \rho^{(b')} \partial_t^2 u_\alpha^{(b)} + \mathbf{b}^*_{,\beta} t_{\alpha\beta}^{(b)} - \mathbf{b}^* g_\alpha \right] dV = \oint_{S_k^-} \mathbf{b}^* \bar{t}_{\alpha\beta}^{(b)} n_\beta \, dS + \int_{V_k} \mathbf{b}^* s_\alpha dV$$

$$\oint_{S_k} \mathbf{b}^* [t_{\alpha\beta}^{(b)} n_\beta] \, dS = 0 \quad ; \quad \oint_{S_k} \mathbf{b}^* [u_\alpha^{(b)}] \, dS = 0 \tag{2.4.9}$$

For the domains intersecting a free surface of the medium, the displacement constraint is relaxed and the traction condition at such a boundary requires the traction in the material to equal any applied tractions, as in (2.4.8).

2.5 Incorporating Discontinuities

The essential generalization of the present development involves the choice of a form of the basis functions that will satisfy all of the relations in either (2.4.8) or (2.4.9). In particular, we consider a basis set b consisting of both the trigonometric basis set of the Fourier method and an additional set of basis functions which are not infinitely differentiable with continuous derivatives. The additional set is used to satisfy the boundary condition constraints on external and/or internal surfaces of material discontinuity in (2.4.8) or (2.4.9) while the remaining continuous set is used to satisfy the volume integral relations involving the equations of motion. Because of their construction and use (to satisfy conservation conditions on surfaces of material discontinuity) the additional functions are referred to as discontinuity functions. In effect, the set of discontinutiy functions provides the extra degrees of freedom required to explicitly satisfy the boundary conditions on the field variables. By construction, the set of discontinuity functions is chosen to be orthogonal to the set of trigonometric functions over the interval of each spatial coordinate, while each member of the

14

discontinuity set is also required to be orthogonal to all other members of the set. (This orthogonal construction is necessary to maintain the efficiency of the computational scheme developed below.)

The trigonometric functions of the Fourier method are defined in terms of a set of wave vectors $\underset{\sim}{k} = \underset{\sim}{k_\alpha} i_\alpha$, which are discretized over each coordinate length X_α in a 3-D system of Cartesian coordinates as

$$\underset{\sim}{k_\alpha} = \frac{2\pi k_\alpha}{X_\alpha} \quad ; \quad -\frac{N_\alpha - 1}{2} \le k_\alpha \le \frac{N_\alpha - 1}{2} \quad \alpha = 1, 2, 3 \qquad (2.5.1)$$

We have adopted indice ranges associated with odd radix Fast Fourier Transforms (FFTs) (Temperton 1983) since these transforms avoid the Nyquist frequency and the associated Nyquist errors that are produced when derivatives are computed using a pseudospectral approximation (Canuto *et al.* 1988; Orrey 1995). The tilde underline of $\underset{\sim}{k_\alpha}$ serves to indicate that the spatial dependence of $\underset{\sim}{k_\alpha}$ is an inverse length, and therefore the index k_α corresponds to a discrete wave number index. From now on, any index with a tilde underline will correspond to a discrete wave number index. In terms of the discrete wave number $\underset{\sim}{k_\alpha}$ for the x_α coordinate, we define a set of 1-D Fourier basis functions with the compact notation

$$e_{(\alpha)} = \left\{ e^{i \underset{\sim}{k_\alpha} x_\alpha} \right\}_{\underset{\sim}{k_\alpha}} \qquad (\text{ no sum on } \alpha) \qquad (2.5.2)$$

where $\{\ \}_{\underset{\sim}{k_\alpha}}$ denotes the set of functions for all values of $\underset{\sim}{k_\alpha}$. A corresponding set of coefficients for an expansion of the displacement component u_γ in the basis functions of (2.5.2) is defined as

$$^{(\alpha)}\hat{u}_\gamma^{(e)} = \left\{ {}^{(\alpha)}\hat{u}_\gamma^{(e)}(\underset{\sim}{k_\alpha}) \right\}_{\underset{\sim}{k_\alpha}} \qquad (2.5.3)$$

Then the 1-D Fourier expansion along the coordinate x_α is

$$^{(\alpha)}\hat{u}_\gamma^{(e)\top} e_{(\alpha)} = \sum_{\underset{\sim}{k_\alpha}} {}^{(\alpha)}\hat{u}_\gamma^{(e)}(\underset{\sim}{k_\alpha}) e^{i \underset{\sim}{k_\alpha} x_\alpha} \qquad (\text{ no sum on } \alpha) \qquad (2.5.4)$$

For expansions of the field variables in terms of both trigonometric and discontinuity functions, we define $d_{(\delta)}$ to be a set of discontinuity functions with a spatial dependence in the δ direction. Then, for the general case of discontinuity functions used in all coordinates directions, the expansion of the displacement component u_γ is

$$u_\gamma^{(b)} = \prod_{\delta=1}^{3} \left({}^{(\delta)}\hat{u}_\gamma^{(e)\top} e_{(\delta)} + {}^{(\delta)}\hat{u}_\gamma^{(d)\top} d_{(\delta)} \right) \qquad (2.5.5)$$

where $^{(\delta)}\hat{u}_\gamma^{(e)}$ and $^{(\delta)}\hat{u}_\gamma^{(d)}$ are sets of (time-dependent) expansion coefficients for the basis functions in the δ direction. The use of the construction in (2.5.5) can be quite flexible, in that the field

15

quantities in a 3-D medium can be represented by using one-dimensional expansions with different basis sets in the different coordinate directions. Let the expansion of (2.5.5) be arranged as a triple product of 1-D Fourier expansions plus a supplementary expansion that contains all of the remaining combinations of $^{(\delta)}\hat{u}_\gamma^{(e)T} e_{(\delta)}$ and $^{(\delta)}\hat{u}_\gamma^{(d)T} d_{(\delta)}$. We denote the supplementary function set as s, which is in general a mixed set of Fourier and discontinuity functions. Then (2.5.5) becomes

$$u_\gamma^{(b)} = \hat{u}_\gamma^{(e)T} e + \hat{u}_\gamma^{(s)T} s \tag{2.5.6}$$

in terms of the set of 3-D Fourier basis functions

$$e = \left\{ e^{i \mathbf{k} \cdot \mathbf{x}} \right\}_{\mathbf{k}} \tag{2.5.7}$$

Eq. (2.5.6) can be conveniently expressed in the general form of (2.2.2) by partitioning the vectors $\hat{u}_\gamma$ and b into Fourier and supplementary contributions:

$$\hat{u}_\gamma = \begin{pmatrix} \hat{u}_\gamma^{(e)} \\ \hat{u}_\gamma^{(s)} \end{pmatrix} \quad ; \quad b = \begin{pmatrix} e \\ s \end{pmatrix} \tag{2.5.8}$$

In a similar manner, the mass density and rheological tensor can be expanded as

$$\rho^{(b')} = \prod_{\delta=1}^{3} \left(^{(\delta)}\hat{\rho}^{(e)T} e_{(\delta)} + ^{(\delta)}\hat{\rho}^{(d')T} d'_{(\delta)} \right) \quad ;$$

$$c_{\alpha\beta\gamma\lambda}^{(b')} = \prod_{\delta=1}^{3} \left(^{(\delta)}\hat{c}_{\alpha\beta\gamma\lambda}^{(e)T} e_{(\delta)} + ^{(\delta)}\hat{c}_{\alpha\beta\gamma\lambda}^{(d')T} d'_{(\delta)} \right) \tag{2.5.9}$$

in terms of the Fourier sets $e_{(\delta)}$ and the material discontinuity sets $d'_{(\delta)}$ for each coordinate x_δ. Arranging these expansions as a triple product of 1-D Fourier expansions plus a supplementary expansion in terms of a basis set s' which contains all remaining combinations of the basis functions, we have

$$\rho^{(b')} = \hat{\rho}^{(e)T} e + \hat{\rho}^{(s')T} s' \equiv \hat{\rho}^T b' \quad ;$$

$$c_{\alpha\beta\gamma\lambda}^{(b')} = \hat{c}_{\alpha\beta\gamma\lambda}^{(e)T} e + \hat{c}_{\alpha\beta\gamma\lambda}^{(s')T} s' \equiv \hat{c}_{\alpha\beta\gamma\lambda}^T b' \tag{2.5.10}$$

where, as discussed in the context of (2.2.4), the material basis set

$$b' = \begin{pmatrix} e \\ s' \end{pmatrix} \tag{2.5.11}$$

can be different than the set b used for the field variables. The discontinuity functions provide an accurate representation of material models whose properties are, in general, different at one endpoint of each coordinate interval than at the other endpoint. This is the case for a single-domain problem, in which the material properties are continuous throughout the problem volume. For a multi-domain problem described by (2.4.9), the representations in (2.5.9) are used in each domain. Discontinuities in material properties exist across the boundaries between domains and the material properties are continuous within each domain.

A simpler numerical algorithm results from the particular choice $\mathbf{d}'_{(\alpha)} = \mathbf{O}_{(\alpha)}$ (where $\mathbf{O}$ denotes the null set) for all α, so that the material properties are represented as

$$\rho^{(e)} = \hat{\rho}^\mathsf{T} \mathbf{e} \quad ; \quad c^{(e)}_{\alpha\beta\gamma\lambda} = \hat{\mathbf{c}}^\mathsf{T}_{\alpha\beta\gamma\lambda} \mathbf{e} \tag{2.5.12}$$

This provides a good approximation to media whose material properties are the same at both endpoints of each coordinate interval and are continuous throughout the problem volume. For single-domain problems, it is still necessary to represent the field variables with (2.5.5), which includes discontinuity functions, if the boundary surface integral in (2.4.8) must be satisfied. For multi-domain problems, discontinuity functions in the field variable representations are necessary to couple the separate domains with boundary conditions. In this study, we provide simulation results of a single-domain method that incorporates the trigonometric basis set expansions of (2.5.12), but we include the formalism for the more general method that uses the expansions of (2.5.9).

With the basis set expansions given by (2.5.5) and (2.5.9), we use the following matrix representation of the governing equations of (2.4.8) for momentum conservation in a single domain:

$$\hat{\mathbf{M}}\,\partial_t^2 \hat{\mathbf{u}}_\alpha + \hat{\mathbf{K}}_{\alpha\gamma}\hat{\mathbf{u}}_\gamma = \hat{\mathbf{g}}_\alpha + \hat{\mathbf{s}}_\alpha + \hat{\mathbf{t}}_\alpha \quad ; \tag{2.5.13}$$

$$\hat{\mathbf{H}}_{\alpha\gamma}\hat{\mathbf{u}}_\gamma = \hat{\mathbf{q}}_\alpha \tag{2.5.14}$$

with the quantities

$$\hat{\mathbf{M}} = \int_{V-S_0} \mathbf{b}^* \left(\hat{\rho}^\mathsf{T} \mathbf{b} \right) \mathbf{b}^\mathsf{T} dV \tag{2.5.15}$$

$$\hat{\mathbf{K}}_{\alpha\gamma} = \int_{V-S_0} \mathbf{b}^*_{,\beta} \left(\hat{\mathbf{c}}^\mathsf{T}_{\alpha\beta\gamma\lambda} \mathbf{b} \right) \mathbf{b}_{,\lambda}{}^\mathsf{T} dV \tag{2.5.16}$$

$$\hat{\mathbf{g}}_\alpha = \int_{V-S_0} \mathbf{b}^* g_\alpha \, dV \tag{2.5.17}$$

$$\hat{\mathbf{s}}_\alpha = \int_{V_S} \mathbf{b}^* s_\alpha \, dV \tag{2.5.18}$$

17

$$\hat{t}_\alpha = \oint_{S_0} \mathbf{b}^* \bar{t}_{\alpha\beta} n_\beta \, dS \tag{2.5.19}$$

and

$$\hat{\mathbf{H}}_{\alpha\gamma} = \oint_{S_0} \mathbf{b}^* \left(\hat{c}_{\alpha\beta\gamma\lambda}^\top \mathbf{b}' \right) \mathbf{b}_{,\lambda}^\top n_\beta \, dS \tag{2.5.20}$$

The mass matrix $\hat{\mathbf{M}}$ and stiffness matrix $\hat{\mathbf{K}}_{\alpha\gamma}$ are evaluated using the orthogonality of the basis functions, while the applied body force terms $\hat{\mathbf{g}}_\alpha$ and $\hat{\mathbf{s}}_\alpha$ and the surface force term $\hat{\mathbf{t}}_\alpha$ are evaluated either analytically, for simple sources, or by specifying nodal source values and using Gaussian quadrature. The generalization to the multi-domain case of eq. (2.4.9) is straightforward, since the single-domain results of (2.5.13) with the quantities in (2.5.15)-(2.5.19) apply to each of the multiple domains (indexed by $k = 0, 1, \dots$), while the boundary condition (2.5.14) is modified to the form

$$^k\hat{\mathbf{H}}_{\alpha\gamma}{}^k\hat{u}_\gamma = {}^{k+1}\hat{\mathbf{H}}_{\alpha\gamma}{}^{k+1}\hat{u}_\gamma \tag{2.5.21}$$

with the superscript k indicating evaluation on the kth interface between the domains k and $k+1$.

3   The Pseudospectral Method for Numerical Approximation

The governing equations (2.5.13) and (2.5.14) are to be solved for the discrete wave number expansion coefficients of the particle displacement field. The only approximation made to obtain (2.5.13) and (2.5.14) was to approximate field variables with truncated discrete wave number expansions. It is now necessary, in order to obtain a numerical solution, to discretize the spatial domain of the problem as well as the wave number domain. This amounts to evaluating the integrals of (2.5.15)-(2.5.20) using Gaussian quadrature. The resulting method is referred to as a pseudospectral method (Orszag 1971).

3.1   Spatial Discretization

Consider first the spatial discretization of the field variables. We have adopted wave number expansions of the form in (2.2.1), in which a different basis set can be used in each coordinate direction. Therefore, let the displacement field expansion of (2.2.1) be expressed as

$$u_\gamma^{(b)} = \prod_{\alpha=1}^{3} {}^{(\alpha)}u_\gamma^{(b)} \equiv \prod_{\alpha=1}^{3} {}^{(\alpha)}\hat{u}_\gamma^\top \, \mathbf{b}_{(\alpha)} \tag{3.1.1}$$

18

where $\mathbf{b}_{(\alpha)}$ is a column vector of basis functions for the α-direction expansion. Now, the basis set in each coordinate direction is defined to be orthonormal as

$$\int_0^{X_\alpha} b_{(\alpha)}^* (x_\alpha, k_\alpha) \, b_{(\alpha)} (x_\alpha, l_\alpha) \, w_{(\alpha)} (x_\alpha) \, dx_\alpha = \delta_{k_\alpha l_\alpha} \tag{3.1.2}$$

for $\alpha = 1, 2, 3$ and any two wavenumbers k_α and l_α of the set in the α-direction, where the star indicates complex conjugate and $w_{(\alpha)} (x_\alpha)$ is the weight function of the orthogonality. Using this orthogonality relation, the expansion coefficients in (3.1.1) are obtained as

$$^{(\alpha)}\hat{u}_\gamma(k_\alpha, t) = \int_0^{X_\alpha} {}^{(\alpha)}u_\gamma^{(b)}(x_\alpha, t) \, b_{(\alpha)}^* (x_\alpha, k_\alpha) \, w_{(\alpha)} (x_\alpha) \, dx_\alpha \tag{3.1.3}$$

However, since $^{(\alpha)}u_\gamma^{(b)}(x_\alpha, t)$ is an expansion in terms of a finite set ($\mathbf{b}_{(\alpha)}$), the integral in (3.1.3) is equal to the Gaussian quadrature sum obtained by discretizing the spatial domain into a set of collocation points. With a pseudospectral approximation, the collocation points are generally chosen as the roots of the first neglected basis function in the (truncated) expansion (Boyd 1989, p. 125). However, it is usually necessary to include the end points of the interval in the set of collocation points, in which case Gauss-Lobatto quadrature is typically used (Canuto *et al.* 1988).

In general, the position vector $\mathbf{x}$ is discretized into the set of grid points

$$\tilde{j}_\alpha = j_\alpha \Delta_\alpha(j_\alpha) \quad ; \quad 0 \leq j_\alpha \leq N_\alpha, \qquad \alpha = 1, 2, 3 \tag{3.1.4}$$

for collocation. From now on, any index with a tilde overline will correspond to the index of a discrete spatial position. The grid point spacing $\Delta_\alpha(j_\alpha)$ is, in general, a function of position and direction. The total number of grid points typically equals the total number of discrete wave numbers in the expansion of (2.2.2). Values of the displacement approximation $u_\gamma^{(b)}(\mathbf{x}, t)$ at the grid points are represented by the vector $\mathbf{u}_\gamma$, with individual components

$$u_\gamma(\mathbf{j}, t) = u_\gamma^{(b)}(\mathbf{x}, t)\Big|_{\mathbf{x} = \tilde{j}_\alpha \mathbf{i}_\alpha} \tag{3.1.5}$$

and the discretized basis function $b(\mathbf{x}, \mathbf{k})$ becomes a matrix operator $\mathbf{B}$ with individual components

$$B(\mathbf{j}, \mathbf{k}) = b(\mathbf{x}, \mathbf{k})\Big|_{\mathbf{x} = \tilde{j}_\alpha \mathbf{i}_\alpha} \tag{3.1.6}$$

The collocation matrix operator $\mathbf{B}$ produces a vector of collocation values from a vector of wave number coefficients:

$$\mathbf{u}_\gamma = \mathbf{B} \, \hat{\mathbf{u}}_\gamma \tag{3.1.7}$$

19

A unique inverse $\mathbf{B}^{-1}$ is defined so that the Gaussian quadrature relation is

$$\hat{\mathbf{u}}_\gamma = \mathbf{B}^{-1}\mathbf{u}_\gamma \tag{3.1.8}$$

The continuous field $u_\gamma^{(\theta)}$ can therefore be expressed as the interpolation of nodal quantities $\mathbf{u}_\gamma$:

$$u_\gamma^{(\theta)} = \left(\mathbf{B}^{-1}\mathbf{u}_\gamma\right)^\top \mathbf{b} \tag{3.1.9}$$

In order to incorporate spatial discretization into the momentum conservation relations (2.5.13) and (2.5.14), the integrals of (2.5.15)-(2.5.20) can be evaluated with continuous quantities using the orthogonality relation (3.1.2), or all quantities can be discretized and the integrals can be evaluated using Gaussian quadrature. In the latter case, the expansion coefficients are expressed in terms of collocation values as in (3.1.8). Because all expansions in (2.5.15)-(2.5.20) are finite, the results of the continuous and discrete treatments of the integrals are equivalent.

In the following subsection, the standard Fourier pseudospectral method is obtained by discretizing the momentum conservation relations and using trigonometric basis functions, while in section 4 the standard method is generalized to the case of both trigonometic and discontinuity basis functions. For both methods, it is necessary to define descretized representations of material strain and stress. In order to do so, we restrict the general basis set $\mathbf{b}$ to be any set for which derivatives of the basis functions in the set also belong to that set. This class of functions is quite broad since it includes all polynomial-based functions. For this class of functions, differentiation with respect to the coordinate x_λ is expressed in terms of a matrix operator $\mathbf{D}_\lambda$:

$$\mathbf{b}_{,\lambda} = \mathbf{D}_\lambda^\top \mathbf{b} \tag{3.1.10}$$

Displacement derivatives are denoted

$$u_{\gamma,\lambda} = \hat{\mathbf{u}}_{\gamma\lambda}^\top \mathbf{b} \tag{3.1.11}$$

where, using (2.2.2) and (3.1.10), the coefficients are

$$\hat{\mathbf{u}}_{\gamma\lambda} = \mathbf{D}_\lambda \,\hat{\mathbf{u}}_\gamma \tag{3.1.12}$$

Combining the previous notation, the collocation derivative of the displacement component u_γ is

$$\mathbf{u}_{\gamma,\lambda} = \mathbf{B}\,\hat{\mathbf{u}}_{\gamma\lambda} = \mathbf{B}\,\mathbf{D}_\lambda\,\mathbf{B}^{-1}\mathbf{u}_\gamma \tag{3.1.13}$$

20

and the procedure for obtaining collocation derivatives of displacement from nodal displacement values is given in terms of matrix operations. Collocation strains follow as

$$\epsilon_{\gamma\lambda} = \tfrac{1}{2}\, \mathbf{B}\Big(\mathbf{D}_\lambda\, \mathbf{B}^{-1}\mathbf{u}_\gamma + \mathbf{D}_\gamma\, \mathbf{B}^{-1}\mathbf{u}_\lambda\Big) \tag{3.1.14}$$

In order to obtain collocation derivatives of the stress tensor, we define a diagonal matrix $\mathbf{C}_{\alpha\beta\gamma\lambda}$ whose components are values of the elastic tensor at the grid points of (3.1.4):

$$C_{\alpha\beta\gamma\lambda}(\mathbf{j},\mathbf{j}) = c_{\alpha\beta\gamma\lambda}(\mathbf{j}) \tag{3.1.15}$$

Then, using the elastic tensor symmetry $c_{\alpha\beta\gamma\lambda} = c_{\alpha\beta\lambda\gamma}$, the collocation stress is

$$t_{\alpha\beta} = \mathbf{C}_{\alpha\beta\gamma\lambda}\, \mathbf{B}\, \mathbf{D}_\lambda\, \mathbf{B}^{-1}\mathbf{u}_\gamma \tag{3.1.16}$$

To obtain the collocation derivative of stress, wave number coefficients are obtained by a forward transform, the coefficients are multiplied by the differentiation matrix, and the collocation derivative of stress is obtained by an inverse transform:

$$t_{\alpha\beta,\beta} = \mathbf{B}\mathbf{D}_\beta\hat{t}_{\alpha\beta} = \mathbf{B}\mathbf{D}_\beta\mathbf{B}^{-1}\mathbf{C}_{\alpha\beta\gamma\lambda}\, \mathbf{B}\, \mathbf{D}_\lambda\, \mathbf{B}^{-1}\mathbf{u}_\gamma \tag{3.1.17}$$

The discretized form of the momentum conservation relations are obtained after multiplying (2.5.13) and (2.5.14) from the left with the collocation matrix operator $\mathbf{B}$. In terms of the matrices

$$\begin{aligned}
\mathbf{M} &= \mathbf{B}\hat{\mathbf{M}}\mathbf{B}^{-1} \\
\mathbf{K}_{\alpha\gamma} &= \mathbf{B}\hat{\mathbf{K}}_{\alpha\gamma}\mathbf{B}^{-1} \\
\mathbf{H}_{\alpha\gamma} &= \mathbf{B}\hat{\mathbf{H}}_{\alpha\gamma}\mathbf{B}^{-1}
\end{aligned} \tag{3.1.18}$$

eqs. (2.5.13) and (2.5.14) become

$$\mathbf{M}\,\partial_t^2\mathbf{u}_\alpha + \mathbf{K}_{\alpha\gamma}\mathbf{u}_\gamma = \mathbf{g}_\alpha + \mathbf{s}_\alpha + \mathbf{t}_\alpha \tag{3.1.19}$$

and

$$\mathbf{H}_{\alpha\gamma}\mathbf{u}_\gamma = \mathbf{t}_\alpha \tag{3.1.20}$$

where $\mathbf{g}_\alpha = \mathbf{B}\hat{\mathbf{g}}_\alpha$, $\mathbf{s}_\alpha = \mathbf{B}\hat{\mathbf{s}}_\alpha$ and $\mathbf{t}_\alpha = \mathbf{B}\hat{\mathbf{t}}_\alpha$. For particular choices of the basis functions $\mathbf{b}$ and $\mathbf{b}'$, (3.1.19) and (3.1.20) provide governing equations for a numerical solution to the discrete displacement field $\mathbf{u}_\alpha$.

21

3.2 The Fourier Pseudospectral Method

The Fourier pseudospectral method is obtained by using the trigonometric basis functions of equation (2.5.7) in the governing equations (3.1.19) and (3.1.20). The resulting method's efficiency is due to the fact that the FFT can be used when evaluating the various expansion coefficients in equation (3.1.19). We show below that the boundary condition equation (3.1.20) vanishes because of the spatial periodicity of the trigonometric basis set. This is a fundamental drawback of the Fourier method for seismic applications.

Using the trigonometric basis (2.5.7) for all previous expansions, we have

$$\mathbf{b} = \mathbf{b}' = \mathbf{e} \tag{3.2.1}$$

and the Fourier expansion of the displacement field u_γ

$$u_\gamma = \hat{\mathbf{u}}_\gamma^\mathsf{T} \mathbf{e} \tag{3.2.2}$$

For trigonometric collocation, the spatial domain is discretized into N_α collocation points evenly spaced by a distance Δx_α along the α coordinate direction, and the coordinate lengths are $X_\alpha = N_\alpha \Delta x_\alpha$ (no sum on α). With discrete spatial positions represented as

$$\bar{j}_\alpha = j_\alpha \Delta x_\alpha \quad ; \quad 0 \le j_\alpha \le N_\alpha - 1, \qquad \alpha = 1, 2, 3 \tag{3.2.3}$$

the discretization of (3.2.2) is

$$u_\gamma(\mathbf{j}) = \sum_{\mathbf{k}} \hat{u}_\gamma(\mathbf{k}) e^{i\mathbf{k}\cdot\bar{\jmath}} \tag{3.2.4}$$

where we have suppressed the explicit time dependence of both the spatial domain and wave number domain representations of displacement. The collocation matrix operator for trigonometric functions is denoted by $\mathbf{E}$, which has individual components $E(\mathbf{j}, \mathbf{k}) = e^{i\mathbf{k}\cdot\bar{\jmath}}$, so that the compact relations between nodal displacement values and wave number coefficients are

$$\mathbf{u}_\gamma = \mathbf{E}\,\hat{\mathbf{u}}_\gamma \quad ; \quad \hat{\mathbf{u}}_\gamma = \mathbf{E}^{-1}\mathbf{u}_\gamma \tag{3.2.5}$$

$\mathbf{E}^{-1}$ is the inverse collocation operator for trigonometric functions:

$$\mathbf{E}^{-1} = \frac{1}{V_N}\mathbf{E}^* \tag{3.2.6}$$

where $V_N = \prod_{\alpha=0}^{3} N_\alpha$. Note that the inverse operator $\mathbf{E}^{-1}$ corresponds to what is typically called the direct Fourier transform, while the direct operator $\mathbf{E}$ corresponds to the typical inverse Fourier transform.

The derivative operator $\mathbf{D}_\lambda$ for the Fourier basis (2.5.7) is a diagonal matrix $\mathbf{D}_\lambda^{(e)}$ with components

$$D_\lambda^{(e)}(\mathbf{k}, \mathbf{k}) = i\underline{k}_\lambda \tag{3.2.7}$$

and the collocation derivative $\mathbf{u}_{\gamma,\lambda}$ is obtained as

$$\mathbf{u}_{\gamma,\lambda} = \mathbf{E}\,\mathbf{D}_\lambda^{(e)}\mathbf{E}^{-1}\mathbf{u}_\gamma \tag{3.2.8}$$

Using the trigonometric basis set $\mathbf{e}$, the inertial term in the differential equation of momentum conservation (2.5.13) becomes

$$\hat{\mathbf{M}}\,\partial_t^2\hat{\mathbf{u}}_\alpha = \mathbf{E}^{-1}\mathbf{M}\,\partial_t^2\mathbf{u}_\alpha \tag{3.2.9}$$

with a diagonal mass matrix $\mathbf{M}$ whose components are

$$M(\mathbf{m}, \mathbf{m}) = V_X\,\rho(\mathbf{m}) \tag{3.2.10}$$

in terms of a collocation representation of density, $\rho = \mathbf{E}\hat{\rho}$, and the problem volume $V_X = \prod_{\alpha=1}^3 X_\alpha$.

The restoring force term in (2.5.13) becomes

$$\hat{\mathbf{K}}_{\alpha\gamma}\hat{\mathbf{u}}_\gamma = -V_X\mathbf{D}_\beta^{(e)}\mathbf{E}^{-1}\mathbf{C}_{\alpha\beta\gamma\lambda}\,\mathbf{E}\,\mathbf{D}_\lambda\,\mathbf{E}^{-1}\mathbf{u}_\gamma \tag{3.2.11}$$

by using a collocation representation of the elastic modulus tensor, $\mathbf{c}_{\alpha\beta\gamma\lambda} = \mathbf{E}\,\hat{\mathbf{c}}_{\alpha\beta\gamma\lambda}$.

From (2.5.17), (2.5.18) and (2.5.19), the external forces are

$$\hat{\mathbf{g}}_\alpha = \int_{V-S_0} \mathbf{e}^* g_\alpha\,dV \tag{3.2.12}$$

$$\hat{\mathbf{s}}_\alpha = \int_{V_S} \mathbf{e}^* s_\alpha\,dV \tag{3.2.13}$$

$$\hat{\mathbf{t}}_\alpha = \oint_{S_0} \mathbf{e}^* \bar{t}_{\alpha\beta} n_\beta\,dS \tag{3.2.14}$$

These integrals are performed either analytically, for simple sources, or the source functions are expanded in Fourier series and the integrals are evaluated using Gaussian quadrature.

Combining the expressions from (3.2.9), (3.2.11), and (3.2.12)-(3.2.14), the differential equation for momentum conservation (2.5.13) becomes

$$\mathbf{M}\,\partial_t^2\mathbf{u}_\alpha - V_X\mathbf{E}\mathbf{D}_\beta\,\mathbf{E}^{-1}\mathbf{C}_{\alpha\beta\gamma\lambda}\,\mathbf{E}\,\mathbf{D}_\lambda^{(e)}\mathbf{E}^{-1}\mathbf{u}_\gamma = \mathbf{g}_\alpha + \mathbf{s}_\alpha + \mathbf{t}_\alpha \tag{3.2.15}$$

23

where $g_\alpha = E\hat{g}_\alpha$, $s_\alpha = E\hat{s}_\alpha$ and $t_\alpha = E\hat{t}_\alpha$ are the collocation representations for the specified external forces on the system, consisting of body forces, internal volume sources and applied tractions on the boundary of the medium, respectively.

Because the collocation mass matrix is diagonal, its inverse is trivially computed. Then (3.2.15) is used to obtain a time history of nodal displacements by solving

$$\partial_t^2 u_\alpha = M^{-1}\left(V_X E D_\beta^{(e)} E^{-1} C_{\alpha\beta\gamma\lambda} E D_\lambda^{(e)} E^{-1} u_\gamma + g_\alpha + s_\alpha + t_\alpha \right) \tag{3.2.16}$$

with a finite difference time-integration scheme. Alternatively, nodal velocities v_α can be stored in addition to the nodal stress values

$$t_{\alpha\beta} = C_{\alpha\beta\gamma\lambda} E D_\lambda^{(e)} E^{-1} u_\gamma \tag{3.2.17}$$

Then, instead of integrating the second-order differential equation (3.2.16) in time, we integrate two coupled, first-order differential equations for velocities and stresses:

$$\partial_t t_{\alpha\beta} = C_{\alpha\beta\gamma\lambda} E D_\lambda^{(e)} E^{-1} v_\gamma \quad ; \tag{3.2.18}$$

$$\partial_t v_\alpha = M^{-1}\left(V_X E D_\beta^{(e)} E^{-1} t_{\alpha\beta} + g_\alpha + s_\alpha + t_\alpha \right) \tag{3.2.19}$$

We use the following explicit leapfrog scheme for the velocity-stress formulation, since the leapfrog scheme is numerically efficient and stable with the Fourier method (Orrey 1995):

$$t_{\alpha\beta}(t + \tfrac{\Delta t}{2}) = t_{\alpha\beta}(t - \tfrac{\Delta t}{2}) + \Delta t\, C_{\alpha\beta\gamma\lambda} E D_\lambda^{(e)} E^{-1} v_\gamma(t) \quad ; \tag{3.2.20}$$

$$\begin{aligned}
v_\alpha(t + \Delta t) = v_\alpha(t) \;&+\; \Delta t\, M^{-1}\Big[V_X E D_\beta^{(e)} E^{-1} t_{\alpha\beta}(t + \tfrac{\Delta t}{2}) \\
&+\; g_\alpha(t + \tfrac{\Delta t}{2}) + s_\alpha(t + \tfrac{\Delta t}{2}) + t_\alpha(t + \tfrac{\Delta t}{2}) \Big]
\end{aligned} \tag{3.2.21}$$

3.3   Inherent Periodicity of the Fourier Method

The periodic boundary conditions of the Fourier method can be explained by considering the boundary integral equation (3.1.20), which must be satisfied as well as the governing equations (3.2.20) and (3.2.21) for a numerical solution. With trigonometric basis functions, we have

$$E \hat{H}_{\alpha\gamma}^{(e)} E^{-1} u_\gamma = t_\alpha \tag{3.3.1}$$

where

$$\hat{H}_{\alpha\gamma}^{(e)} = \oint_{S_0} e^* \left(\hat{c}_{\alpha\beta\gamma\lambda}^\top e \right) e_{,\lambda}^\top n_\beta \, dS \tag{3.3.2}$$

24

If the surface S_0 is taken to be a planar surface with constant x_3, then $n_\beta = n_3$ and the surface integral (3.3.2) with explicit indices becomes

$$\hat{H}^{(e)}_{\alpha\gamma}(\mathbf{k},\mathbf{l}) = (il_\lambda)e^{i(l_3 - k_3 + l_3)x_3}\hat{c}_{\alpha\beta\gamma\lambda}(\mathbf{j})\int_0^{X_2}\int_0^{X_1}\prod_{\alpha=1}^{2}\left[e^{i(l_\alpha - k_\alpha + l_\alpha)x_\alpha}\right]dx_1dx_2 \tag{3.3.3}$$

Evaluating the integral and using $X_\alpha = N_\alpha\Delta x_\alpha$ (no sum on α) for $\alpha = 1,2,3$, gives

$$\hat{H}^{(e)}_{\alpha\gamma}(\mathbf{k},\mathbf{l}) = \Delta x_1\Delta x_2(il_\lambda)\hat{c}_{\alpha\beta\gamma\lambda}(\overset{3}{\mathbf{k}} - \overset{3}{\mathbf{l}})e^{i(l_3 - k_3 + l_3)x_3} \tag{3.3.4}$$

Here $\overset{3}{\mathbf{k}}$ denotes the projection of $\mathbf{k}$ onto the plane with normal n_3. Because of the periodicity of the exponential in x_3 over the computational interval $[0, X_3]$, we have that

$$\hat{H}^{(e)}_{\alpha\gamma}(\mathbf{k},\mathbf{l})\bigg|_{x_3 = 0} = \hat{H}^{(e)}_{\alpha\gamma}(\mathbf{k},\mathbf{l})\bigg|_{x_3 = X_3} = \Delta x_1\Delta x_2(il_\lambda)\hat{c}_{\alpha\beta\gamma\lambda}(\overset{3}{\mathbf{k}} - \overset{3}{\mathbf{l}}) \tag{3.3.5}$$

Then, since the displacement coefficients $\hat{u}_\gamma$ are wavenumber coefficients and therefore independent of the spatial coordinates,

$$\hat{\mathbf{H}}^{(e)}_{\alpha\gamma}\bigg|_{x_3 = 0}\hat{\mathbf{u}}_\gamma = \hat{\mathbf{H}}^{(e)}_{\alpha\gamma}\bigg|_{x_3 = X_3}\hat{\mathbf{u}}_\gamma \tag{3.3.6}$$

Given the relationship in (3.1.18) between $\hat{\mathbf{H}}^{(e)}_{\alpha\gamma}$ and $\mathbf{H}^{(e)}_{\alpha\gamma}$ and the relationship (3.1.8) between $\hat{\mathbf{u}}_\gamma$ and $\mathbf{u}_\gamma$, it is evident that the boundary condition (3.1.20) at $x_3 = 0$ and $x_3 = X_3$ are identical. The general case in which S_0 is not planar is the same, although more complicated to illustrate analytically.

This coupling of the boundary conditions leads to the familiar wraparound effect of the Fourier method, in which the stress conditions at one domain boundary (in this case at $x_3 = 0$) are reproduced at the other boundary (in this case at $x_3 = X_3$) for each spatial coordinate interval. Figure 3 demonstrates the wraparound effect for a 2-D Fourier pseudospectral wavefield simulation using the governing equations (3.2.20) and (3.2.21). An impulsive vertical displacement point source was applied just below the top-most boundary, and the boundary condition (3.3.1) was not applied at any of the domain boundaries. Because of the periodicity of the basis functions, however, the coupling expressed in (3.3.6) still applies and a wavefield is produced at both ends of the computational domain. The leading wave is a compressional (P) wave and the following wave is a shear (S) wave.

Figure 4 shows the same problem as that shown in Figure 3 except in this case an explicit zero traction condition ($t_\alpha = 0$) was applied at the top-most boundary so that $\mathbf{H}_{\alpha\gamma}\mathbf{u}_\gamma = 0$. Here it is

25

evident that the top and bottom boundaries, at $x_3 = 0$ and $x_3 = X_3$, respectively, are still coupled via (3.3.6), but due to the zero traction condition the coupling is different than in Figure 3. In this example there is a required relationship between the stress components at each boundary, whereas in the previous example there was none. In this example the S-wave is followed by a boundary (surface) wave confined to the zones near the boundaries at $x_3 = 0$ and $x_3 = X_3$. The effect of the boundary coupling between these surfaces is to leak energy from the top surface, where the physically relevant traction-free condition applies, through the bottom surface and into the lower part of the computational space. The surface wave that is produced is a poor approximation to the exact surface wave solution for this problem, and the error increases with increasing propagation distance from the source.

Evidently the continuous and periodic nature of the trigonometric functions of the Fourier method makes them inappropriate for an accurate solution to a traction-free boundary condition. In general, their continuity limits their usefulness for synthesizing wavefields in discontinuous material structures. The basis set of the Fourier method must be supplemented with additional functions in order to efficiently incorporate surfaces of discontinuity.

4 The Generalized Fourier Method

4.1 Discontinuity Functions

Boundary conditions on surfaces of discontinuity can be satisfied by using the general expansion of (2.5.5), which contains discontinuity functions. The set of discontinuity functions must include at least one function whose value at one endpoint of its coordinate interval is not equal to its value at the other endpoint. We refer to such a function as being *discontinuous across the endpoints of its coordinate interval.* A simple choice for such a function is the sawtooth function illustrated in Figure 5 along with its truncated Fourier series representation. Let $d^{(I)}(x_3)$ represent the 1-D sawtooth discontinuity function obtained by making the sawtooth orthogonal to all Fourier basis functions in the x_3 coordinate direction. The superscript (I) identifies this specific discontinuity function and indicates that it is linear in its argument. Making the function orthogonal to all Fourier terms amounts to subtracting the Fourier interpolation of the sawtooth from the sawtooth.

26

The discontinuity function over unit length is

$$d^{(I)}(x_3) = x_3 - \frac{1}{2} + \sum_{k_3 \neq 0} \frac{1}{i\underline{k}_3} e^{i\underline{k}_3 x_3} \tag{4.1.1}$$

where $\underline{k}_3 = 2\pi k_3$ and the limit on the sum incorporates all Fourier wave numbers except zero. This function is also plotted in Figure 5. The sawtooth discontinuity function by itself is not sufficient to satify boundary conditions on tractions, because the function's derivative

$$d^{(I)\prime}(x_3) = \sum_{k_3} e^{i\underline{k}_3 x_3} \tag{4.1.2}$$

is continuous across the endpoints of its coordinate interval. However, the sawtooth function is appropriate for handling displacement discontinuities across the coordinate interval endpoints, which do not involve derivatives. Therefore, we retain it in the set of discontinuity functions and consider the addition of a function whose derivative is discontinuous across the coordinate interval endpoints.

One of the simplest functions whose derivative is discontinuous across the x_3 coordinate interval endpoints is x_3^2, but the discontinuity function must be orthogonal to all Fourier basis functions as well as to the sawtooth. A quadratic discontinuity function which meets these criteria over the interval $[0, 1]$ is

$$d^{(II)}(x_3) = \frac{x_3(x_3-1)}{2} + \frac{1}{12} + \sum_{k_3 \neq 0} \frac{1}{(i\underline{k}_3)^2} e^{i\underline{k}_3 x_3} \tag{4.1.3}$$

with derivative

$$d^{(II)\prime}(x_3) = d^{(I)}(x_3) \tag{4.1.4}$$

The superscript (II) indicates that the function is quadratic in its argument, in accordance with the notation of the sawtooth in (4.1.1). The quadratic discontinuity function is plotted in Figure 6 with a normalized amplitude of 0.5.

Note that the quadratic discontinuity function itself is continuous across $x_3 = 0$ and $x_3 = 1$ but that its derivative, which is the sawtooth discontinuity function, is discontinuous. That is, the quadratic discontinuity function is C_0-continuous across its endpoints. Therefore, by using the quadratic and sawtooth functions in the generalized Fourier method for a problem with discontinuities, the portion of the solution that is synthesized by the Fourier series is C_1-continuous, with Fourier coefficients that decay with wave number $\underline{k}_3$ as $\underline{k}_3^{-1}$. The C_0-continuous and discontinuous portions are synthesized by the discontinuity functions. The supplementary coefficients

corresponding to the sawtooth function contribute to discontinuities in displacement, while those corresponding to the quadratic function contribute to discontinuities in strain.

4.2 Pseudospectral Approximation with Discontinuity Functions

In this section, we obtain pseudospectral approximations to the displacement field and its derivatives using a mixed basis set of trigonometric functions and the sawtooth and quadratic discontinuity functions in x_3 and only trigonometric functions in x_1 and x_2. The formalism developed here is used in the following section to obtain a weak Galerkin formulation of momentum conservation.

Using the sawtooth and quadratic discontinuity functions in the supplementary basis set of (2.5.6), there are two supplementary basis functions:

$$s^{(I)}(\overset{3}{\mathbf{k}}) = e_{(1)}(k_1)e_{(2)}(k_2)d^{(I)} \quad ; \quad s^{(II)}(\overset{3}{\mathbf{k}}) = e_{(1)}(k_1)e_{(2)}(k_2)d^{(II)} \tag{4.2.1}$$

In terms of the basis set

$$\mathbf{b} = \begin{pmatrix} \mathbf{e} \\ \mathbf{s}^{(I)} \\ \mathbf{s}^{(II)} \end{pmatrix} \tag{4.2.2}$$

the approximation to the displacement field $u_\gamma(\mathbf{x}, t)$ is

$$u_\gamma^{(b)}(\mathbf{x}) = \sum_{\mathbf{k}} \hat{u}_\gamma^{(e)}(\mathbf{k})\, e^{i\mathbf{k}\cdot\mathbf{x}} + \sum_{\overset{3}{\mathbf{k}}} \left[\hat{u}_\gamma^{(I)}(\overset{3}{\mathbf{k}})\, d^{(I)}(x_3) + \hat{u}_\gamma^{(II)}(\overset{3}{\mathbf{k}})\, d^{(II)}(x_3) \right] e^{i\overset{3}{\mathbf{k}}\cdot\overset{3}{\mathbf{x}}} \tag{4.2.3}$$

where we have made the time-dependence implicit for the displacement and its expansion coefficients. Discretizing this field at the collocation points of the trigonometric functions, we have

$$u_\gamma(\mathbf{j}) = \sum_{\mathbf{k}} \hat{u}_\gamma^{(e)}(\mathbf{k})\, e^{i\mathbf{k}\cdot\mathbf{j}} + \sum_{\overset{3}{\mathbf{k}}} \left[\hat{u}_\gamma^{(I)}(\overset{3}{\mathbf{k}})\, d^{(I)}(j_3) + \hat{u}_\gamma^{(II)}(\overset{3}{\mathbf{k}})\, d^{(II)}(j_3) \right] e^{i\overset{3}{\mathbf{k}}\cdot\overset{3}{\mathbf{j}}} \tag{4.2.4}$$

Since the supplementary functions $\mathbf{s}^{(I)}$ and $\mathbf{s}^{(II)}$ are trigonometric functions in the coordinates x_1 and x_2, the supplementary coefficients $\hat{u}_\gamma^{(I)}(\overset{3}{\mathbf{k}})$ and $\hat{u}_\gamma^{(II)}(\overset{3}{\mathbf{k}})$ are related to the sets of coefficients $u_\gamma^{(I)}(\overset{3}{\mathbf{j}})$ and $u_\gamma^{(II)}(\overset{3}{\mathbf{j}})$ in the discrete space $\overset{3}{\mathbf{j}}$ as

$$u_\gamma^{(P)}(\overset{3}{\mathbf{j}}) = \sum_{\overset{3}{\mathbf{k}}} \hat{u}_\gamma^{(P)}(\overset{3}{\mathbf{k}})\, e^{i\overset{3}{\mathbf{k}}\cdot\overset{3}{\mathbf{j}}} \quad , \quad P = I, II \tag{4.2.5}$$

28

with

$$\hat{u}_\gamma^{(P)}(\overset{3}{\mathbf{k}}) = \frac{1}{N_1 N_2} \sum_{\overset{3}{\mathbf{j}}} u_\gamma^{(P)}(\overset{3}{\mathbf{j}}) e^{-i\overset{3}{\mathbf{k}}\cdot\overset{3}{\mathbf{j}}} \tag{4.2.6}$$

Therefore, the sets of coefficients

$$\mathbf{u}_\gamma = \begin{pmatrix} \mathbf{u}_\gamma^{(e)} \\ \mathbf{u}_\gamma^{(I)} \\ \mathbf{u}_\gamma^{(II)} \end{pmatrix} \quad \text{and} \quad \hat{\mathbf{u}}_\gamma = \begin{pmatrix} \hat{\mathbf{u}}_\gamma^{(e)} \\ \hat{\mathbf{u}}_\gamma^{(I)} \\ \hat{\mathbf{u}}_\gamma^{(II)} \end{pmatrix} \tag{4.2.7}$$

are related to one another as in (3.1.7) and (3.1.8),

$$\mathbf{u}_\gamma = \mathbf{B}\,\hat{\mathbf{u}}_\gamma \quad ; \quad \hat{\mathbf{u}}_\gamma = \mathbf{B}^{-1}\mathbf{u}_\gamma \tag{4.2.8}$$

by defining a block diagonal collocation matrix operator $\mathbf{B}$ and its inverse $\mathbf{B}^{-1}$:

$$\mathbf{B} = \begin{bmatrix} \mathbf{E} & \mathbf{O} & \mathbf{O} \\ \mathbf{O} & \mathbf{B}^{(I)} & \mathbf{O} \\ \mathbf{O} & \mathbf{O} & \mathbf{B}^{(II)} \end{bmatrix} \quad ; \quad \mathbf{B}^{-1} = \begin{bmatrix} \mathbf{E}^{-1} & \mathbf{O} & \mathbf{O} \\ \mathbf{O} & \mathbf{B}^{(I)-1} & \mathbf{O} \\ \mathbf{O} & \mathbf{O} & \mathbf{B}^{(II)-1} \end{bmatrix} \tag{4.2.9}$$

$\mathbf{O}$ is a null matrix of size $N_1 N_2 \times N_1 N_2$, $\mathbf{E}$ is the collocation matrix operator for trigonometric functions, and $\mathbf{B}^{(I)}$ and $\mathbf{B}^{(II)}$ are discrete trigonometric functions in x_1 and x_2:

$$B^{(P)}(\overset{3}{\mathbf{j}},\overset{3}{\mathbf{k}}) = e^{i\overset{3}{\mathbf{k}}\cdot\overset{3}{\mathbf{j}}} \quad , \quad P = I, II \tag{4.2.10}$$

with inverses

$$\mathbf{B}^{(P)-1} = \frac{1}{N_1 N_2}\mathbf{B}^{(P)*}, \tag{4.2.11}$$

For a numerical implementation of the generalized method, it is convenient to define differentiation of the basis functions in terms of a diagonal differentiation matrix. Let

$$\mathbf{b}_{,\lambda} = \mathbf{D}_\lambda^{\mathsf{T}}\,^{(\lambda)}\mathbf{b} \tag{4.2.12}$$

with a diagonal matrix $\mathbf{D}_\lambda$ and the basis set

$$^{(\lambda)}\mathbf{b} = \begin{pmatrix} \mathbf{e} \\ ^{(\lambda)}\mathbf{s}^{(I)} \\ ^{(\lambda)}\mathbf{s}^{(II)} \end{pmatrix} \tag{4.2.13}$$

29

With the modified supplementary functions

$$^{(\lambda)}s^{(I)}\left(\overset{3}{\mathbf{k}}\right) = e_{(1)}(k_1)e_{(2)}(k_2)\left[d^{(I)}[1-\delta(\lambda-3)] + \sum_{k_3}e^{ik_3z_3}\delta(\lambda-3)\right]$$

$$^{(\lambda)}s^{(II)}\left(\overset{3}{\mathbf{k}}\right) = e_{(1)}(k_1)e_{(2)}(k_2)\left[d^{(II)}[1-\delta(\lambda-3)] + d^{(I)}\delta(\lambda-3)\right] \tag{4.2.14}$$

the matrix

$$\mathbf{D}_\lambda = \begin{bmatrix} \mathbf{D}_\lambda^{(e)} & \mathbf{O} & \mathbf{O} \\ \mathbf{O} & \mathbf{D}_\lambda^{(I)} & \mathbf{O} \\ \mathbf{O} & \mathbf{O} & \mathbf{D}_\lambda^{(II)} \end{bmatrix} \tag{4.2.15}$$

has the submatrix $\mathbf{D}_\lambda^{(e)}$ of (3.2.7) and the two submatrices

$$D_\lambda^{(P)}(\overset{3}{\mathbf{k}},\overset{3}{\mathbf{k}}) = ik_\lambda[1-\delta(\lambda-3)] + \frac{1}{X_3}\delta(\lambda-3) \quad , \quad P = I, II \tag{4.2.16}$$

4.3 Galerkin's Method with a Mixed Basis Set

Using the mixed basis set of trigonometric and discontinuity functions, we derive a system of algebraic equations for the set of displacement coefficients in (4.2.7) using the differential equation of momentum conservation that was given by (3.1.19):

$$\mathbf{M}\,\partial_t^2\mathbf{u}_\alpha + \mathbf{K}_{\alpha\gamma}\mathbf{u}_\gamma = \mathbf{g}_\alpha + \mathbf{s}_\alpha + \mathbf{t}_\alpha \tag{4.3.1}$$

The quantities $\mathbf{M}$, $\mathbf{K}_{\alpha\gamma}$, $\mathbf{g}_\alpha$, $\mathbf{s}_\alpha$ and $\mathbf{t}_\alpha$ are obtained by first evaluating the integrals of the corresponding quantities $\hat{\mathbf{M}}$, $\hat{\mathbf{K}}_{\alpha\gamma}$, $\hat{\mathbf{g}}_\alpha$, $\hat{\mathbf{s}}_\alpha$ and $\hat{\mathbf{t}}_\alpha$ which are given by (2.5.15) through (2.5.19), and then using the collocation matrix operator $\mathbf{B}$ of (4.2.9) and its inverse to transform these quantities and obtain (4.3.1) in explicit form.

In this section we present the explicit expressions for $\mathbf{M}$ and $\mathbf{K}_{\alpha\gamma}$ that are obtained by using the purely trigonometric representations of material parameters of (2.5.12). Of course, doing so restricts the realm of possible material models that can be included to those whose properties are continuous and periodic. Nevertheless, the resulting method is simple and sufficiently general for simulations involving a free surface boundary. In the most general implementation of the generalized Fourier method, the material parameters would be represented by mixed set expansions which contain basis functions that are discontinuous across the endpoints of their coordinate interval. In Appendix A, we discuss the form of the matrices $\mathbf{M}$ and $\mathbf{K}_{\alpha\gamma}$ that result from using a mixed set expansion containing the sawtooth discontinuity function and the trigonometric functions.

Using the trigonometric representations of material parameters would be overly restrictive for material models that contain a jump in parameters across coordinate interval endpoints, such as the model illustrated in Figure 7. The trigonometric interpolation of the elastic velocities contains significant Gibbs oscillations at the top and bottom of the model due to the mismatch in parameter values. However, a more accurate approximation to the layered model is obtained by utilizing the lower-most region of the grid to effectively blend together the upper-most and lower-most velocity values, as shown in Figure 8. The improved accuracy of the structure approximation is necessary for simulations in which the top boundary is a free surface. Because in this study we approximate absorbing boundary conditions at the base of the model, as well as along the vertical faces of the model, by using the attenuation scheme of Cerjan *et al.* (1985), the lower-most region corresponds to a region of attenuation and the wavefield within this region is excluded from the results. Therefore, the structural modification at the base does not matter. However, the structure gradient within the attenuating region must be small enough that significant impedance mismatch and accompanying reflections are avoided.

Using a trigonometric representation of mass density, the wave number domain mass matrix

$$\hat{\mathbf{M}} = \int_V \mathbf{b}^* \left(\hat{\rho}^\mathsf{T} \mathbf{e} \right) \mathbf{b}^\mathsf{T} dV \tag{4.3.2}$$

with the mixed basis set (4.2.2) is partitioned as

$$\hat{\mathbf{M}} = \begin{bmatrix} \hat{\mathbf{M}}^{(e)} & \mathbf{O} & \mathbf{O} \\ \mathbf{O} & \hat{\mathbf{M}}^{(I)} & \mathbf{O} \\ \mathbf{O} & \mathbf{O} & \hat{\mathbf{M}}^{(II)} \end{bmatrix} \tag{4.3.3}$$

where the superscripts on the submatrices indicate the basis functions used in the integral of (4.3.2). The matrix is block diagonal because the discontinuity functions are orthogonal to the trigonometric terms and to one another. The submatrix $\hat{\mathbf{M}}^{(e)}$ is the mass matrix of the Fourier method. Defining the integrals

$$\hat{I}^{(P)}(j_3) = \frac{1}{X_3} \int_0^{X_3} e^{i j_3 x_3} d^{(P)*}(x_3) d^{(P)}(x_3) \, dx_3 \quad , \quad P = I, II \tag{4.3.4}$$

the matrices $\hat{\mathbf{M}}^{(I)}$ and $\hat{\mathbf{M}}^{(II)}$ are expressed in terms of the quantities

$$I^{(P)}(n_3) = \frac{1}{N_3} \sum_{j_3} e^{-i j_3 \tilde{n}_3} \hat{I}^{(P)}(j_3) \tag{4.3.5}$$

31

as

$$\hat{M}^{(P)}(\overset{3}{k},\overset{3}{l}) = \frac{V_X}{N_1 N_2} \sum_{\mathbf{n}} \rho(\mathbf{n}) I^{(P)}(n_3) e^{-i(\overset{3}{k}-\overset{3}{l})\cdot\overset{3}{\mathbf{n}}} \tag{4.3.6}$$

Combining these matrices with the coefficients $\hat{u}_\alpha^{(P)}(\overset{3}{l})$ and transforming with $\mathbf{B}^{(P)}$ for $P = I, II$, we obtain inertial terms in collocation space:

$$B^{(P)}(\overset{3}{m},\overset{3}{k}) \, \hat{M}^{(P)}(\overset{3}{k},\overset{3}{l}) \, \partial_t^2 \hat{u}_\alpha^{(P)\overset{3}{}}(\overset{3}{l}) = V_X \sum_{m_3} \rho(\mathbf{m}) \, I^{(P)}(m_3) \, \partial_t^2 u_\alpha^{(P)}(\overset{3}{m}) \tag{4.3.7}$$

Equation (4.3.7) can be written in matrix form as

$$\mathbf{B}^{(P)} \hat{\mathbf{M}}^{(P)} \partial_t^2 \hat{\mathbf{u}}_\alpha^{(P)} = \mathbf{M}^{(P)} \partial_t^2 \mathbf{u}_\alpha^{(P)} \tag{4.3.8}$$

with the diagonal matrix $\mathbf{M}^{(P)}$ whose elements are

$$M^{(P)}(\overset{3}{m},\overset{3}{m}) = V_X \sum_{m_3} \rho(\mathbf{m}) I^{(P)}(m_3) \tag{4.3.9}$$

Thus we retain the matrix form $\mathbf{M}\,\partial_t^2 \mathbf{u}_\alpha$ for the inertial term in collocation space, with the diagonal mass matrix

$$\mathbf{M} = \begin{bmatrix} \mathbf{M}^{(e)} & \mathbf{O} & \mathbf{O} \\ \mathbf{O} & \mathbf{M}^{(I)} & \mathbf{O} \\ \mathbf{O} & \mathbf{O} & \mathbf{M}^{(II)} \end{bmatrix} \tag{4.3.10}$$

The submatrix $\mathbf{M}^{(e)}$ is the collocation space matrix (3.2.10) of the Fourier method. In practice, we compute the supplementary matrices of (4.3.9) before time-stepping the algebraic equations of the generalized Fourier method. In the general 3-D case in which density values are stored for each node in the computational grid, storing the quantities $\sum_{m_3} \rho(\mathbf{m}) I^{(I)}(m_3)$ and $\sum_{m_3} \rho(\mathbf{m}) I^{(II)}(m_3)$ requires two additional arrays of size $N_1 \times N_2$, compared to the storage of the mass density $\rho(\mathbf{m})$ in the Fourier method. [1]

Using the representation (4.2.12) for differentiation, the stiffness matrix $\hat{\mathbf{K}}_{\alpha\gamma}$ of (2.5.16) with the mixed basis set becomes

$$\hat{\mathbf{K}}_{\alpha\gamma} = \int_{V_X} \left(\mathbf{D}_\beta \, {}^{(\beta)}\mathbf{b}\right)^* \left(\hat{c}_{\alpha\beta\gamma\lambda}^\top \mathbf{e}\right) \left(\mathbf{D}_\lambda \, {}^{(\lambda)}\mathbf{b}\right)^\top d^3 x \tag{4.3.11}$$

---

[1] Storage requirements are reduced significantly if no redundant values of the material properties are stored, so that all nodes with the same corresponding value of mass density are associated with the same component of the mass density array.

where we have made use of the fact that $\mathbf{D}_\lambda = \mathbf{D}_\lambda{}^\top$ for a diagonal matrix. Defining the matrix

$$\mathbf{G}_{\alpha\beta\gamma\lambda} = \mathbf{B}\hat{\mathbf{G}}_{\alpha\beta\gamma\lambda}\mathbf{B}^{-1} \tag{4.3.12}$$

where

$$\hat{\mathbf{G}}_{\alpha\beta\gamma\lambda} = \int_{V_X} {}^{(\lambda)}\mathbf{b}^* \left(\hat{\mathbf{c}}_{\alpha\beta\gamma\lambda}^\top \mathbf{e}\right) {}^{(\lambda)}\mathbf{b}^\top d^3x \tag{4.3.13}$$

the collocation space restoring force $\mathbf{K}_{\alpha\gamma}\mathbf{u}_\gamma$ is

$$\mathbf{K}_{\alpha\gamma}\mathbf{u}_\gamma = \mathbf{B}\mathbf{D}_{\hat{\beta}}^*\mathbf{B}^{-1}\mathbf{G}_{\alpha\beta\gamma\lambda}\mathbf{B}\mathbf{D}_\lambda\mathbf{B}^{-1}\mathbf{u}_\gamma \tag{4.3.14}$$

The matrix $\mathbf{G}_{\alpha\beta\gamma\lambda}$ is partitioned as

$$\mathbf{G}_{\alpha\beta\gamma\lambda} = \begin{bmatrix} \mathbf{G}_{\alpha\beta\gamma\lambda}^{(ee)} & \mathbf{G}_{\alpha\beta\gamma\lambda}^{(eI)} & \mathbf{O} \\ \mathbf{G}_{\alpha\beta\gamma\lambda}^{(Ie)} & \mathbf{G}_{\alpha\beta\gamma\lambda}^{(II)} & \mathbf{G}_{\alpha\beta\gamma\lambda}^{(I\,II)} \\ \mathbf{O} & \mathbf{G}_{\alpha\beta\gamma\lambda}^{(II\,I)} & \mathbf{G}_{\alpha\beta\gamma\lambda}^{(II\,II)} \end{bmatrix} \tag{4.3.15}$$

where the superscripts indicate the basis functions used in the integral of (4.3.13). The contribution $\mathbf{G}_{\alpha\beta\gamma\lambda}^{(ee)}$ is just the elastic modulus matrix of (3.1.15) scaled to the problem volume:

$$\mathbf{G}_{\alpha\beta\gamma\lambda}^{(ee)} = V_X \mathbf{C}_{\alpha\beta\gamma\lambda} \tag{4.3.16}$$

The supplementary contributions to $\mathbf{G}_{\alpha\beta\gamma\lambda}$ are given in Appendix A. There the restoring force $\mathbf{K}_{\alpha\gamma}\mathbf{u}_\gamma$ is combined with the inertial term $\mathbf{M}\,\partial_t^2\mathbf{u}_\alpha$ and the source terms $\mathbf{g}_\alpha$, $\mathbf{s}_\alpha$ and $\mathbf{t}_\alpha$ for a mixed basis set to obtain a velocity-stress formulation of the differential equations of momentum conservation.

It remains to compute the source terms $\mathbf{g}_\alpha$, $\mathbf{s}_\alpha$ and $\mathbf{t}_\alpha$ for the mixed basis set. Using the basis set (4.2.2) in the applied body force terms (2.5.17) and (2.5.18) gives the representations

$$\hat{\mathbf{g}}_\alpha = V_X \begin{pmatrix} \hat{\mathbf{g}}_\alpha^{(e)} \\ \mathcal{D}^{(I)}\hat{\mathbf{g}}_\alpha^{(I)} \\ \mathcal{D}^{(II)}\hat{\mathbf{g}}_\alpha^{(II)} \end{pmatrix} \quad \text{and} \quad \hat{\mathbf{s}}_\alpha = V_X \begin{pmatrix} \hat{\mathbf{s}}_\alpha^{(e)} \\ \mathcal{D}^{(I)}\hat{\mathbf{s}}_\alpha^{(I)} \\ \mathcal{D}^{(II)}\hat{\mathbf{s}}_\alpha^{(II)} \end{pmatrix} \tag{4.3.17}$$

where $\left(\hat{\mathbf{g}}_\alpha^{(e)}, \hat{\mathbf{g}}_\alpha^{(I)}, \hat{\mathbf{g}}_\alpha^{(II)}\right)$ and $\left(\hat{\mathbf{s}}_\alpha^{(e)}, \hat{\mathbf{s}}_\alpha^{(I)}, \hat{\mathbf{s}}_\alpha^{(II)}\right)$ are the sets of coefficients of the body force expansions and $\mathcal{D}^{(I)}$ and $\mathcal{D}^{(II)}$ are, respectively, the sawtooth and quadratic discontinuity function normalizations:

$$\mathcal{D}^{(P)} = \frac{1}{X_3}\int_0^{X_3} d^{(P)*}(x_3)d^{(P)*}(x_3)\,dx_3 \quad , \quad P = I, II \tag{4.3.18}$$

33

Since the supplementary basis functions are primarily localized at bounding surfaces, however, it is sufficiently general to use only a Fourier expansion of the body force densities. Then only the uppermost partition of $\hat{g}_\alpha$ and $\hat{s}_\alpha$ is non-zero in (4.3.17).

For the geometry of the problem considered here, the applied surface traction term (2.5.19) becomes

$$^0\hat{t}_\alpha = \int_0^{X_2}\int_0^{X_1} \mathbf{b}^* \bar{t}_{\alpha 3}\, dx_1 dx_2 \bigg|_{x_3 = 0}$$

and

$$^X\hat{t}_\alpha = \int_0^{X_2}\int_0^{X_1} \mathbf{b}^* \bar{t}_{\alpha 3}\, dx_1 dx_2 \bigg|_{x_3 = X_3} \tag{4.3.19}$$

for the surfaces at $x_3 = 0$ and $x_3 = X_3$, respectively. Since we are using a basis set that is continuous in the coordinates x_1 and x_2, it is sufficient to expand $\bar{t}_{\alpha 3}$ as

$$\bar{t}_{\alpha 3}(\mathbf{x})\bigg|_{x_3 = 0} = \sum_{\overset{3}{\mathbf{k}}} {}^0\hat{t}_{\alpha 3}(\overset{3}{\mathbf{k}})e^{i\overset{3}{\mathbf{k}}\overset{3}{\mathbf{x}}} \quad ;$$

$$\bar{t}_{\alpha 3}(\mathbf{x})\bigg|_{x_3 = X_3} = \sum_{\overset{3}{\mathbf{k}}} {}^X\hat{t}_{\alpha 3}(\overset{3}{\mathbf{k}})e^{i\overset{3}{\mathbf{k}}\overset{3}{\mathbf{x}}} \tag{4.3.20}$$

with expansion coefficients $^0\hat{t}_{\alpha 3}(\overset{3}{\mathbf{k}})$ and $^X\hat{t}_{\alpha 3}(\overset{3}{\mathbf{k}})$. Then the surface tractions of (4.3.19) become

$$^0\hat{t}_\alpha = X_1 X_2 \begin{pmatrix} ^0\hat{t}_{\alpha 3} \\ ^0\hat{t}_{\alpha 3}\, d^{(I)}(0) \\ ^0\hat{t}_{\alpha 3}\, d^{(II)}(0) \end{pmatrix} \quad ; \quad {}^X\hat{t}_\alpha = X_1 X_2 \begin{pmatrix} ^X\hat{t}_{\alpha 3} \\ ^X\hat{t}_{\alpha 3}\, d^{(I)}(X_3) \\ ^X\hat{t}_{\alpha 3}\, d^{(II)}(X_3) \end{pmatrix} \tag{4.3.21}$$

and the source term t_α in (4.3.1) is composed of

$$^0t_\alpha = \mathbf{B}\, ^0\hat{t}_\alpha \quad \text{and} \quad {}^Xt_\alpha = \mathbf{B}\, ^X\hat{t}_\alpha \tag{4.3.22}$$

for the contributions on the surfaces at $x_3 = 0$ and $x_3 = X_3$, respectively.

4.4 Boundary Conditions

The applied surface tractions of (4.3.22) are incorporated into the present development of the generalized Fourier method by way of the boundary integral equation (3.1.20),

$$\mathbf{B}\,\hat{\mathbf{H}}_{\alpha\gamma}\,\mathbf{B}^{-1}\mathbf{u}_\gamma = \mathbf{t}_\alpha \tag{4.4.1}$$

34

where

$$\hat{\mathbf{H}}_{\alpha\gamma} = \oint_{S_0} \mathbf{b}^* \left(\bar{\mathbf{c}}_{\alpha\beta\gamma\lambda}^{\mathsf{T}} \mathbf{e} \right) \mathbf{b}_{,\lambda}^{\mathsf{T}} n_\beta \, dS \tag{4.4.2}$$

and the bounding surface S_0 corresponds to the coordinate planes at $x_3 = 0$ and $x_3 = X_3$. Here we address the particular case of a traction-free boundary at $x_3 = 0$ to represent the Earth's surface. This condition is applied in conjunction with a zero-displacement condition at $x_3 = X_3$, since these conditions together provide relatively simple expressions for the supplementary expansion coefficients of the displacement field.

For the case of a traction-free surface at $x_3 = 0$ and isotropic media, the boundary integral equation (3.1.20) becomes

$$t_{\alpha3}^{(e)}(\mathbf{m})\delta(m_3) \;+\; \mu(\mathbf{m})\delta(m_3) \sum_1 e^{i\underset{\sim}{1}\cdot\overset{3}{\underset{\sim}{\mathbf{m}}}} \Bigg\{ i\underset{\sim}{l}_\alpha \left[\hat{u}_3^{(I)}(\overset{3}{\underset{\sim}{1}}) d^{(I)} + \hat{u}_3^{(II)}(\overset{3}{\underset{\sim}{1}}) d^{(II)} \right]$$

$$+ \; \hat{u}_\alpha^{(I)}(\overset{3}{\underset{\sim}{1}}) d^{(I)\prime} + \hat{u}_\alpha^{(II)}(\overset{3}{\underset{\sim}{1}}) d^{(II)\prime} \Bigg\} \Bigg|_{x_3 = 0} = 0 \quad \alpha = 1,2 \tag{4.4.3}$$

and

$$t_{33}^{(e)}(\mathbf{m})\delta(m_3) +$$

$$\sum_1 e^{i\underset{\sim}{1}\cdot\overset{3}{\underset{\sim}{\mathbf{m}}}} \Bigg\{ \lambda(\mathbf{m}) \left[i\underset{\sim}{l}_1 \left(\hat{u}_1^{(I)}(\overset{3}{\underset{\sim}{1}}) d^{(I)} + \hat{u}_1^{(II)}(\overset{3}{\underset{\sim}{1}}) d^{(II)} \right) + i\underset{\sim}{l}_2 \left(\hat{u}_2^{(I)}(\overset{3}{\underset{\sim}{1}}) d^{(I)} + \hat{u}_2^{(II)}(\overset{3}{\underset{\sim}{1}}) d^{(II)} \right) \right]$$

$$+ \; [\lambda(\mathbf{m}) + 2\mu(\mathbf{m})] \left[\hat{u}_3^{(I)}(\overset{3}{\underset{\sim}{1}}) d^{(I)\prime} + \hat{u}_3^{(II)}(\overset{3}{\underset{\sim}{1}}) d^{(II)\prime} \right] \Bigg\} \Bigg|_{x_3 = 0} \delta(m_3) = 0 \tag{4.4.4}$$

and we have three sets of equations for the six sets of unknowns $\hat{u}_\alpha^{(I)}$ and $\hat{u}_\alpha^{(II)}$, $\alpha = 1, 2, 3$. Three additional sets of equations are obtained from the zero displacement condition at $x_3 = X_3$:

$$\sum_{k_3} \hat{u}_\alpha^{(e)}(\mathbf{k}) + \hat{u}_\alpha^{(I)}(\overset{3}{\underset{\sim}{\mathbf{k}}}) d^{(I)}(X_3) + \hat{u}_\alpha^{(II)}(\overset{3}{\underset{\sim}{\mathbf{k}}}) d^{(II)}(X_3) = 0 \tag{4.4.5}$$

These sets of equations are used to express the sawtooth discontinuity function expansion coefficients in terms of the Fourier and quadratic coefficients, since the sawtooth function serves to synthesize discontinuities in displacement across the endpoints of the x_3 coordinate interval. The resulting equations for the sawtooth coefficients are combined with the zero traction equations (4.4.3) and (4.4.4) to obtain equations for the quadratic coefficients.

The zero displacement condition at $x_3 = X_3$ is not an optimal treatment of the boundary condition at the base of the computation space, since it requires the use of the costly attenuation scheme of Cerjan *et al.* (1985) to simulate a radiation condition. This reduces the generalized method's efficiency. In addition, combining the zero displacement condition with the zero traction condition restricts the possible material structure models that can be handled with the method to models with constant elastic moduli at all nodes at $x_3 = 0$. Because the boundary conditions for traction involve the products of strain and elastic moduli, combining them with the constraints on displacement at $x_3 = X_3$ results in equations in wave number space that involve both displacement coefficients and the discrete convolutions of displacement coefficients with elastic moduli coefficients. The convolutions are in the x_1- and x_2-coordinate directions, so the only way the displacement coefficients can be efficiently isolated (at each time step) is to assume no variation in the elastic moduli at $x_3 = 0$. Then the only non-zero modulus coefficients are those that correspond to the wave numbers $k_1 = 0$ and $k_2 = 0$. Thus, the constraints restrict the possible material structure models to those with homogeneous elastic moduli values at the location of the free surface. The use of other possible boundary conditions is discussed in section 6.

4.5 Curvilinear Coordinates

The generalized Fourier method, as formulated above in Cartesian coordinates, admits discontinuities only on coordinate planes that traverse a rectangular volume. Irregular interfaces can be incorporated into the method by using a coordinate transformation that maps the irregular interfaces in the physical space into coordinate planes in a Cartesian computational space. The numerical method is formulated in the computational space, and quantities in the computational space are related to their associated quantities in the physical space by an inverse transformation. We incorporate a mapping between Cartesian and general curvilinear coordinates by transforming the equations for momentum conservation (2.5.13) and (2.5.14) from the physical space into the computational space for solution. The transformation properties of the field quantities in (2.5.13) and (2.5.14) are derived in Washizu (1968). These properties are used in Appendix B to derive the integral formulation of momentum conservation in the curvilinear computational space. As the use of coordinate transformations in pseudospectral methods is well established (Fornberg 1988, Tessmer *et al.* 1992; Tessmer and Kosloff 1994), here we provide merely an overview.

Let a general curvilinear coordinate system **x** designate the physical space, and define a trans-

formation $T(\mathbf{x}) = \mathbf{x}'$ that maps the physical space into the computational space with Cartesian coordinates $\mathbf{x}'$. Coordinate directions in the physical space are labeled with the dummy indices α, β, γ and λ, while coordinate directions in the computational space are labeled with corresponding dummy indices ϕ, χ, ψ and ω. With the Jacobian of the transformation

$$J = \left| \frac{\partial x_\alpha}{\partial x'_\phi} \right| \neq 0 \tag{4.5.1}$$

a unique inverse transformation exists and

$$\frac{\partial x_\alpha}{\partial x'_\phi} \frac{\partial x'_\phi}{\partial x_\beta} = \delta_{\alpha\beta} \tag{4.5.2}$$

For a given transformation, the Jacobian and the coefficients $\frac{\partial x_\alpha}{\partial x'_\phi}$ and $\frac{\partial x'_\chi}{\partial x_\beta}$ are obtained at collocation points and then included in the integral formulation of momentum conservation by using Fourier interpolation of the nodal values. Either the transformation $x_\alpha = x_\alpha(x'_\phi)$ is specified analytically, in which case the Jacobian and coefficients are obtained exactly, or x_α is specified at a set of discrete points in the physical space which maps to a set of collocation points in the computational space. The discrete locations in the physical space are chosen to match some geometrical features, for example some surface topography or a curved internal interface. Once enough points are specified to sufficiently discern the given features, the remaining points in the physical space are obtained by interpolation. Fornberg (1988) uses a bicubic spline interpolation, which also provides the derivatives $\frac{\partial x_\alpha}{\partial x'_\phi}$. However, the derivatives can be approximated with two-sided finite differences within the grid and one-sided finite differences on the grid borders.

In this study we apply a coordinate transformation to reduce the physical space's grid spacing in the vertical direction in the vicinity of the traction-free surface, as illustrated in Figure 12. As shown in the following section, a moderate reduction of grid spacing greatly improves the accuracy of the surface waves computed with the generalized Fourier method. We have chosen an analytic transformation that is symmetric about the middle of the vertical coordinate interval, but it is sufficient to cluster grid points only near the top boundary of the model for improved surface wave accuracy. The symmetric tranformation, however, admits a simple inverse mapping so that source and receiver positions can be easily specified.

5 SIMULATION EXAMPLES

In this section, the accuracy of solutions using the generalized Fourier method (GFM) is tested for problems involving a free surface boundary condition. For each problem, the source was applied as a delta function in space and time. The leapfrog time-stepping scheme of (3.2.20) and (3.2.21) was used with a time step chosen small enough that numerical dispersion is neglible (Kosloff and Baysal 1982).

5.1 Lamb's Problem

For Lamb's problem, an impulsive source on the surface of a homogeneous half-space, we compare the GFM solution to the analytic solution and to the solution obtained using a fourth-order finite difference method. For the following comparisons, the P-wave and S-wave velocities of the medium are 5 km/s and 3 km/s, respectively, with a mass density of 2.5 g/cm^3. The grid spacing used was 1 km in each coordinate direction except where otherwise noted. For these values, the Rayleigh wave velocity is about 2.74 km/s, and the frequency of the Rayleigh wave with a wavelength of 2 km, corresponding to Nyquist sampling of two nodes per wavelength, is 1.37 Hz. Except where otherwise noted, we low-pass filter the results with a corner frequency of 0.5 Hz, which corresponds to a grid sampling of the Rayleigh wave of about 5.5 grid points per wavelength.

The kinetic energy density field of the GFM solution to Lamb's problem is shown in Figure 9, where the source was applied in the middle of the upper-most boundary at a depth of 1 km (one grid spacing). The field was low-pass filtered in the wavenumber domain to remove high spatial frequencies. Notice the presence of very small disturbances at the base of the grid, which propagate at the Rayleigh wave velocity, and the (weak) P-wave disturbance propagating from the base, which was caused by the shallow source. These disturbances result from the incomplete decoupling of the top and bottom of the grid by the finite set of discontinuity functions. The displacement comparison of the analytic and GFM solutions is shown in Figure 10. The largest error in the figure between the GFM solution and the exact solution is less than about twenty percent. Figure 11 compares the GFM and analytic solutions after low-pass filtering the traces with a cutoff frequency of 0.25 Hz. At this frequency, the smallest wavelength of the Rayleigh wave corresponds to a length of about 11 grid points, and the GFM solution is nearly exact. However, the body waves are greatly oversampled at this frequency. For example, the P-wave is sampled at about 20 grid points

per wavelength. Therefore, such extreme low-pass filtering is wasteful from the standpoint of the problem's computer memory and operation count requirements.

On the other hand, such oversampling is necessary to obtain accurate surface wave results using a low-order finite difference method. Figure 12 compares the analytic solution to Lamb's problem to the results from a staggered-grid finite difference method which is fourth-order accurate in space and second-order accurate in time (Levander 1988). In our version of the method, however, the treatment of the traction-free boundary condition is a combination of fourth-order and second-order spatial approximations. The solutions in Figure 12 were low-pass filtered with a corner frequency of 0.25 Hz and should be compared to those of the GFM method in Figure 11 since the source was applied at a depth of 1 km. The finite difference solution exhibits a large amount of dispersion caused by the spatial discretization. Higher-frequency energy is delayed. When the finite difference solution was low-pass filtered with a cut-off frequency of 0.125 Hz, the Rayleigh wave was sampled at about 22 grid points per wavelength and we found the Rayleigh wave fit to be qualitatively better than the GFM fit of Figure 10, where the Rayleigh wave was sampled at about 5.5 grid points per wavelength. However, the finite difference fit at 0.125Hz was not as good as the GFM fit of Figure 11, where the Rayleigh wave was sampled at about 11 grid points per wavelength. Therefore, it appears that the generalized Fourier method produces Rayleigh wave solutions for Lamb's problem that are comparable in accuracy to the solutions of the finite difference method when between one half and one fourth as many grid points per minimum wavelength are used.

The error in the numerical solutions, at a given frequency, can be reduced by reducing the vertical grid spacing in the vicinity of the free surface with a coordinate transformation. Although the reduced grid spacing necessitates a smaller time-step size, it is more efficient, from a memory requirement standpoint, to cluster grid points near the boundary rather than to reduce the low-pass cutoff frequency. Figure 14 compares the GFM and analytic solutions obtained using the grid of Figure 13, in which the vertical grid spacing has been reduced in the vicinity of the surface so that $min(\Delta x_2) = 0.5$ km. The horizontal displacement solution is significantly better than the solution of Figure 10. Further reduction of the vertical grid spacing in the vicinity of the free surface improves the GFM solutions, particularly for the horizontal displacment, but the marginal improvement in accuracy is at the expense of a large increase in the number of iterations required to compute over the same time duration. It appears that the optimal configuration for efficiently computing highly-accurate surface waves with the GFM algorithm is moderate grid clustering near

the boundary, such as that used for the simulation of Figure 14.

5.2   Layer Over a Half-Space

In order to test the accuracy of the generalized Fourier method in heterogeneous media, we have compared GFM solutions to the solutions obtained by a normal mode method (Harvey 1981) for vertically-layered material structure models. The normal mode method produces highly accurate and efficient Green's functions for layered media, except for the contributions from very high phase velocities that correspond to energy propagating with nearly normal incidence upon material layers. To ensure the accuracy of the normal mode solutions that were used for comparison in this paper, we compared some of the normal mode solutions to the solutions obtained by the discrete wave number integration method of Apsel and Luco (1983).

In the generalized Fourier method simulations performed with the following 2-D heterogeneous material models, reflections from the left-hand, right-hand and bottom grid edges were minimized by using a variation of the damping technique of Cerjan *et al.* (1985). We find that applying strong damping at the lower-most nodes of the grid adversely affects the Rayleigh wave solutions along the top of the grid. This is an artifact of the incomplete decoupling of the top and bottom boundaries with this method. Strongly damping the disturbances at the base of the grid in Figure 9 affects the Rayleigh wave at the surface as well. Instead of applying the strongest level of damping at the base of the grid, we use a level of damping that gradually increases from the base to a distance of several grid points above the base, and then gradually decreases with further distance from the base. This minimizes the effect on the real surface waves at the free surface.

We compare the velocity time series obtained with the generalized Fourier and normal mode methods for an explosive source at a depth of 1 km in the layer over half-space structure of Figure 15. The structure is intended to represent a crude model of the crust and upper mantle. The source was applied at a depth of 1 km as an impulse in space and time, velocity time-histories were recorded on the free surface of the 2-D space, and the results were low-pass filtered. Because the geometry of the normal mode method is cylindrical and that of the generalized Fourier method is Cartesian, a gain factor was applied to the normal mode traces to remove the geometric spreading of the Rayleigh wave. Therefore, the trace amplitudes of the body wave phases do not match at all source-receiver distances. Figure 16 compares the GFM and normal mode solutions for a corner frequency of 1.0 Hz. At this frequency, the smallest wavelength in the wavefield corresponds to a

40

distance of about 3.5 km. This is about the smallest wavelength that can be accurately represented with the generalized Fourier method for the given velocity model and a grid spacing of 1 km in both coordinate directions. At higher frequencies, the grid-point-per-wavelength sampling is insufficient to accurately represent all phases in the wavefield. The mismatch between the GFM and normal mode solutions at the trailing edge of the Rayleigh wave may be caused, in part, by the damping technique employed in the GFM method to prevent reflections from the base of the grid. That is, the very low-frequency oscillations of the GFM solution about the normal mode solution for times later than the arrival time of the Rayleigh wave may be low-frequency reflections from the damping region. On the other hand, the low-frequency mismatch may be due to the normal mode method, which exhibits error at low frequencies from the application of a high-velocity cap layer at depth to trap modes between the cap layer and the free surface (Harvey 1981).

5.3 Layer Over a Half-Space with Q.

Whereas realistic models of earth structure must account for dissipative mechanisms, we have incorporated anelastic attenuation into the generalized Fourier method by applying the method of Emmerich and Korn (1987). In their method, frequency-dependent Q is approximated as the effect of a superposition of relaxation mechanisms. This time-domain approach is much more computationally expensive than the simple t^* technique of Vidale and Helmberger (1988), but it is valid for any level of attenuation and makes it possible to specify distinct levels of attenuation within different regions of the problem space. We have tested the method and its effect on the GFM surface wave solution by applying it to the layer over half-space problem and comparing the solution to the solution obtained with Harvey's normal mode method. In the normal mode method, anelasticity is included by specifying imaginary components of material moduli which are frequency dependent, and the approximation is accurate only for weakly attenuating media. (See Aki and Richards 1981, Chapter 5.) Therefore, for both compressional and shear waves, we chose a constant Q of 300 in the upper layer and a constant Q of 1000 in the half-space. This Q model was included in both the GFM and normal mode simulations used to produce the velocity traces in Figure 17. The simulations used to produce Figure 17 were identical to those used to produce Figure 16 except for the addition of anelasticity. A gain factor was applied to the normal mode traces to remove the geometric spreading of the Rayleigh wave. The GFM and normal mode results match very well for the given Q values.

41

5.4   A Thin, Low-Velocity Layer

In order to test the accuracy of the GFM results in heterogeneous media with a coordinate transformation included, we have used the computational grid of Figure 13 to obtain accurate GFM simulations in the material model of Figure 18. The model is identical to the layer over half-space structure except for the addition of the thin layer at the top. For this model, the coordinate transformation is used to increase resolution within the thin layer without oversampling the remainder of the model space. The coordinate transformation reduces the grid spacing in the vicinity of the free surface from a uniform spacing of 500 meters to a minimum spacing of 300 meters. The top layer of the structure is 1100 meters thick. Figure 19 compares the horizontal and vertical velocity traces of the GFM and normal mode solutions for an explosive source applied at a depth of 650 meters. The traces were recorded on the free surface and low-pass filtered with a corner frequency of 0.5 Hz. A gain factor was applied to the normal mode traces to remove the geometric spreading of the Rayleigh wave. The low-velocity layer causes the Rayleigh wave to be highly dispersive. The GFM solution would be much less accurate if the coordinate transformation were not used, because the uniform grid spacing of 500 meters does not include sufficent nodes within the low-velocity layer. With the coordinate transformation included, 4 nodes in the vertical direction are included in the top layer.

5.5   A Randomized, Layered Structure

GFM synthetics were computed for the layered crust and upper mantle model of Figure 20, and for this model with the addition of random variations in velocity values about their mean values. Our intent was to demonstrate the stability of the generalized Fourier method for models containing strong, small-scale lateral variations in material structue. For the randomized medium, a self-similar autocorrelation function was used with a correlation length of 5.0 km in both the horizontal and vertical directions. The rms fluctuations in the velocity model change from layer to layer in depth (with decreasing fluctuations with depth) and also decrease within lateral zones at greater distances from the explosion source. The strongest fluctuations were 25 % rms within the source region, which were meant to approximate a tectonic environment. Figures 21(a) and 21(b) compare the free surface vertical velocity time series for the models without and with randomization, respectively. Evidently the effect of the random fluctuations is to reduce the amplitude of the R_g phase as a function of distance from the source and to increase the amplitudes and complexities of

42

the P_g and L_g phases. Since this effect is generally observed, we conclude that random fluctuations are responsible for the relatively large L_g observed relative to R_g at greater distances from the source. In this case, the L_g energy is largely derived from scattering from R_g, with an associated rapid attenuation of R_g with distance and a relative growth of L_g amplitudes.

5.6 A Basin Structure

In the final example, we test the effects on GFM crustal phase simulations of the large-scale lateral variation in structure illustrated in Figure 22. This structure is intended to approximate the occurrence of a sedimentary basin along the source-receiver path. Figure 23 shows the seismograms obtained from a simulation through the structure of Figure 22. These results should be compared to those in Figure 21(a) since the velocity structure was the same for both simulations, except for the presence of the basin. Clearly the L_g phase is strongly affected by the basin structure, with reduced amplitudes upon emergence from the basin. That is, this large-scale structure had the effect of "blocking" L_g. The P and P_g phases are similarly influenced by the basin and mantle uplift, and R_g energy is reflected upon incidence on the basin.

6   CONCLUSIONS

The generalization of the Fourier pseudospectral method developed in this study involved supplementing the Fourier method's trigonometric basis set with discontinuity functions and using the weak Galerkin form of weighted residuals to approximate the governing equations for momentum conservation. With the particular choice of the sawtooth and quadratic discontinuity functions, accurate simulations were obtained for problems with a traction-free surface. In principle, other forms of discontinuity functions could be used in a generalization of the Fourier method, as long as they suitably handle the discontinuous portion of an approximate solution. They must be orthogonal to one another and to the Fourier basis set, and each additional function must be a degree higher in continuity than the previous one if adding the function is to improve convergence. A systematic method for obtaining a set of polynomial-based discontinuity functions up to a specified degree of continuity is given in Orrey (1995), and the possibility of using other non-polynomial-based functions is discussed there.

The natural extension of the existing generalized Fourier method, with the sawtooth and

43

quadratic discontinuity functions in the x_3-coordinate direction only, is to couple horizontal interfaces with boundary conditions and create a layered structure. The material properties would be heterogeneous but continuous in each layer, and discontinuities would exist at layer boundaries. In a more general multi-domain method, discontinuity functions would be included in all coordinate directions to create a spectral element method (Patera 1984). In order to produce a multi-domain method with the generalized Fourier method, however, it is necessary that the decoupling of coordinate interval endpoints is complete. In the existing method, with the sawtooth and quadratic discontinuity functions, coordinate interval endpoints are not completely decoupled. This is evidenced by the presence of waves at the base of the grid in Figure 9. Therefore, it may be necessary to include additional discontinuity functions in a multi-domain method. On the other hand, the surface wave solutions of Lamb's problem were improved in the existing method by using a coordinate transformation (Figure 10 versus Figure 14), so using a coordinate transformation with the sawtooth and quadratic discontinuity functions may provide sufficient decoupling for a multi-domain method.

The system memory and operation count requirements of the generalized Fourier method are not significantly larger than those of the standard Fourier method. The number of supplementary functions in the generalized method is neglible compared to the number of Fourier basis functions, and the computations required to apply boundary conditions are performed only over a 1-D space (lines) for 2-D problems and a 2-D space (planes) for 3-D problems. Because of the high wavefield sampling efficiency of pseudospectral methods, the generalized Fourier method may prove most useful for 3-D problems. In 3-D, there are 9 field variables and 3 material parameters to be stored at a single time step in the leapfrog velocity-stress formulation. However, it is usually not necessary to store independent material parameters at every node in the problem space. In practice, the memory requirements for storing the material parameters can be effectively neglected in 3-D problems. Therefore, it is typically necessary to store about $9 \times 4 = 36$ bytes per node for single precision computations. Then propagation to a distance d, measured in minimum wavelengths, with a method that requires a sampling of N nodes per minimum wavelength requires a storage (in bytes) of

$$S = 36 \, (Nd)^3$$

in three dimensions. For a fixed propagation distance, the storage scales as the cube of sampling, and optimal sampling is highly desirable.

44

One of the most pressing topics for increasing the efficiency of the generalized Fourier method is the approximation of radiation boundary conditions. Using the attenuation method of Cerjan *et al.* (1985) wastes a considerable amount of available grid to remove unwanted reflections (and wraparound from the periodicity of the Fourier method) at grid edges. The zones of attenuation used in the simulations in this study were about 5 minimum wavelengths in length. One possible means of more accurately and efficiently simulating a radiation condition at $x_3 = X_3$ is to use a paraxial approximation at $x_3 = X_3$ (Clayton and Engquist 1977; Chang and McMechan 1989). Kosloff *et al.* (1990) use such a paraxial approximation in their Chebyshev-Fourier pseudospectral method by constraining the ingoing characteristic variables of their algebraic system to be zero at the base of the computational space. Incorporating such a radiation condition into the generalized Fourier method is a topic of our current research.

References

Aki, K., and P. G. Richards, 1980. *Quantitative Seismology, Theory and Methods*, volume 1, W. H. Freeman and Company, New York.

Apsel, R. J. and J. E. Luco, 1983. On the Green's functions for a layered half-space, part II, *Bull. Seism. Soc. Am.*, **73**, 931–951.

Archambeau, C. B. and J. B. Minster, 1978. Dynamics in prestressed media with moving phase boundaries: a continuum theory of failure in solids, *Geophys. J. R. astr. Soc.*, **52**, 65–96.

Boyd, J. P., 1989. *Chebyshev and Fourier Spectral Methods*, Lecture Notes in Engineering, Springer-Verlag, Berlin.

Canuto, C., M. Y. Hussaini, A. Quarteroni, and T. A. Zang, 1988. *Spectral Methods in Fluid Dynamics*, Springer Series in Computational Physics, Springer Verlag, New York.

Cerjan, C., D. Kosloff, R. Kosloff, and M. Reshef, 1985. A nonreflecting boundary condition for discrete acoustic and elastic wave equations, *Geophysics*, **50**, 705–708.

Chang, W.-F. and G. A. McMechan, 1989. Absorbing boundary conditions for 3-D acoustic and elastic finite-difference calculations, *Bull. Seism. Soc. Am.*, **79**, 211–218.

Clayton, R. and B. Engquist, 1977. Absorbing boundary conditions for acoustic and elastic wave equations, *Bull. Seism. Soc. Am.*, **67**, 1529–1540.

Daudt, C. R., L. W. Braile, R. L. Nowack, and C. S. Chiang, 1989. A comparison of finite-difference and Fourier method calculations of synthetic seismograms, *Bull. Seism. Soc. Am.*, **79**, 1210–1230.

Emmerich, H. and M. Korn, 1987. Incorporation of attenuation into time-domain computations of seismic wave fields, *Geophysics*, **52**, 1252–1264.

Finlayson, B. A., 1972. *The Method of Weighted Residuals and Variational Principles*, Academic Press, New York.

Fornberg, B., 1988. The pseudospectral method: accurate representation of interfaces in elastic calculations, *Geophysics*, **53**, 625–637.

Harvey, D., 1981. Seismogram synthesis using normal mode superposition: the locked mode approximation, *Geophys. J. R. Astr. Soc.*, **66**, 37–61.

Kosloff, D. and E. Baysal, 1982. Forward modeling by a Fourier method, *Geophysics*, **47**, 1402–1412.

Kosloff, D., D. Kessler, A. Filho, E. Tessmer, A. Behle, and R. Strahilevitz, 1990. Solution of the equations of dynamic elasticity by a Chebyshev spectral method, *Geophysics*, **55**, 734–748.

Kosloff, D. and H. Tal-Ezer, 1993. A modified Chebyshev pseudospectral method with an $O(N^{-1})$ time step restriction, *J. Comp. Phys.*, **104**, 457–469.

Levander, A. R., 1988. Fourth-order finite-difference P-SV seismograms, *Geophysics*, **53**, 1425–1436.

Orrey, J. L., 1995. A generalized Fourier pseudospectral method for elastodynamics, *PhD thesis*, University of Colorado, Boulder.

Orszag, S. A., 1971. Numerical simulation of incompressible flows within simple boundaries: I. Galerkin (spectral) representations, *Stud. Appl. Math.*, **50**, 293–327.

Patera, A. T., 1984. A spectral element method for fluid dynamics: laminar flow in a channel expansion, *J. Comp. Phys.*, **54**, 468-488.

Richtmyer, R. D. and K. W. Morton, 1967. *Difference Methods for Initial-Value Problems*, John Wiley and Sons, New York.

Temperton, C., 1983. Self-sorting mixed-radix fast Fourier transforms, *J. Comp. Phys.*, **52**, 1–23.

Tessmer, E., D. Kessler, D. Kosloff, and A. Behle, 1992. Multi-domain Chebyshev-Fourier method for the solution of the equations of motion of dynamic elasticity, *J. Comp. Phys.*, **100**, 355–363.

Tessmer, E. and D. Kosloff, 1994. 3-D elastic modeling with surface topography by a Chebyshev spectral method, *Geophysics*, **59**, 464–473.

Trefethen, L. N., 1988. Lax-stability vs. eigenvalue stability of spectral methods, In Morton, K. W. and M. J. Baines, editors, *Numerical Methods for Fluid Dynamics III*, New York, Clarendon.

Vidale, J. E., 1990. Comment on a comparison of finite-difference and Fourier method calculations of synthetic seismograms by C. R. Daudt *et al*, *Bull. Seism. Soc. Am.*, **80**, 493–495.

Vidale, J. E. and D. V. Helmberger, 1988. Elastic finite-difference modeling of the 1971 San Fernando, California earthquake, *Bull. Seism. Soc. Am.*, **78**, 122–141.

Washizu, K., 1968. *Variational Methods in Elasticity and Plasticity*, volume 9 of *International Series of Monographs in Aeronautics and Astronautics*, Pergammon Press, New York.

Witte, D. C., 1989. The pseudospectral method for simulating wave propogation, *PhD thesis*, Columbia University.

Appendix A

The contributions to the matrix $G_{\alpha\beta\gamma\lambda}$ of (4.3.15) from the supplementary functions of (4.2.14) are the following:

$$
\begin{aligned}
G^{(eI)}_{\alpha\beta\gamma\lambda}(\mathbf{n}, \overset{3}{\mathbf{n}}) &= \delta(\lambda-3)N_3 c_{\alpha\beta\gamma\lambda}(\mathbf{n})\delta(n_3) \\
G^{(Ie)}_{\alpha\beta\gamma\lambda}(\overset{3}{\mathbf{n}}, \mathbf{n}) &= \delta(\beta-3)c_{\alpha\beta\gamma\lambda}(\mathbf{n})\delta(n_3) \\
G^{(II)}_{\alpha\beta\gamma\lambda}(\overset{3}{\mathbf{n}}, \overset{3}{\mathbf{n}}) &= \sum_{n_3} c_{\alpha\beta\gamma\lambda}(\mathbf{n}) \\
&\quad \cdot \Big[\delta(\beta-3)\delta(\lambda-3)N_3\delta(n_3) + [1-\delta(\beta-3)][1-\delta(\lambda-3)] \Big] I^{(I)}(n_3) \\
G^{(III)}_{\alpha\beta\gamma\lambda}(\overset{3}{\mathbf{n}}, \overset{3}{\mathbf{n}}) &= [1-\delta(\beta-3)]\delta(\lambda-3)\sum_{n_3} c_{\alpha\beta\gamma\lambda}(\mathbf{n})I^{(I)}(n_3) \\
G^{(III)}_{\alpha\beta\gamma\lambda}(\overset{3}{\mathbf{n}}, \overset{3}{\mathbf{n}}) &= \delta(\beta-3)[1-\delta(\lambda-3)]\sum_{n_3} c_{\alpha\beta\gamma\lambda}(\mathbf{n})I^{(I)}(n_3) \\
G^{(IIII)}_{\alpha\beta\gamma\lambda}(\overset{3}{\mathbf{n}}, \overset{3}{\mathbf{n}}) &= \sum_{n_3} c_{\alpha\beta\gamma\lambda}(\mathbf{n}) \\
&\quad \cdot \Big[\delta(\beta-3)\delta(\lambda-3)I^{(I)}(n_3) + [1-\delta(\beta-3)][1-\delta(\lambda-3)]I^{(II)}(n_3) \Big]
\end{aligned}
\tag{A.1}
$$

Examining the submatrices of $G_{\alpha\beta\gamma\lambda}$ in (A.1), it is evident that all submatrices other than $G^{(eI)}_{\alpha\beta\gamma\lambda}$ are nonsymmetric in the indices α and β. Therefore, the quantity $G_{\alpha\beta\gamma\lambda}\mathbf{B}\mathbf{D}_\lambda\mathbf{B}^{-1}\mathbf{u}_\gamma$ is also nonsymmetric in α and β. The contributions to $G_{\alpha\beta\gamma\lambda}\mathbf{B}\mathbf{D}_\lambda\mathbf{B}^{-1}\mathbf{u}_\gamma$ from the submatrix $G^{(ee)}_{\alpha\beta\gamma\lambda}$ of (4.3.16) are the nodal values of stress in the Fourier method,

$$
t_{\alpha\beta} = C_{\alpha\beta\gamma\lambda}\,\mathbf{E}\,\mathbf{D}_\lambda\,\mathbf{E}^{-1}\mathbf{u}_\gamma
\tag{A.2}
$$

which are symmetric, but the supplementary contributions to $G_{\alpha\beta\gamma\lambda}\mathbf{B}\mathbf{D}_\lambda\mathbf{B}^{-1}\mathbf{u}_\gamma$ do not correspond to stress field contributions from the supplementary basis functions. That is, they are not the products of the modulus tensor and strain

$$
c_{\alpha\beta\gamma\lambda}\,\hat{\mathbf{u}}^{(P)\top}_\gamma\mathbf{D}^{(P)}_\lambda{}^{(\lambda)}\mathbf{s}^{(P)} \qquad P = I, II
$$

evaluated at collocation points. Therefore, storing $G_{\alpha\beta\gamma\lambda}\mathbf{B}\mathbf{D}_\lambda\mathbf{B}^{-1}\mathbf{u}_\gamma$ is more costly than storing a symmetric quantity in a coupled first-order differential equation formulation.

It is possible to store symmetric quantities, however, by dividing $G_{\alpha\beta\gamma\lambda}$ into three separate matrices as follows. Let

$$
G_{\alpha\beta\gamma\lambda} = {}^{(\beta)}\Phi\, C_{\alpha\beta\gamma\lambda}\,{}^{(\lambda)}\Psi
\tag{A.3}
$$

48

where

$$
{}^{(\beta)}\Phi = \begin{bmatrix} \mathbf{1} & \mathbf{O} & \mathbf{O} \\ {}^{(\beta)}\!\Delta^{(Ie)} & {}^{(\beta)}\!\Delta^{(II)} & \mathbf{O} \\ \mathbf{O} & {}^{(\beta)}\!\Delta^{(II)} & {}^{(\beta)}\!\Delta^{(II\!I)} \end{bmatrix} \quad ; \quad {}^{(\lambda)}\Psi = \begin{bmatrix} \mathbf{1} & {}^{(\lambda)}\!\Delta^{(eI)} & \mathbf{O} \\ \mathbf{O} & {}^{(\lambda)}\!\Delta^{(II)} & {}^{(\lambda)}\!\Delta^{(I\!I\!I)} \\ \mathbf{O} & \mathbf{O} & {}^{(\lambda)}\!\Delta^{(I\!I\!I)} \end{bmatrix}
\tag{A.4}
$$

and

$$
\mathbf{C}_{\alpha\beta\gamma\lambda} = \begin{bmatrix} \mathbf{C}^{(e)}_{\alpha\beta\gamma\lambda} & \mathbf{O} & \mathbf{O} \\ \mathbf{O} & \mathbf{C}^{(I)}_{\alpha\beta\gamma\lambda} & \mathbf{O} \\ \mathbf{O} & \mathbf{O} & \mathbf{C}^{(I\!I)}_{\alpha\beta\gamma\lambda} \end{bmatrix}
\tag{A.5}
$$

with the following submatrices:

$$
\begin{aligned}
{}^{(\beta)}\!\Delta^{(Ie)}(\overset{3}{\mathbf{n}},\mathbf{n}) &= \delta(\beta-3)\delta(n_3) \\
{}^{(\beta)}\!\Delta^{(II)}(\overset{3}{\mathbf{n}},\overset{3}{\mathbf{n}}) &= [1-\delta(\beta-3)] \\
{}^{(\beta)}\!\Delta^{(II)}(\overset{3}{\mathbf{n}},\overset{3}{\mathbf{n}}) &= \delta(\beta-3) \\
{}^{(\beta)}\!\Delta^{(I\!I\!I)}(\overset{3}{\mathbf{n}},\overset{3}{\mathbf{n}}) &= [1-\delta(\beta-3)] \\
{}^{(\lambda)}\!\Delta^{(eI)}(\mathbf{n},\overset{3}{\mathbf{n}}) &= N_3\delta(\lambda-3)\delta(n_3) \\
{}^{(\lambda)}\!\Delta^{(II)}(\overset{3}{\mathbf{n}},\overset{3}{\mathbf{n}}) &= [1-\delta(\lambda-3)] \\
{}^{(\lambda)}\!\Delta^{(I\!I)}(\overset{3}{\mathbf{n}},\overset{3}{\mathbf{n}}) &= \delta(\lambda-3) \\
{}^{(\lambda)}\!\Delta^{(I\!I\!I)}(\overset{3}{\mathbf{n}},\overset{3}{\mathbf{n}}) &= [1-\delta(\lambda-3)]
\end{aligned}
\tag{A.6}
$$

and

$$
\begin{aligned}
C^{(e)}_{\alpha\beta\gamma\lambda}(\mathbf{n},\mathbf{n}) &= c_{\alpha\beta\gamma\lambda}(\mathbf{n}) \\
C^{(I)}_{\alpha\beta\gamma\lambda}(\overset{3}{\mathbf{n}},\overset{3}{\mathbf{n}}) &= \sum_{n_3} I^{(I)}(n_3)c_{\alpha\beta\gamma\lambda}(\mathbf{n}) \\
C^{(I\!I)}_{\alpha\beta\gamma\lambda}(\overset{3}{\mathbf{n}},\overset{3}{\mathbf{n}}) &= \sum_{n_3} I^{(I\!I)}(n_3)c_{\alpha\beta\gamma\lambda}(\mathbf{n})
\end{aligned}
\tag{A.7}
$$

Then we define the vector $\tau_{\alpha\beta}$ as

$$
\tau_{\alpha\beta} = \mathbf{C}_{\alpha\beta\gamma\lambda}\,{}^{(\lambda)}\Psi\,\mathbf{B}\,\mathbf{D}_\lambda\,\mathbf{B}^{-1}\mathbf{u}_\gamma
\tag{A.8}
$$

which is symmetric in the indices α and β. The purely trigonometric contribution to $\tau_{\alpha\beta}$ is the collocation domain stress of the Fourier method. Combining the restoring force (4.3.14) with the

inertial terms of (4.3.7) and the source terms in (4.3.1), the differential equation of momentum conservation (4.3.1) becomes the coupled set of equations

$$\partial_t \tau_{\alpha\beta} = C_{\alpha\beta\gamma\lambda}{}^{(\lambda)}\Psi \, B \, D_\lambda \, B^{-1} \, v_\gamma \tag{A.9}$$

and

$$\partial_t v_\alpha = M^{-1}\left(-V_X \, B \, D_\beta^* \, B^{-1}{}^{(\beta)}\Phi \, \tau_{\alpha\beta} + g_\alpha + s_\alpha + t_\alpha\right) \tag{A.10}$$

These equations are the generalized analogue of equations (3.2.18) and (3.2.19) of the Fourier method.

In the most general implementation of the generalized Fourier method, the basis set expansions of the material properties would involve functions which are discontinuous across the endpoints of their coordinate intervals. Here we discuss the additional contributions to the mass and stiffness matrices which result from considering mass density and elastic moduli expansions in terms of the trigonometric and sawtooth discontinuity basis functions:

$$\rho^{(\theta)} = \hat\rho^{(e)T}\,e + \hat\rho^{(I)T}s^{(I)} \; ; \quad c_{\alpha\beta\gamma\lambda}^{(\theta)} = \hat c_{\alpha\beta\gamma\lambda}^{(e)T}e + \hat c_{\alpha\beta\gamma\lambda}^{(I)T}s^{(I)} \tag{A.11}$$

For these expansions, the mass matrix (4.3.10) of the generalized method has the form

$$M = \begin{bmatrix} M^{(ee)} & M^{(eI)} & M^{(eII)} \\ M^{(Ie)} & M^{(II)} & M^{(III)} \\ M^{(IIe)} & M^{(III)} & M^{(IIII)} \end{bmatrix} \tag{A.12}$$

and the matrix $G_{\alpha\beta\gamma\lambda}$ of (4.3.14) is partitioned as

$$G_{\alpha\beta\gamma\lambda} = \begin{bmatrix} G_{\alpha\beta\gamma\lambda}^{(ee)} & G_{\alpha\beta\gamma\lambda}^{(eI)} & G_{\alpha\beta\gamma\lambda}^{(eII)} \\ G_{\alpha\beta\gamma\lambda}^{(Ie)} & G_{\alpha\beta\gamma\lambda}^{(II)} & G_{\alpha\beta\gamma\lambda}^{(III)} \\ G_{\alpha\beta\gamma\lambda}^{(IIe)} & G_{\alpha\beta\gamma\lambda}^{(III)} & G_{\alpha\beta\gamma\lambda}^{(IIII)} \end{bmatrix} \tag{A.13}$$

The additional terms in the matrix $G_{\alpha\beta\gamma\lambda}$ do not add significantly more computation to the method, but the fact that the mass matrix M is no longer diagonal makes its inversion at each discrete time step more difficult. A satisfactory means of treating problems with material models that are discontinuous across the endpoints of coordinate intervals may be to use only a (continuous and periodic) trigonometric expansion for the mass density while including discontinuity functions in the modulus tensor expansion. For earth models in which mass density can be treated as approximately constant, such a treatment is obviously sufficient.

Appendix B

As in section 4.5, let a general curvilinear coordinate system $\mathbf{x}$ designate the physical space, and define a transformation $T(\mathbf{x}) = \mathbf{x}'$ that maps the physical space into the computational space with Cartesian coordinates $\mathbf{x}'$. Coordinate directions in the physical space are labeled with the dummy indices α, β, γ and λ, while coordinate directions in the computational space are labeled with corresponding dummy indices ϕ, χ, ψ and ω. From now on, when the position vector $\mathbf{x}'$ is not explicit, the prime is placed on a subscript or superscript. For example, $\mathbf{b}_{,\chi}(\mathbf{x}')$ is written as $\mathbf{b}_{,\chi'}$.

An integral formulation of momentum conservation in the curvilinear computational space is obtained by transforming the quantities in (2.5.13) and (2.5.14). Upon transformation to the primed system, the volume element dV transforms as $dV = J dV'$. Therefore, the inertial term $\hat{\mathbf{M}} \, \partial_t^2 \hat{u}_\alpha$ becomes

$$\hat{\mathbf{M}} \, \partial_t^2 \hat{u}_\alpha = \int_{V'} \mathbf{b}^* \rho^{(b)} \mathbf{b}^\top J \, dV' \, \partial_t^2 \hat{u}_\alpha \tag{B.1}$$

where $\rho^{(b)}$ is the basis set expansion of the density that is specified in the physical space $\mathbf{x}(\mathbf{x}')$. Since mass is invariant with respect to a coordinate transformation, the density transforms as $\rho' = J\rho$. The transformation has been performed only to evaluate the integral in the computational space; the displacement coefficients $\hat{u}_\alpha$ still correspond to displacement components in the physical space.

In order to transform the restoring force $\hat{K}_{\alpha\gamma} \hat{u}_\gamma$, the chain rule is applied to the basis functions $\mathbf{b}$ as

$$\mathbf{b}_{,\beta}(\mathbf{x}) = \mathbf{b}_{,\chi}(\mathbf{x}') \frac{\partial x'_\chi}{\partial x_\beta} \tag{B.2}$$

and the modulus $c_{\alpha\beta\gamma\lambda}$ is expressed as a contravariant tensor of rank four:

$$c_{\alpha\beta\gamma\lambda} = c_{\phi'\chi'\psi'\omega'} \frac{\partial x_\alpha}{\partial x'_\phi} \frac{\partial x_\beta}{\partial x'_\chi} \frac{\partial x_\gamma}{\partial x'_\psi} \frac{\partial x_\lambda}{\partial x'_\omega} \tag{B.3}$$

Then

$$\hat{K}_{\alpha\gamma} \hat{u}_\gamma = \int_{V'} \mathbf{b}^*_{,\chi'} c^{(b)}_{\alpha\chi'\gamma\omega'} \mathbf{b}_{,\omega'} J \, dV' \, \hat{u}_\gamma \tag{B.4}$$

where

$$c^{(b)}_{\alpha\chi'\gamma\omega'} = c^{(b)}_{\alpha\beta\gamma\lambda} \frac{\partial x'_\chi}{\partial x_\beta} \frac{\partial x'_\omega}{\partial x_\lambda} \tag{B.5}$$

and $c^{(b)}_{\alpha\beta\gamma\lambda}$ is the basis set expansion of the modulus that is specified in the physical space.

Components of the body forces $\hat{g}_\alpha$ and $\hat{s}_\alpha$ and the surface force $\hat{t}_\alpha$ in the physical space are expressed in terms of their components in the computational space, where they are applied. The body force density $g_{\phi'}$ in the computational space is obtained from components in the the physical space by the transformation

$$g_{\phi'} = g_\alpha \frac{\partial x'_\phi}{\partial x_\alpha} J \tag{B.6}$$

Upon transformation, the body force becomes

$$\hat{g}_\alpha = \int_{V'} \mathbf{b}^* g_{\phi'}^{(b)} \frac{\partial x_\alpha}{\partial x'_\phi} dV' \tag{B.7}$$

where $g_{\phi'}^{(b)}$ is the basis set expansion of the body force density in the computational space. A similar argument holds for $\hat{s}_\alpha$.

Applied tractions $\bar{t}_{\phi'\chi'}$ in the computational space are obtained from the components $\bar{t}_{\alpha\beta}$ in the physical space by the transformation

$$\bar{t}_{\phi'\chi'} = \bar{t}_{\alpha\beta} \frac{\partial x'_\phi}{\partial x_\alpha} \frac{\partial x'_\chi}{\partial x_\beta} \tag{B.8}$$

The surface element $n_\alpha dS = dS_\alpha$ transforms as $dS_\alpha = J\frac{\partial x'_\phi}{\partial x_\alpha} dS_{\phi'}$, and the applied surface force term becomes

$$\hat{t}_\alpha = \oint_{S'} \mathbf{b}^* \bar{t}_{\phi'\chi'}^{(b)} n_{\chi'} \frac{\partial x_\alpha}{\partial x'_\phi} J dS' \tag{B.9}$$

where $\bar{t}_{\phi'\chi'}^{(b)} n_{\chi'}$ is the basis set expansion of the applied tractions in the computational space.

Combining terms, the weak form of momentum conservation becomes

$$\int_{V'} \mathbf{b}^* \rho^{(b)} \mathbf{b}^\top J dV' \partial_t^2 \hat{u}_\alpha$$

$$+ \int_{V'} \mathbf{b}^*_{,\chi'} c_{\alpha\chi'\gamma\omega'}^{(b)} \mathbf{b}_{,\omega'} J dV' \hat{u}_\gamma = \int_{V'} \mathbf{b}^* \left[g_{\phi'}^{(b)} + s_{\phi'}^{(b)} \right] \frac{\partial x_\alpha}{\partial x'_\phi} dV'$$

$$+ \oint_{S'} \mathbf{b}^* \bar{t}_{\phi'\chi'}^{(b)} n_{\chi'} \frac{\partial x_\alpha}{\partial x'_\phi} J dS' \tag{B.10}$$

For a given transformation, the Jacobian and transformation coefficients $\frac{\partial x_\alpha}{\partial x'_\phi}$ and $\frac{\partial x'_\chi}{\partial x_\beta}$ are obtained at collocation points. Then the integrals in equation (B.10) are performed by approximating the Jacobian and metric coefficients with their Fourier interpolants, in the same manner as the density, modulus, and applied forces are approximated. The modulus-Jacobian combination in equation (B.10) becomes

$$c_{\alpha\chi'\gamma\omega'}^{(e)}(\mathbf{x}(x'))J(x') = \frac{1}{V_N} \sum_{\mathbf{j}} c_{\alpha\chi'\gamma\omega'}(\mathbf{j}) J(\mathbf{j}) \sum_{\mathbf{k}} e^{-i\mathbf{k}\cdot(\mathbf{j}-\mathbf{x}')} \tag{B.11}$$

where

$$c_{\alpha\chi'\gamma\omega'}(\mathbf{j})J(\mathbf{j}) = \left[c_{\alpha\beta\gamma\lambda}(\mathbf{x}(\mathbf{x}'))\frac{\partial x'_\chi}{\partial x_\beta}(\mathbf{x}')\frac{\partial x'_\omega}{\partial x_\lambda}(\mathbf{x}')\,J(\mathbf{x}')\right]\Bigg|_{\mathbf{x}' = j_\alpha \Delta x'_\alpha \mathbf{i}_\alpha} \tag{B.12}$$

The quantities $\rho^{(t)}J$, $g_{\phi'}^{(t)}\frac{\partial x_\alpha}{\partial x'_\phi}$, $s_{\phi'}^{(t)}\frac{\partial x_\alpha}{\partial x'_\phi}$ and $\bar{t}_{\phi'\chi'}^{(t)} n_{\chi'}\frac{\partial x_\alpha}{\partial x'_\phi}J$ are similarly represented. The integral formulation of momentum conservation that has been given above reduces to a differential formulation in which the chain rule is applied to the spatial derivatives to incorporate the effects of the transformation.

The boundary condition constraints of section 4.4 are applied in the computational space. The stress tensor $t_{\alpha\beta}$ in the physical space is expressed in terms of spatial derivatives in the computational space, i.e.

$$\begin{aligned} t_{\alpha\beta} &= c_{\alpha\beta\gamma\lambda}\,u_{\gamma,\lambda} \\ &= c_{\alpha\beta\gamma\omega'}\,u_{\gamma,\omega'} \end{aligned} \tag{B.13}$$

and the modulus tensor $c_{\alpha\beta\gamma\omega'}$ is obtained from the modulus tensor $c_{\alpha\beta\gamma\lambda}$ in the physical space as

$$c_{\alpha\beta\gamma\omega'} = c_{\alpha\beta\gamma\lambda}\frac{\partial x'_\omega}{\partial x_\alpha} \tag{B.14}$$

The displacement constraint of (4.4.5) remains unchanged.

Figure Captions

Figure 1: Schematic treatment of complicated earth models with the generalized Fourier method. The physical model is mapped to a Cartesian computational space in which all surfaces of discontinuity are Cartesian coordinate planes. Discontinuous variations in material parameters are indicated by thin black lines and continuous variations are indicated by thicker gray lines. Within the nth domain, the sets of trigonometric functions $e^n_{(1)}$ and $e^n_{(3)}$, in the x_1 and x_3 coordinate directions, respectively, are supplemented by the sets of discontinuity functions $d^n_{(1)}$ and $d^n_{(3)}$. With the discontinuity functions included, boundary conditions can be applied.

Figure 2: Schematic illustration of 1-D endpoint decoupling with discontinuity functions. The periodic spatial domain of the Fourier method, shown in (a), is modified by the introduction of the discontinuity function set $d_{(2)}$ to produce the domain of (b), which is nonperiodic in x_2 with bounding surfaces S_2.

Figure 3: Energy density snapshot of a Fourier method wavefield from an impulsive vertical displacement point source applied just below the top-most boundary. The wraparound phenomenon is due to the periodic nature of the basis set.

Figure 4: Energy density snapshot of a Fourier method wavefield from an impulsive vertical displacement point source with a traction-free boundary condition applied.

Figure 5: The sawtooth discontinuity function. The function is the difference between a sawtooth and the Fourier expansion of a sawtooth.

Figure 6: The quadratic discontinuity function. The function is orthogonal to the sawtooth discontinuity function and to all Fourier terms.

Figure 7: Trigonometric interpolation of an elastic velocity model. The actual model is shown as a dotted line.

Figure 8: Trigonometric interpolation of a periodic elastic velocity model. The actual model is made periodic by tapering the velocities and density within a region of attenuation.

Figure 9: Normalized kinetic energy density field of the GFM solution to Lamb's problem.

Figure 10: Comparison of GFM and analytic displacement solutions to Lamb's problem.

Figure 11: Comparison of GFM and analytic displacement solutions to Lamb's problem with a low-pass cutoff frequency of 0.25 Hz, or half the cutoff frequency used for Figure 10.

Figure 12: Comparison of the fourth-order finite difference and analytic displacement solutions to Lamb's problem. The wavelength of the Rayleigh wave at this frequency corresponds to about 11 grid points.

Figure 13: Spatial domain with grid points clustered in the vicinity of the traction-free surface.

Figure 14: Comparison of GFM and analytic displacement solutions to Lamb's problem when the vertical grid spacing in the GFM simulation was reduced in the vicinity of the free surface so that $min(\Delta x_2) = 0.5\Delta x_1$.

Figure 15: Layer over half-space velocity model used for comparisons of the GFM and normal mode methods.

Figure 16: Comparison of the horizontal (left) and vertical (right) component velocity solutions to the layer over half-space problem using the GFM and normal mode methods. The solid lines are the GFM solutions and the dashed lines are the normal mode solutions. The solutions were low-pass filtered with a corner frequency of 1.0 Hz.

Figure 17: Same as Figure 16 except anelasticity was included in the simulation. A constant Q of 300 was used for waves in the top layer of the structure, and a constant Q of 1000 was used for waves in the half-space.

Figure 18: A thin, low-velocity layer model used for a comparison of GFM and normal mode simulations.

Figure 19: Comparison of horizontal (left) and vertical (right) velocity component solutions to the thin, low-velocity layer problem from the GFM and normal mode methods. The solid line is the GFM solution, and the dashed line is the normal mode solution. The solutions were low-pass filtered with a corner frequency of 0.5 Hz.

Figure 20: Layered velocity model of the earth's crust and upper mantle.

Figure 21: Vertical velocity GFM synthetics computed for an explosion source in (a) the layered earth model of Figure 20 and (b) the layered earth model with the addition of random variations

in elastic velocity values about their mean values. The strongest fluctuations were 25 % rms within the source region.

Figure 22: Basin structure used to generate the seismograms in Figure 23. Light shades indicate low velocities and dark shades indicate high velocities. The basin and its associated mantle uplift span a source-receiver range of 70 km to 270 km, and the basin extends to a depth of 10 km.

Figure 23: GFM generated seismograms from an explosive source at a depth of 1 km in the layered, basin structure of Figure 22.

Physical Space

Computational Space
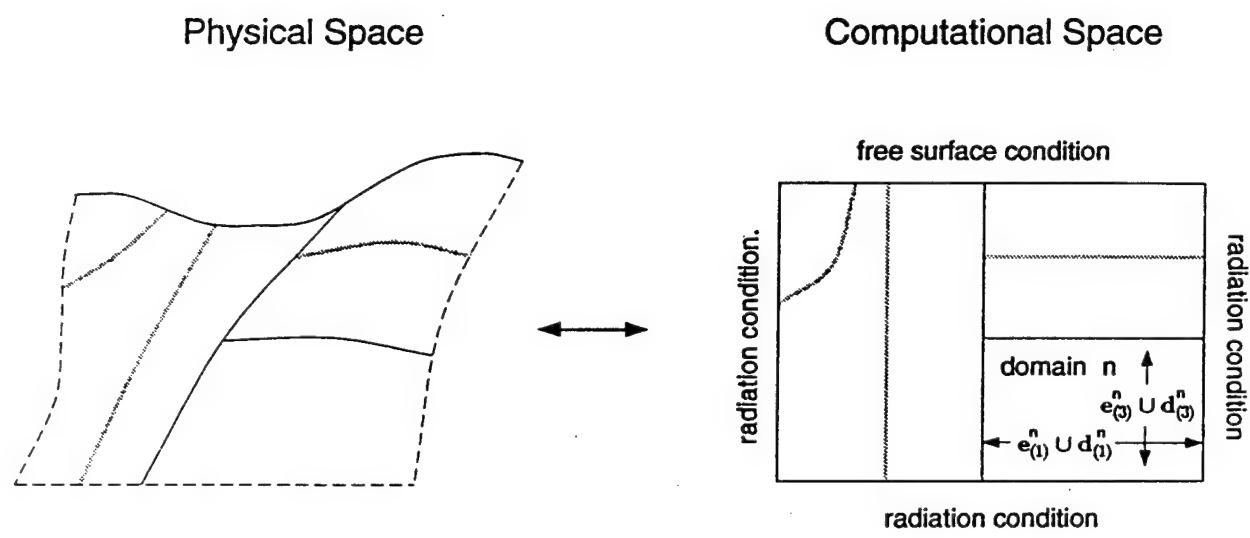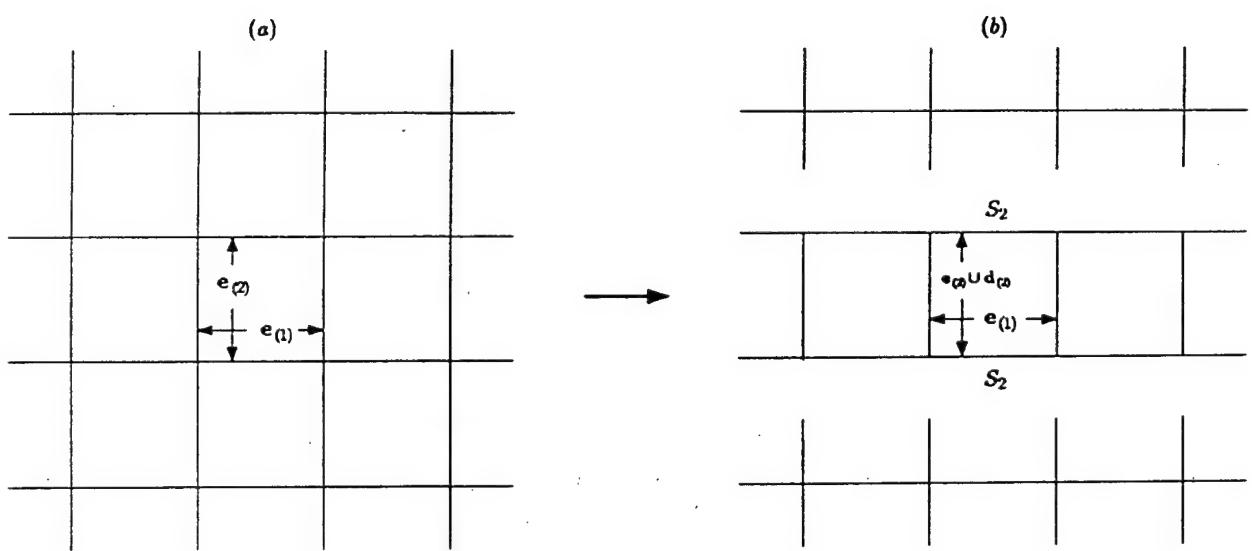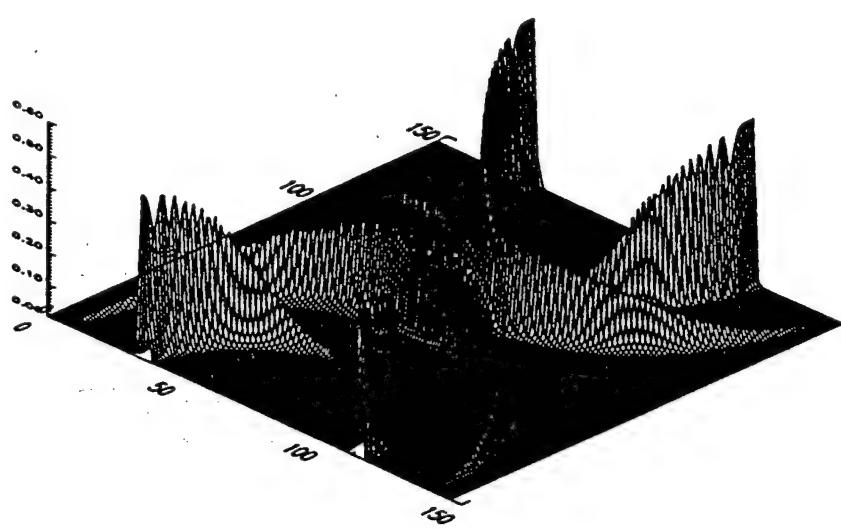
Figure 1:

Figure 2:

Figure 3:
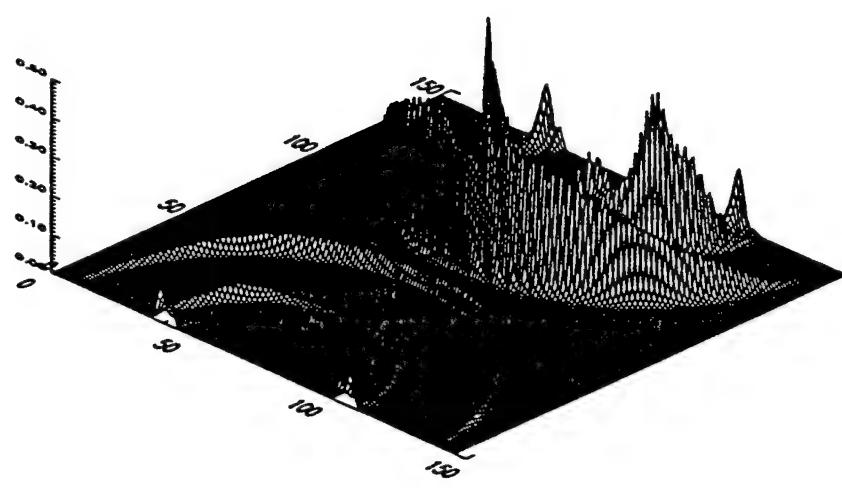
Figure 4:
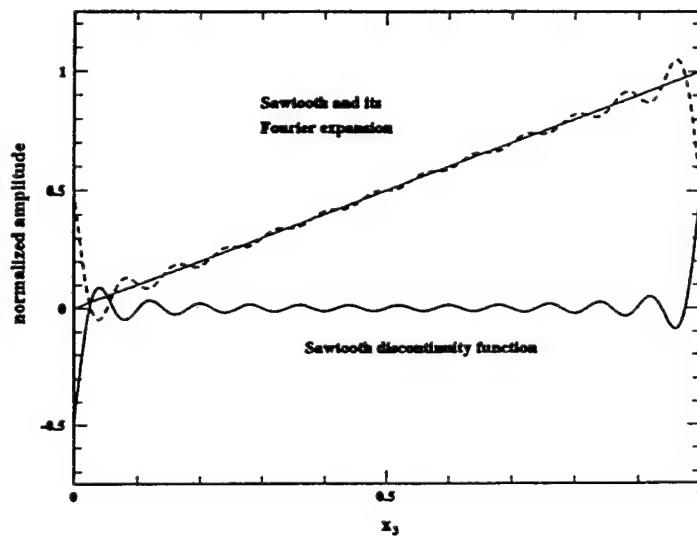
Figure 5:
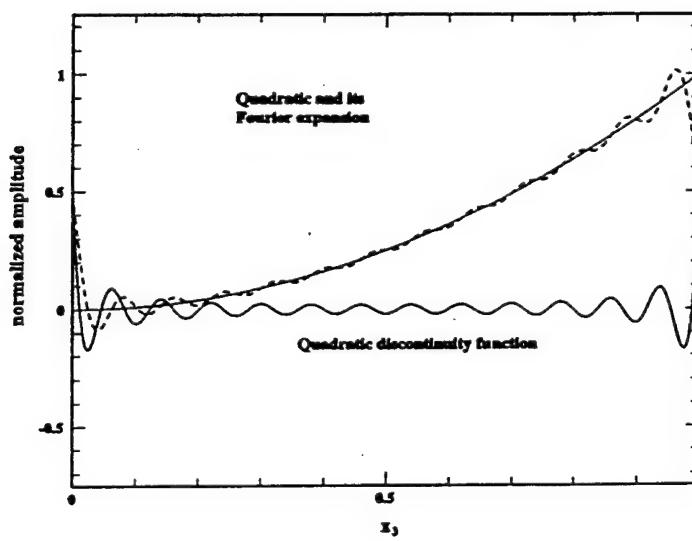
Figure 6:
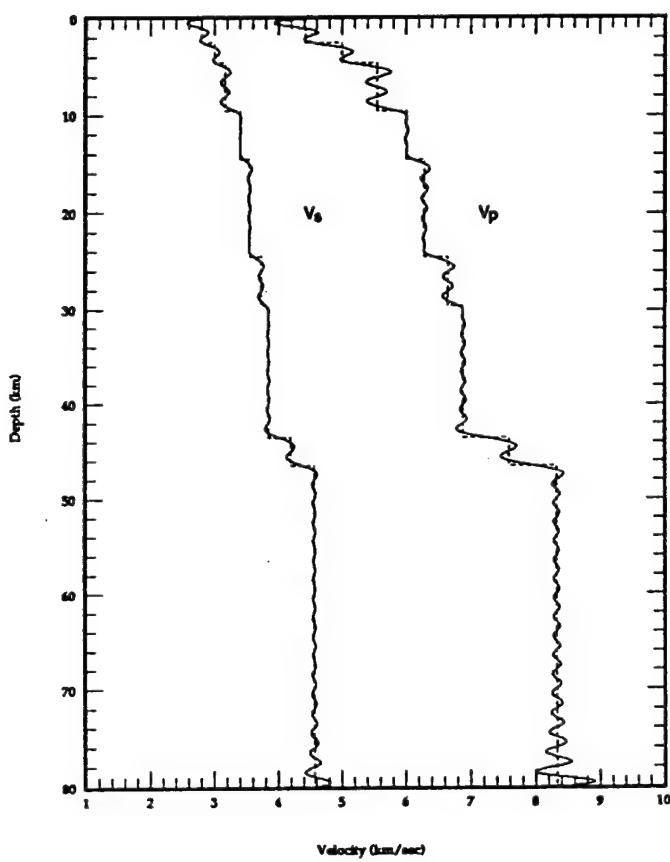
Figure 7:
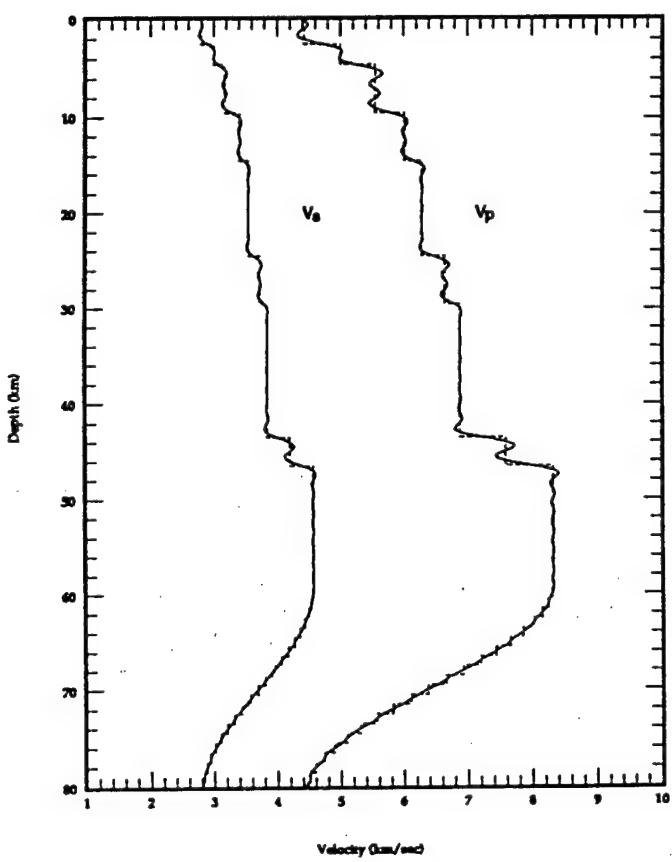
Figure 8:
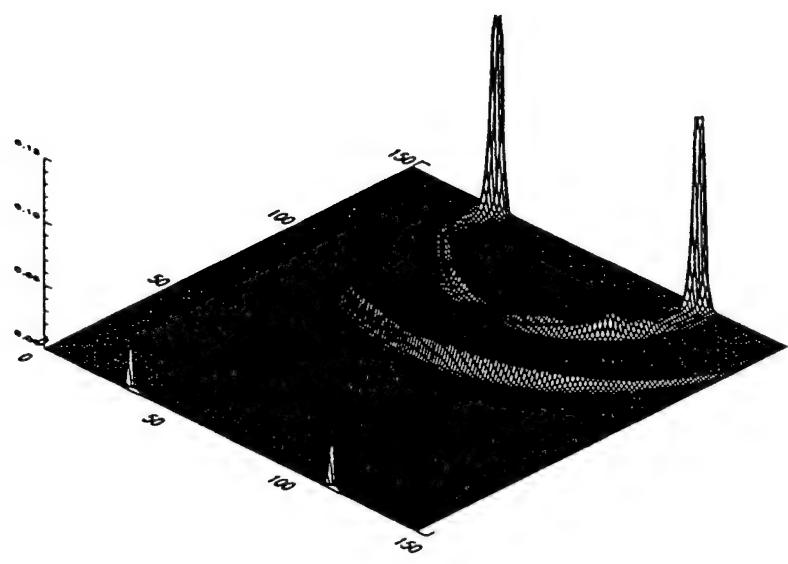
Figure 9:
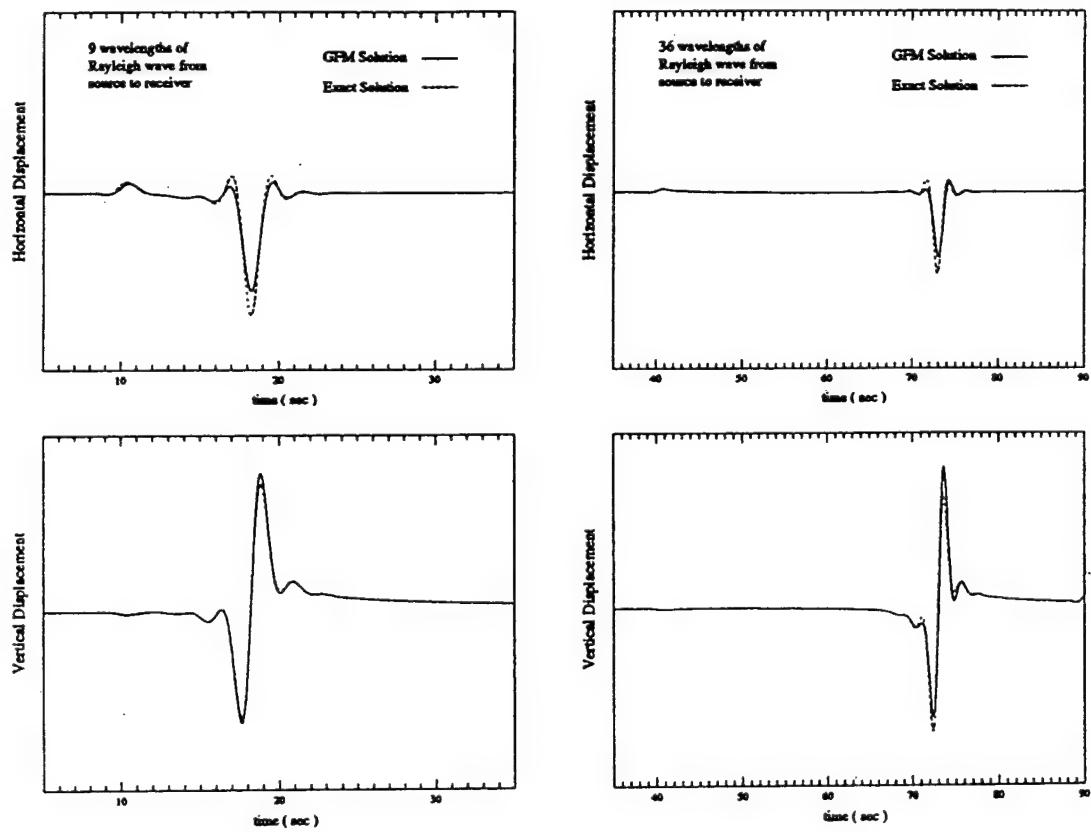
Figure 10:
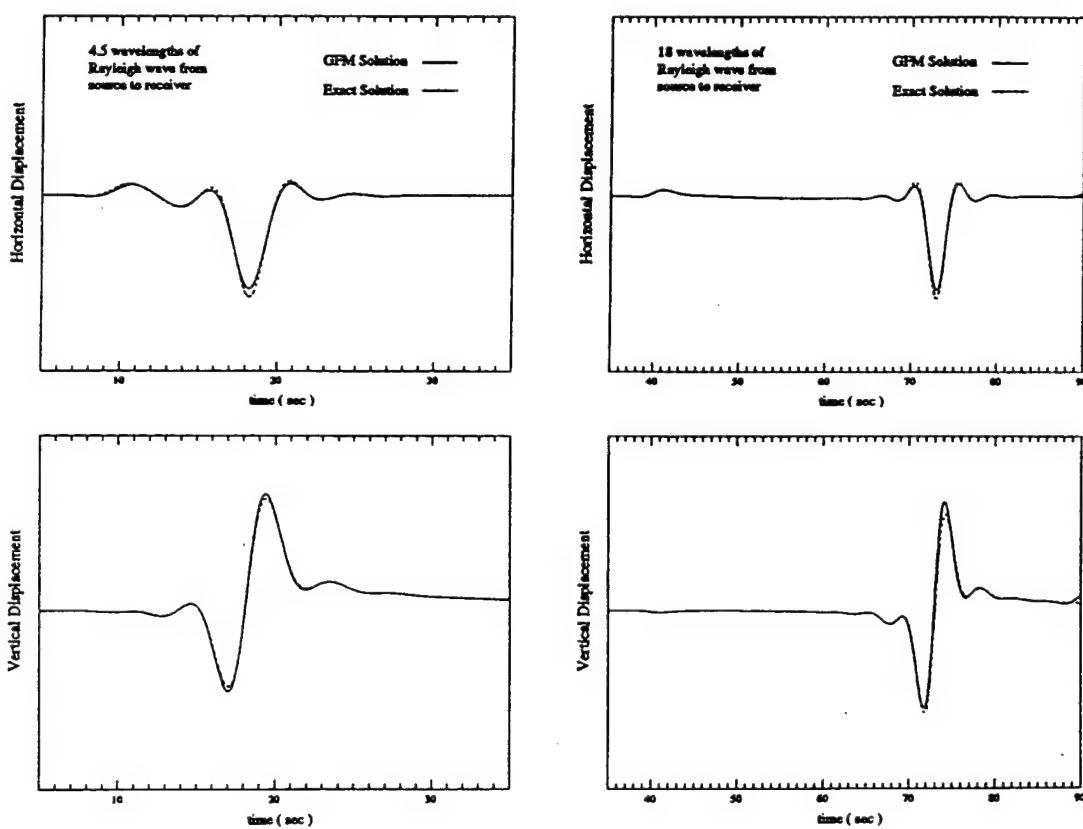
Figure 11:

Figure 12:

Free Surface
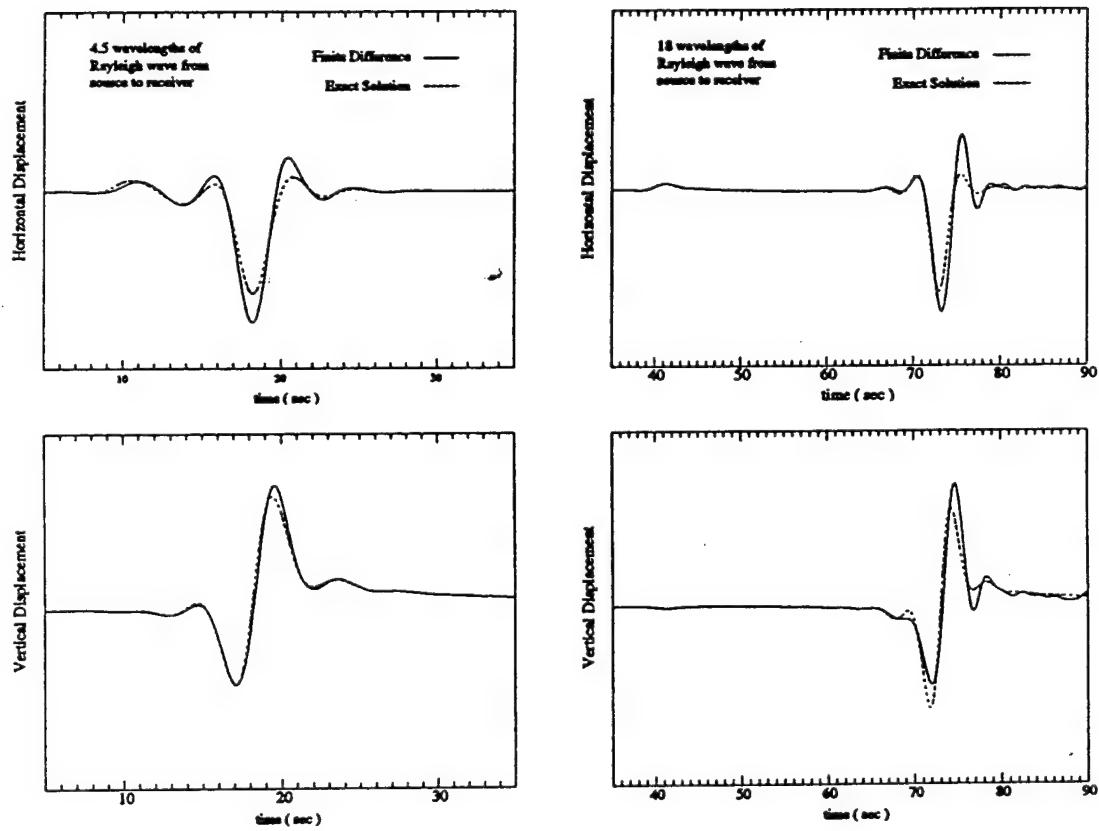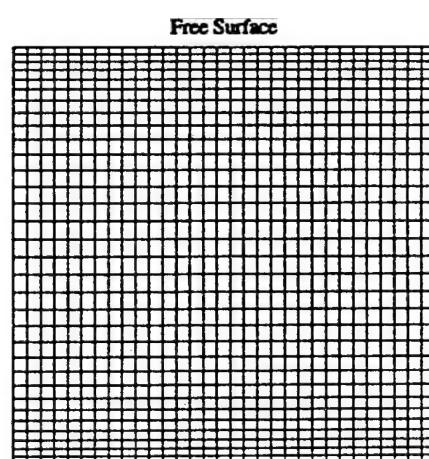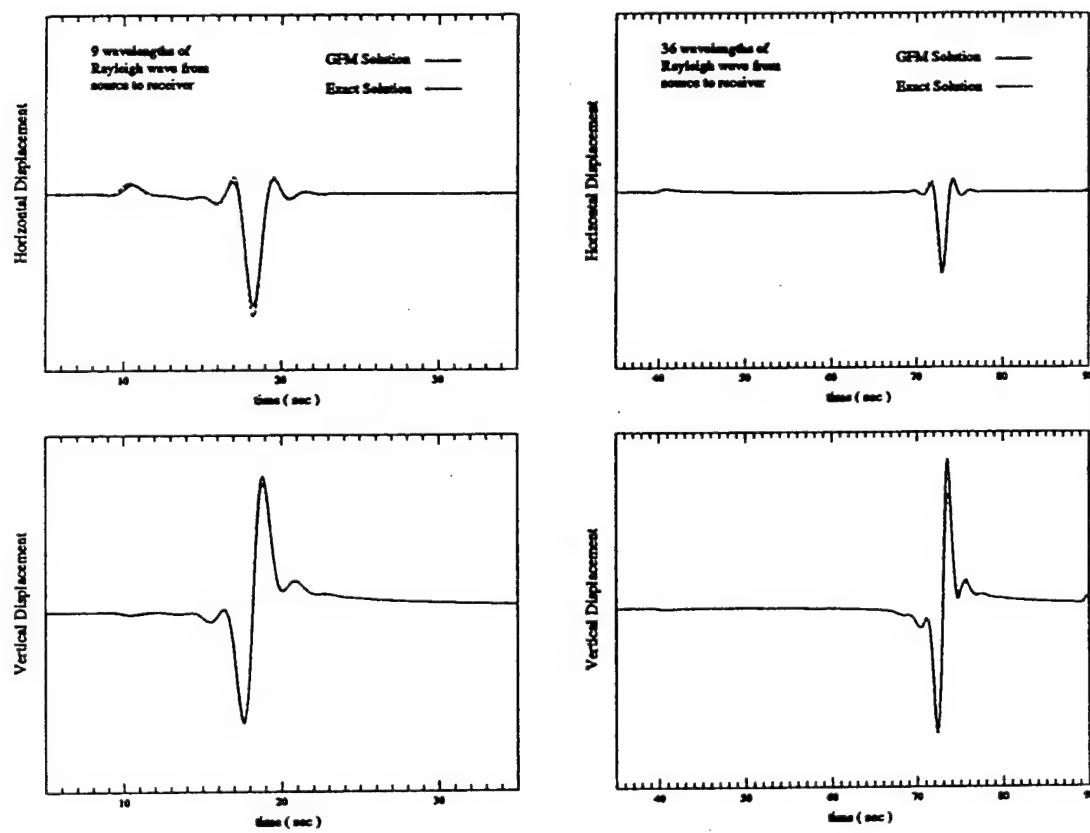
Figure 13:

Figure 14:
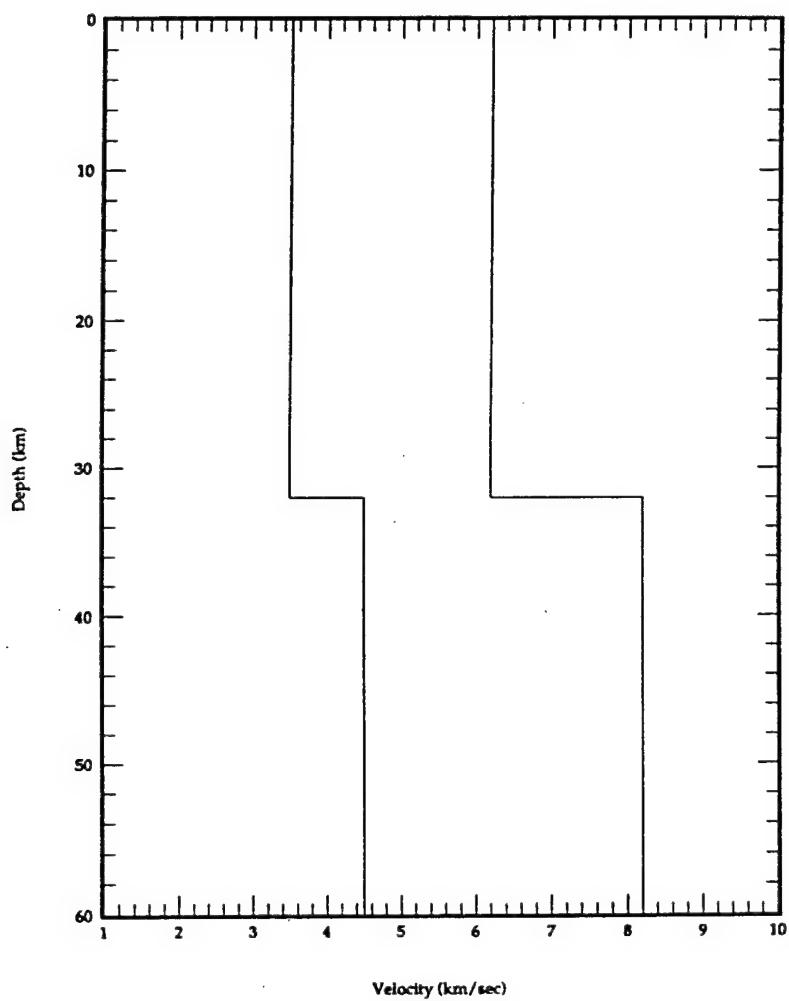
Figure 15:
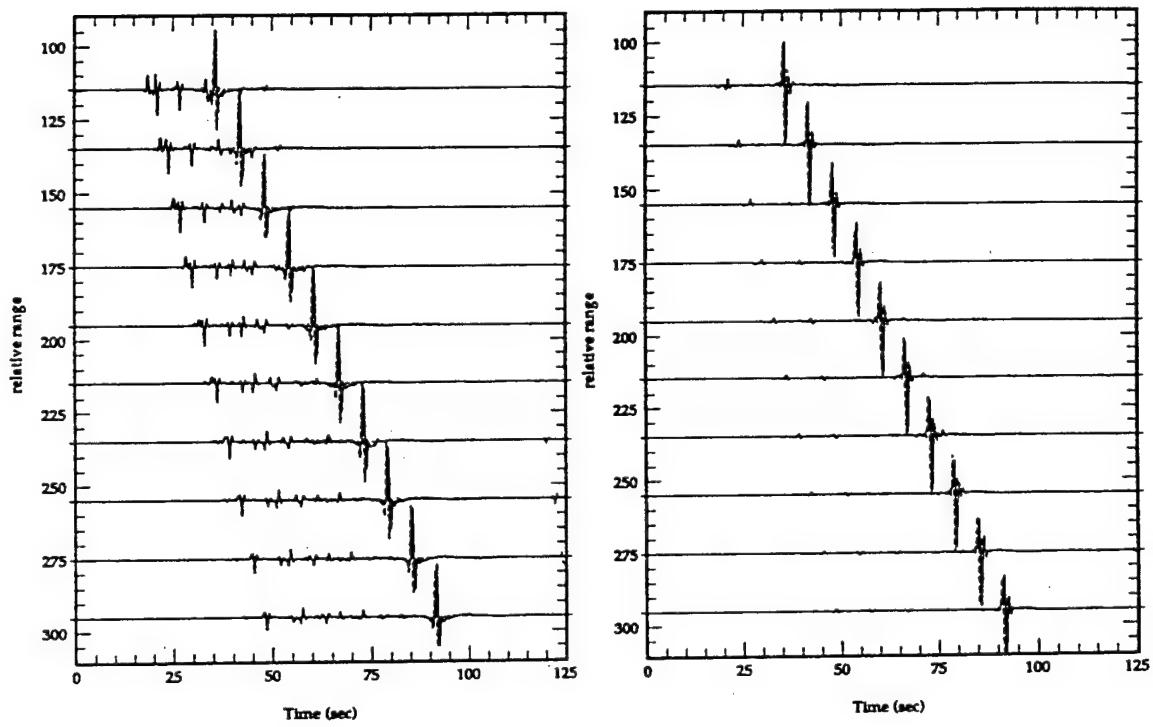
Figure 16:
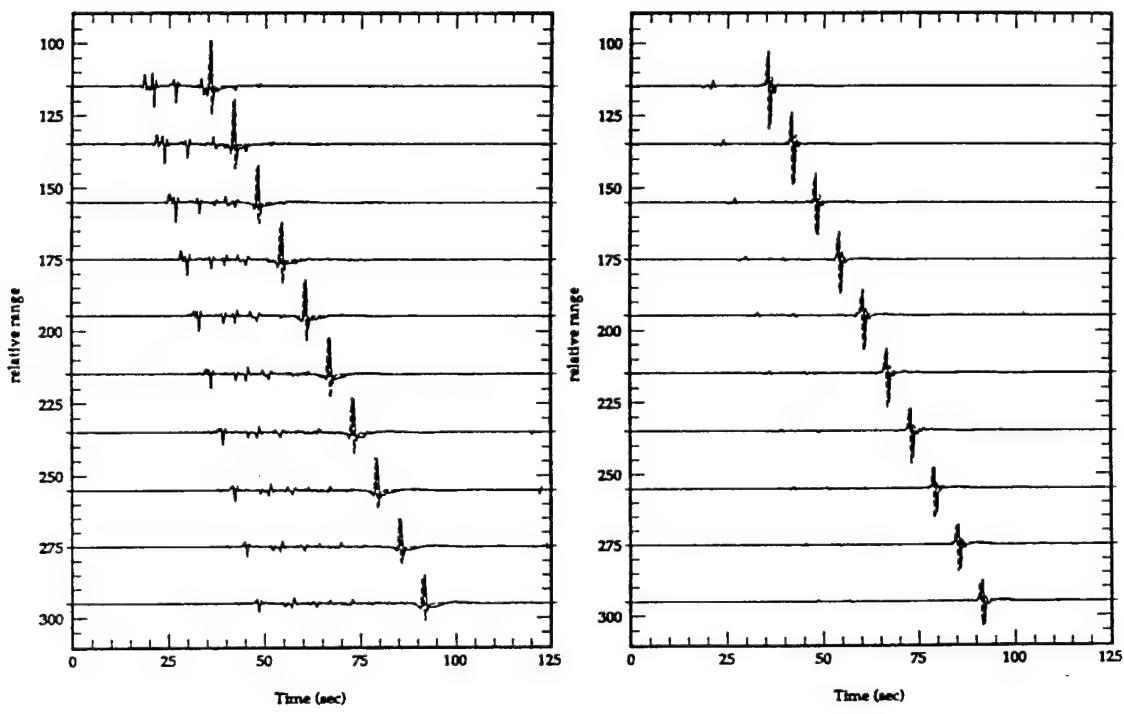
Figure 17:
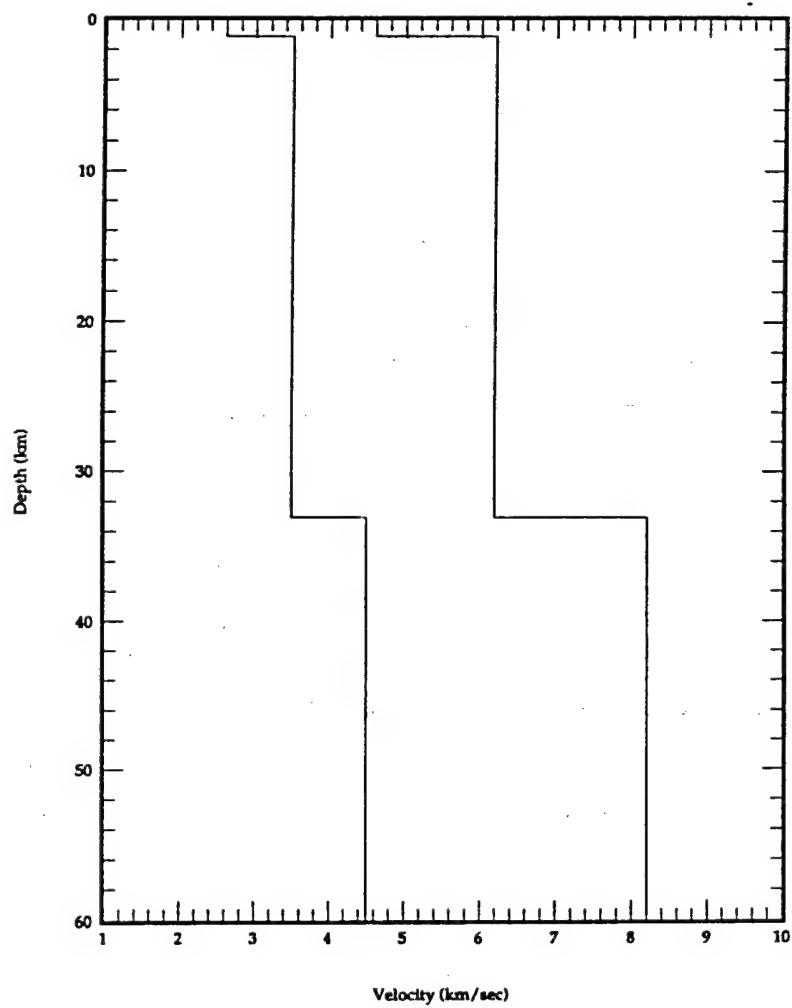
Figure 18:
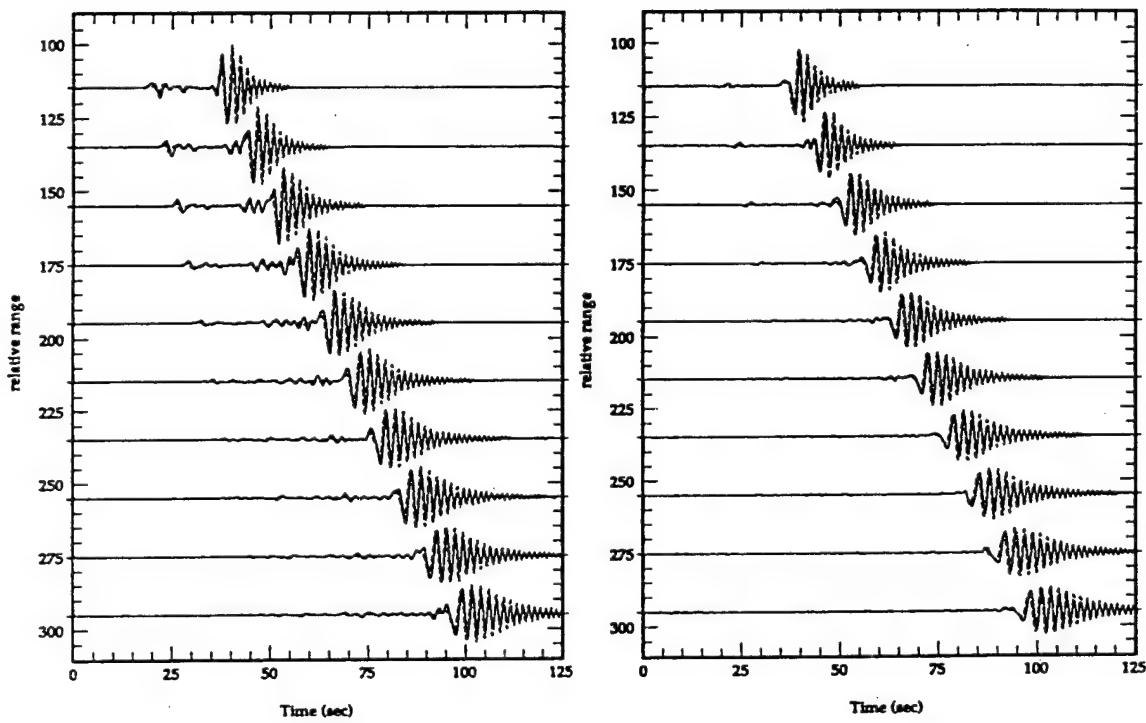
Figure 19:
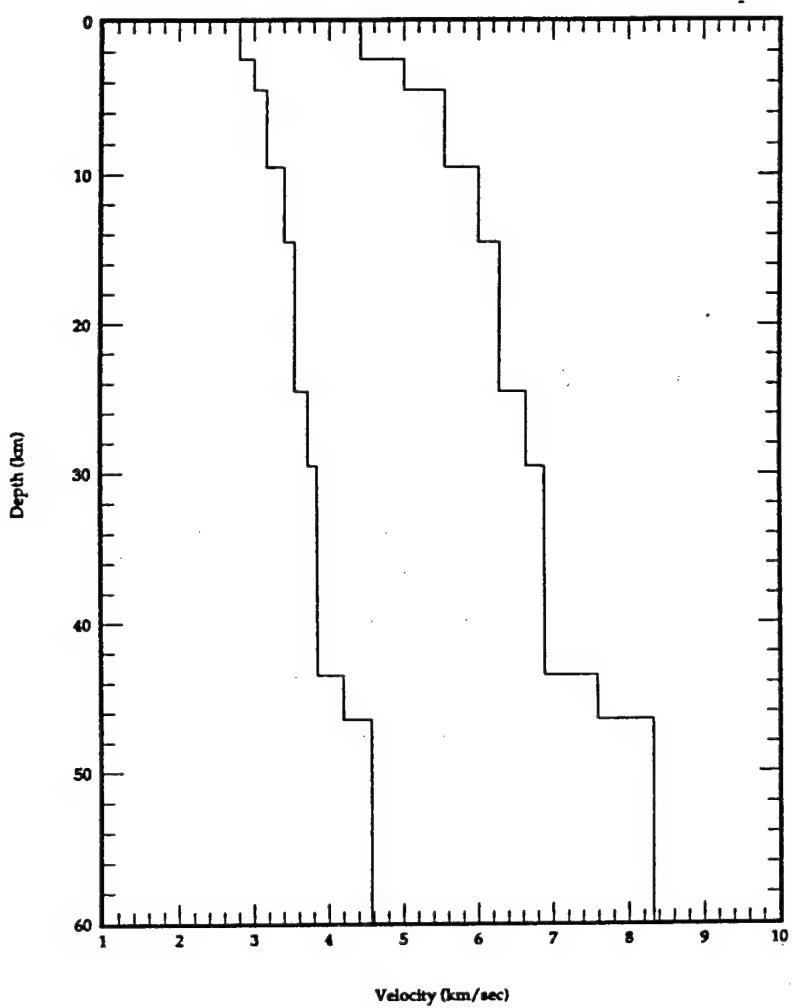
Figure 20:
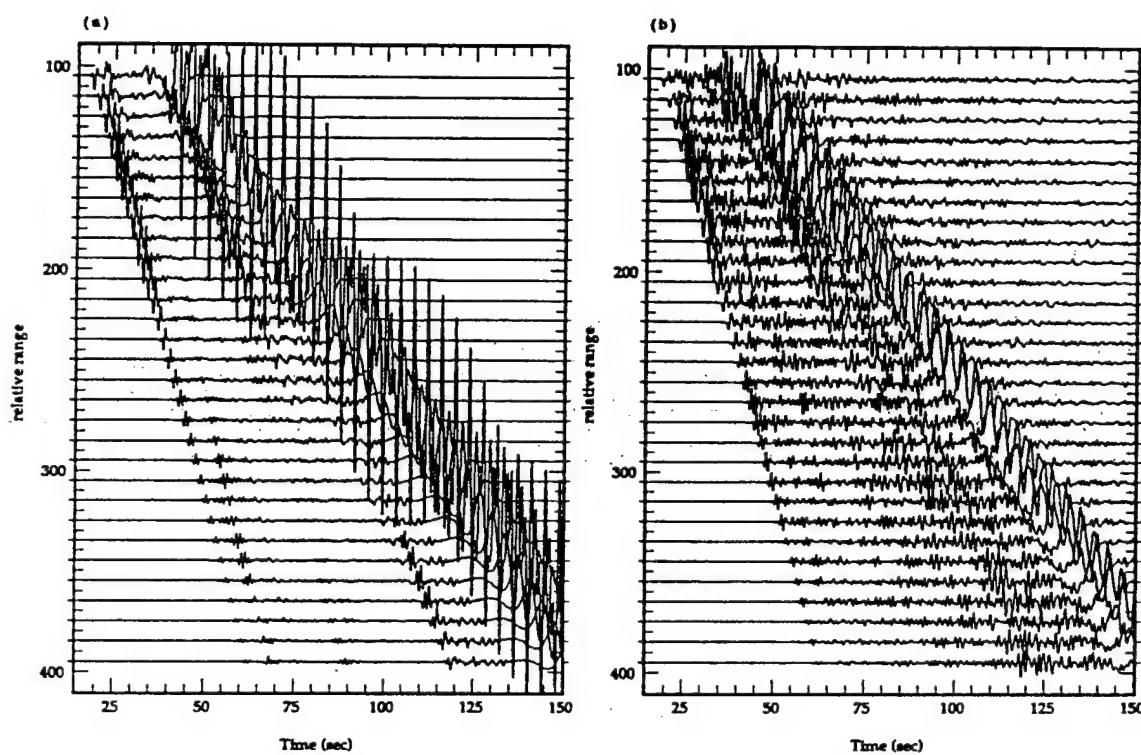
Figure 21:
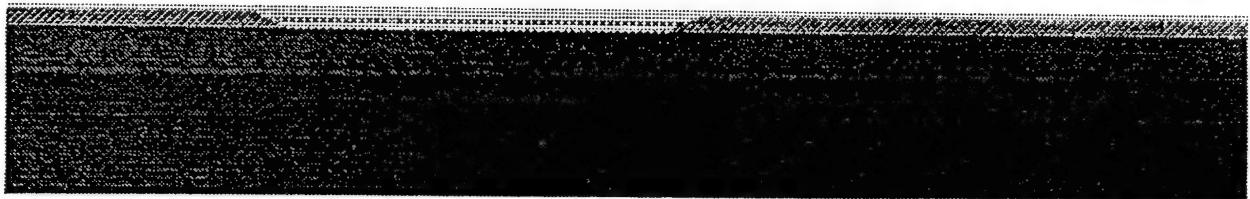
Figure 22:
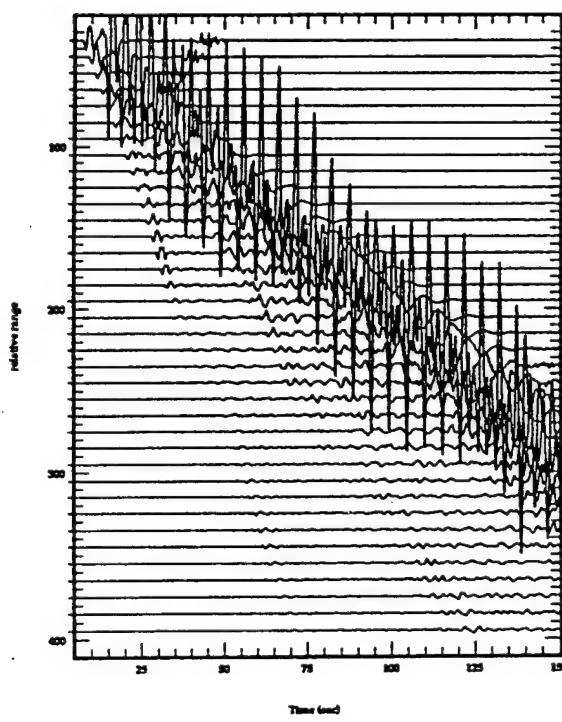
Figure 23:

Part II

Wave Propagation in Laterally Varying Media: A Mode Expansion Method

C. B. Archambeau

Department of Physics, University of Colorado

Boulder, Colorado

Wave Propagation in Laterally Varying Media:
A Mode Expansion Method

by
Charles Archambeau
Department of Physics
Theoretical and Applied Geophysics Group
University of Colorado
Boulder, CO. 80309

Abstract

An analytical approach, using modes defined on subregions of the medium, has been developed to model seismic wave propagation in media with vertically and horizontally variable elastic and anelastic properties. The approach is also applicable to acoustic waves in fluid media and electromagnetic wave propagation in laterally varying media. The restriction on the medium variability is that it can be represented by step function variations in its properties in both the vertical and horizontal directions.

The method makes use of normal mode expansions of the wave field in partitioned sub-regions of the medium within which the medium is uniform in the lateral directions. Thus, the medium is partitioned into laterally uniform zones and complete normal mode solutions are obtained for each horizontally layered zone. In the analytical development the "zonal eigenvalues and eigenfunctions" are generated by treating each zone as a layered half space or radially layered sphere, as is appropriate for medium geometry. The resulting sets of modes are then used as a bases for expansions of Greens functions in the layered subregions. The Greens function expansions are then used in Greens function surface integral representations that give the displacement fields in each zone. These representations apply at the common boundaries between the zones where continuity of displacement and traction is required. Therefore, the integral expressions for the displacements and tractions from adjacent zones can be equated along their common (vertical) boundaries as required for continuity. Then introducing eigenfunction expansions for the displacement and traction fields appearing in the integrals allows the integrations along the boundary surfaces to be performed. Consequently, boundary continuity equations reduce to algebraic equations in the unknown coefficients of the zonal eigenfunction expansions for the displacement field. This reduction to algebraic form allows a "lateral propagator" for the wave field to be defined when the method is applied to all the zones and vertical boundaries making up the medium.

In application this "lateral propagator " is very similar to the classical "vertical propagator", but now performs the function of coupling modes between the various zones. The theory is exact when the lateral variations are actually discontinuous step changes in properties. Consequently, when the actual changes can be well approximated as a sequence of steps, the method should be superior in computational accuracy and speed to numerical methods.

Table of Contents

Wave Propagation in Laterally Varying Media: A Modal Expansion Method

by

Charles B. Archambeau

Zonal Partitioning and Green's Function Representations

Consider a two dimensionally varying elastic-anelastic medium, as indicated in Figure 1. In each zone V_α, $\alpha = 1, 2, \cdots M$, the medium varies in the vertical direction (z), but is uniform in the horizontal direction (y or ρ). The supposition is that the laterally varying medium can be approximated by a series of step variations in material properties in the same way as is done in the vertical direction.

In V_α we have for the frequency domain displacement field $^{(\alpha)}\mathbf{u}$ at any point r within V_α:

$$^{(\alpha)}u_i(\mathbf{r}, \omega) = \frac{1}{4\pi} \int_{\Sigma_\alpha + \Sigma_{\alpha-1}} \left[t_j(\mathbf{r}_o)^{(\alpha)}G_j^i(\mathbf{r}, \mathbf{r}_o; \omega) - u_j(\mathbf{r}_o)^{(\alpha)}g_j^i(\mathbf{r}, \mathbf{r}_o; \omega) \right] d a_o \qquad (1)$$

where $^{(\alpha)}G_j^i$ and $^{(\alpha)}g_j^i$ are the zonal displacement and traction Greens' functions appropriate for the zone or region V_α.[*] The vertical boundary surfaces of V_α are Σ_α and $\Sigma_{\alpha-1}$, as indicated in Figure 1. Here we assume no sources inside V_α and that the Green's functions satisfy all internal boundary conditions on all horizontal layers in V_α. (In this case there are no surface integrals over internal boundaries in (1)). Green's functions in V_α can be written in terms of the eigenvalues k_α and eigenfunctions $^{(\alpha)}\psi$ for this zone as [**]:

---

[*] Summation over repeated coordinate indices is used throughout. Coordinate indices will appear as lower case latin subscripts and superscripts. The summation convention does *not* apply to any indices appearing in parenthesis.

[**] Throughout this development the "sum" over the eigenvalues k_α will be written as a discrete summation but it should be understood that in an unbounded medium, such as a layered half space, part of the wave number spectrum will be continuous. In this case the "sum" over k_α must be interpreted as a generalized summation involving a regular sum over the discrete part of the spectrum plus an integration over the continuous part of the wave number spectrum.
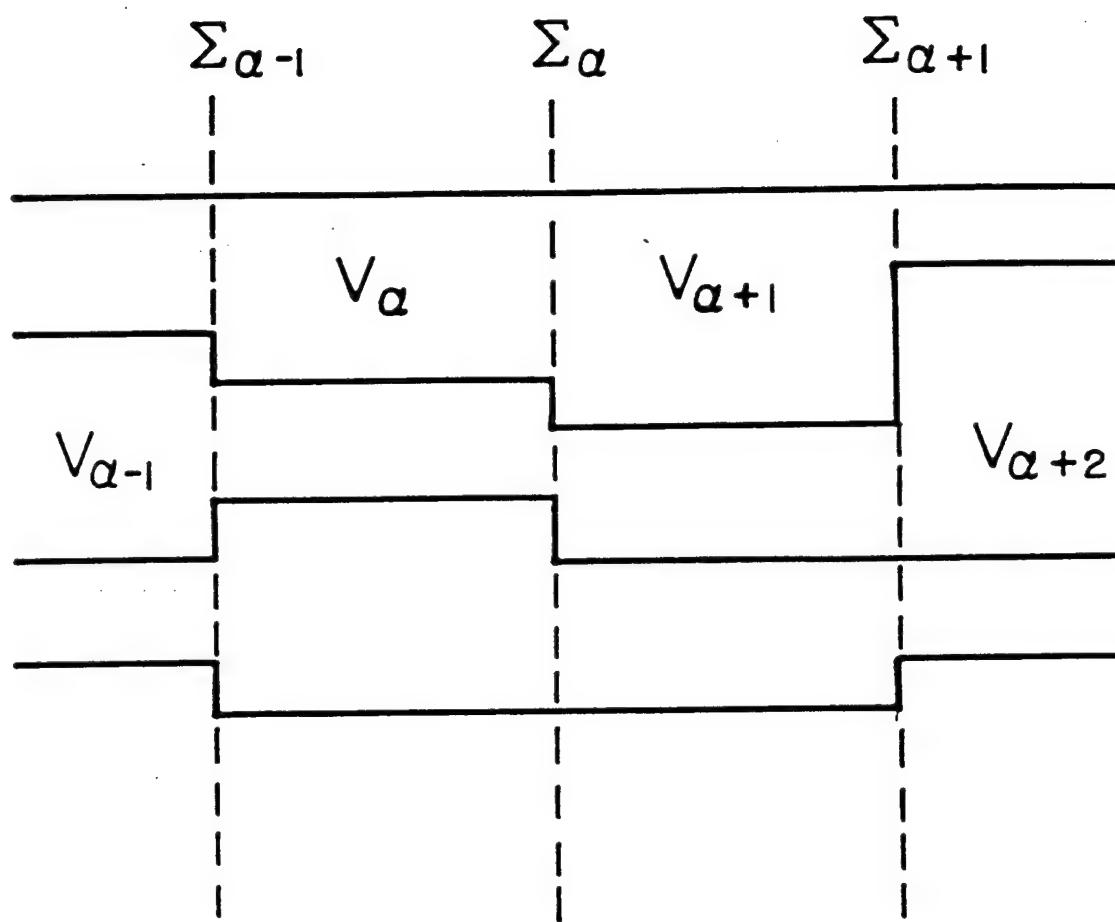
Figure 1.   Zonal partitioning of a vertically and laterally
             varying medium into subregions of uniform
             horizontal layering.

$$^{(\alpha)}G_j^i(\mathbf{r}, \mathbf{r_o}; \omega) = 4\pi \sum_{m,k_\alpha} \frac{^{(\alpha)}\overline{\psi}_j(\mathbf{r_o}, k_\alpha) \, ^{(\alpha)}\psi_i(\mathbf{r}, k_\alpha)}{N_\alpha(k_\alpha, \omega)} \tag{2}$$

where $^{(\alpha)}\overline{\psi}_i$ is the complex conjugate of $^{(\alpha)}\psi_i$ and N_α is a normalization constant which may be a function of frequency ω and the wave number k_α. Since the $^{(\alpha)}\psi_j$ are eigenfunctions for the region V_α, this Green's function satisfies all boundary conditions along the horizontal boundaries in V_α. (For details see Harvey, 1983.)

Further, since:

$$^{(\alpha)}g_j^i(\mathbf{r}; \mathbf{r_o}; \omega) = n_k^{(o)} \left[C_{kjln}^{(o)} \frac{\partial ^{(\alpha)}G_n^i(\mathbf{r}, \mathbf{r_o}; \omega)}{\partial x_l^{(o)}} \right]$$

where $n_k^{(o)}$ is the surface normal to Σ_α and $\Sigma_{\alpha-1}$ and $x_l^{(o)}$ are *source coordinate* variables, then

$$^{(\alpha)}g_j^i(\mathbf{r}; \mathbf{r_o}; \omega) = 4\pi \sum_{m,k_\alpha} \frac{^{(\alpha)}\overline{\Psi}_j(\mathbf{r_o}, k_\alpha) ^{(\alpha)}\psi_i(\mathbf{r}, k_\alpha)}{N_\alpha(k_\alpha, \omega)} \tag{3}$$

Here m is the angular index for cylindrical coordinates, k_α the horizontal wave number corresponding to the modes in V_α and where:

$$^{(\alpha)}\overline{\Psi}_j(\mathbf{r_o}, k_\alpha) = n_k^{(o)} C_{kjln}^{(o)} \frac{\partial}{\partial x_l^\rho} \left[^{(\alpha)}\psi_n(\mathbf{r_o}, k_\alpha) \right] \tag{4}$$

Because of the horizontal layering in V_α, the eigenfunctions $^{(\alpha)}\psi_j$ and $^{(\alpha)}\Psi_j$ are defined sectionally, that is:

$$^{(\alpha)}\psi_j = \left\{ ^{(\alpha)}\psi_j^{(s)}(z) \mid z_{s-1} \le z \le z_s \right\}_1^N$$

with (s) the horizontal layer index in V_α.

For the horizontally layered region V_α we have that:

$$\left. \begin{array}{l} ^{(\alpha)}G_j^i = ^{(\alpha)}_R G_j^i + ^{(\alpha)}_L G_j^i \\ ^{(\alpha)}g_j^i = ^{(\alpha)}_R R g_j^i + ^{(\alpha)}_L g_j^i \end{array} \right\} \tag{5}$$

Here $^{(\alpha)}_R G^j_j$ and $^{(\alpha)}_L G^j_j$ are the Rayleigh and Love type Green's displacement functions (with similar names for the associated Green's tractions) and where

$$
\left.
\begin{aligned}
^{(\alpha)}_R G^j_j(\mathbf{r}, \mathbf{r}_o; \omega) &= 4\pi \sum_{m, {}_Rk_\alpha} \frac{^{(\alpha)}_R\psi_j(\mathbf{r}_o, {}_Rk_\alpha)\ ^{(\alpha)}_R\psi_i(\mathbf{r}, {}_Rk_\alpha)}{N^{(R)}_\alpha(k_\alpha, \omega)} \\
^{(\alpha)}_L G^j_j(\mathbf{r}, \mathbf{r}_o; \omega) &= 4\pi \sum_{m, {}_Lk_\alpha} \frac{^{(\alpha)}_L\Psi_j(\mathbf{r}_o, {}_Lk_\alpha)\ ^{(\alpha)}_L\overline{\psi}_j(\mathbf{r}_o, {}_Lk_\alpha)}{N^{(L)}_\alpha(k_\alpha, \omega)}
\end{aligned}
\right\}
\tag{6}
$$

with ${}_Rk_\alpha$ and ${}_Lk_\alpha$ representing the Rayleigh and Love type mode eigenvalues. Likewise:

$$
\left.
\begin{aligned}
^{(\alpha)}_R g^j_j(\mathbf{r}, \mathbf{r}_o; \omega) &= 4\pi \sum_{m, {}_Rk_\alpha} \frac{^{(\alpha)}_R\overline{\Psi}_j(\mathbf{r}_o, {}_Rk_\alpha)\ ^{(\alpha)}_R\psi_i(\mathbf{r}, {}_Rk_\alpha)}{N^{(R)}_\alpha(k_\alpha, \omega)} \\
^{(\alpha)}_L g^j_j(\mathbf{r}, \mathbf{r}_o; \omega) &= 4\pi \sum_{m, {}_Lk_\alpha} \frac{^{(\alpha)}_L\overline{\Psi}_j(\mathbf{r}_o, {}_Lk_\alpha)\ ^{(\alpha)}_L\psi_i(\mathbf{r}, {}_Lk_\alpha)}{N^{(L)}_\alpha(k_\alpha, \omega)}
\end{aligned}
\right\}
\tag{7}
$$

In cylindrical coordinates (ρ, ϕ, z), the eigenfunctions are (see, for example, Harvey, 1981):

$$
\left.
\begin{aligned}
^{(\alpha)}_R\psi(\mathbf{r}, {}_Rk_\alpha) &= {}^{(\alpha)}D_m(z; {}_Rk_\alpha)\, \mathbf{P}({}_Rk_\alpha\rho, \phi) \\
&\quad + {}^{(\alpha)}E_m(z; {}_Rk_\alpha)\, \mathbf{B}({}_Rk_\alpha\rho, \phi) \\
^{(\alpha)}_R\Psi(\mathbf{r}, {}_Rk_\alpha) &= {}^{(\alpha)}R_m(z; {}_Rk_\alpha)\, \mathbf{P}_m({}_Rk_\alpha\rho, \phi) \\
&\quad + {}^{(\alpha)}S_m(z; {}_Rk_\alpha)\, \mathbf{B}_m({}_Rk_\alpha\, \rho, \phi)
\end{aligned}
\right\}
\tag{8}
$$

$$
\left.
\begin{aligned}
^{(\alpha)}_L\psi(\mathbf{r}, {}_Lk_\alpha) &= {}^{(\alpha)}F_m(z; {}_Lk_\alpha)\, \mathbf{C}_m({}_Lk_\alpha\rho, \phi) \\
^{(\alpha)}_L\Psi(\mathbf{r}, {}_Lk_\alpha) &= {}^{(\alpha)}T_m(z; {}_Lk_\alpha)\, \mathbf{C}_m({}_Lk_\alpha\rho, \phi)
\end{aligned}
\right\}
\tag{9}
$$

Here $\mathbf{P}$, $\mathbf{B}$ and $\mathbf{C}$ are the vector cylindrical harmonics defined as:

$$
\left.
\begin{aligned}
\mathbf{P}_m(k\rho, \phi) &\equiv \hat{\mathbf{e}}_z J_m(k\rho)e^{im\phi} \\
\mathbf{B}_m(k\rho, \phi) &\equiv \left[\hat{\mathbf{e}}_\rho \frac{\partial}{\partial(k\rho)} + \hat{\mathbf{e}}_\phi \left[\frac{1}{k\rho}\right] \frac{\partial}{\partial\phi}\right] J_m(k\rho)e^{im\phi} \\
\mathbf{C}_m(k\rho, \phi) &\equiv \left[\hat{\mathbf{e}}_\rho \left[\frac{1}{k\rho}\right] \frac{\partial}{\partial\phi} - \hat{\mathbf{e}}_\phi \frac{\partial}{\partial(k\rho)}\right] J_m(k\rho)e^{im\phi}
\end{aligned}
\right\}
\tag{10}
$$

where

$$J_m(k\rho) = H_m^{(1)}(k\rho) + H_m^{(2)}(k\rho)$$

with J_m the cylindrical Bessel function and $H_m^{(1)}$ and $H_m^{(2)}$ the cylindrical Hankel functions. These vector functions are clearly such that $P_m \cdot B_m = P_m \cdot C_m = B_m \cdot C_m = 0$ and also have the usual functional orthogonality. (**e.g.** Stratton 1941, Morse and Feshbach, 1953). Here $\hat{e}_z$, $\hat{e}_\rho$ and $\hat{e}_\phi$ are the unit vectors in cylindrical coordinates. The various "stress-displacement" functions $^{(\alpha)}D_m$, $^{(\alpha)}E_m$, $^{(\alpha)}R_m \cdots {}^{(\alpha)}T_m$ in (8) are the same as those usually appearing in the ordinary developments for a laterally *homogeneous* layered half space -- such as described in Harkrider (1964); Ben Menahem and Singh (1972), or Harvey (1981).

Similar representations for the eigenfunctions can be given in cartesian and spherical coordinates. (In the latter case the eigenfunctions $_R\psi$ and $_L\psi$ are usually termed spheroidal and torsional; and **P**, **B** and **C** become vector spherical harmonics). The choice of cylindrical coordinates implies rotational symmetry, that is that the medium is partitioned into zones V_α which are cylindrical shells, with Figure 1 depicting a cross section at fixed ϕ. If cartesian coordinates are used, then Figure 1 represents a cross section at constant y, with properties constant in the $\pm$y directions. In the development that immediately follows cylindrical coordinates will be used; however the cartesian and spherical representations are also appropriate and the development and results are analogous to those for the cylindrical choice.

"Forward" and "Backward Propagating" Mode Expansions

In addition to the eigenfunction expansions of the Green's functions in V_α, we can also expand the displacements and tractions, appearing in (1) in terms of eigenfunctions in V_α. In particular, $^{(\alpha)}u_j(r_o)$ and $^{(\alpha)}t_j(r_o)$ may be expanded in terms of "forward" and "backward" propagating modes as:

$$
\left.\begin{array}{l}
^{(\alpha)}u_j(\mathbf{r}_0, \omega) = {}^{(\alpha)}u_j^{(1)}(\mathbf{r}_0, \omega) + {}^{(\alpha)}u_j^{(2)}(\mathbf{r}_0, \omega) \\
^{(\alpha)}t_j(\mathbf{r}_0, \omega) = {}^{(\alpha)}t_j^{(1)}(\mathbf{r}_0, \omega) + {}^{(\alpha)}t_j^{(2)}(\mathbf{r}_0, \omega) ,
\end{array}\right\} \tag{11}
$$

where the superscripts (1) and (2) denote modes propagating in the positive and negative radial (ρ) directions. Specifically,

$$
\left.\begin{array}{l}
^{(\alpha)}u_j(\mathbf{r}_0, \omega) = \displaystyle\sum_{m', k_\alpha'} \left[{}^{(\alpha)}a_{m'}^{(1)}(k_\alpha')\, {}^{(\alpha)}\psi_j^{(1)}(\mathbf{r}_0, k_\alpha') + {}^{(\alpha)}a_{m'}^{(2)}(k_\alpha')\, {}^{(\alpha)}\psi_j^{(2)}(\mathbf{r}_0, k_\alpha') \right] \\[2ex]
^{(\alpha)}t_j(\mathbf{r}_0, \omega) = \displaystyle\sum_{m', k_\alpha'} \left[{}^{(\alpha)}a_{m'}^{(1)}(k_\alpha')\, {}^{(\alpha)}\Psi_j^{(1)}(\mathbf{r}_0, k_\alpha') + {}^{(\alpha)}a_{m'}^{(2)}(k_\alpha')\, {}^{(\alpha)}\Psi_j^{(2)}(\mathbf{r}_0, k_\alpha') \right]
\end{array}\right\} \tag{12}
$$

where

$$
^{(\alpha)}\psi^{(p)}(\mathbf{r}_0, R k_\alpha') = \left[{}^{(\alpha)}D_{m'}(z_0; k_\alpha')\, \mathbf{P}_{m'}^{(p)} + {}^{(\alpha)}E_{m'}(z_0; k_\alpha')\mathbf{B}_{m'}^{(p)} + {}^{(\alpha)}F_{m'}(z_0; k_\alpha')\, \mathbf{C}_{m'}^{(p)} \right] e^{im'\phi}
$$

$$
^{(\alpha)}\Psi^{(p)}(\mathbf{r}_0, k_\alpha') = \left[{}^{(\alpha)}R_{m'}(z_0; k_\alpha')\, \mathbf{P}_{m'}^{(p)} + {}^{(\alpha)}S_{m'}(z_0; k_\alpha')\, \mathbf{B}_{m'}^{(p)} + T_{m'}(z_0; k_\alpha')\, \mathbf{C}_{m'}^{(p)} \right] e^{im'\phi} \tag{13}
$$

with

$$
\left.\begin{array}{l}
\mathbf{P}_{m'}^{(p)} = \hat{\mathbf{e}}_z\, H_{m'}^{(p)}(k_\alpha'\rho) \; ; \; p = 1, 2 \\[2ex]
\mathbf{B}_{m'}^{(p)} = \left[\hat{\mathbf{e}}_\rho\, \dfrac{\partial}{\partial(k_\alpha'\rho)} + \hat{\mathbf{e}}_\phi \left[\dfrac{im'}{k_\alpha'\rho} \right] \right] H_{m'}^{(p)}(k_\alpha'\rho) \\[3ex]
\mathbf{C}_{m'}^{(p)} = \left[\hat{\mathbf{e}}_\rho \left[\dfrac{im'}{k_\alpha'\rho} \right] - \hat{\mathbf{e}}_\phi\, \dfrac{\partial}{\partial(k_\alpha'\rho)} \right] H_{m'}^{(p)}(k_\alpha'\rho)
\end{array}\right\} \tag{14}
$$

The coefficients $^{(\alpha)}a_m^{(p)}(k_\alpha)$ are to be determined from boundary conditions at Σ_α and $\Sigma_{\alpha-1}$; these conditions bring the continuity of displacement and traction on these surfaces. On the other hand, of course, all the functions $^{(\alpha)}D_m^{(p)}$, $^{(\alpha)}E_m^{(p)}$, $^{(\alpha)}F_m^{(p)}$, $^{(\alpha)}R_m^{(p)}$, $^{(\alpha)}S_m^{(p)}$, and $^{(\alpha)}T_m^{(p)}$ are known functions of the coordinate variables and the intrinsic material properties of the internal horizontal layers, since they are provided by the usual one-dimensional propagator approach in a layered half space (**e.g.**, Harvey, 1981). The explicit forms of the functions are included in the

Appendix 1.

Given that G_j^i and g_j^i in (1) can be split into Rayleigh and Love type Green's functions, as defined in (5)-(9), then it follows that $^{(\alpha)}u_j$ can also be split into modal sums involving only $_R^{(\alpha)}\psi_j$ and $_L^{(\alpha)}\psi_j$. Therefore:

$$^{(\alpha)}u_j = \sum_{p=1}^{2} {}^{(\alpha)}u_j^{(p)} = \sum_{p=1}^{2} \left[{}_R^{(\alpha)}u_j^{(p)} + {}_L^{(\alpha)}u_j^{(p)} \right] \tag{15}$$

where

$$\sum_{p=1}^{2} {}_R^{(\alpha)}u_j^{(p)}(\mathbf{r}_o, \omega) = \sum_{m', {}_Rk_\alpha} \left[{}_R^{(\alpha)}a_{m'}^{(1)}({}_Rk_\alpha') \, {}_R^{(\alpha)}\psi_j^{(1)} + {}_R^{(\alpha)}a_{m'}^{(2)}({}_Rk_\alpha') \, {}_R^{(\alpha)}\psi_j^{(2)} \right]$$

$$\sum_{p=1}^{2} {}_L^{(\alpha)}u_j^{(p)}(\mathbf{r}_o, \omega) = \sum_{m', {}_Lk_\alpha} \left[{}_L^{(\alpha)}a_{m'}^{(1)}({}_Lk_\alpha') \, {}_L^{(\alpha)}\psi_j^{(1)} + {}_L^{(\alpha)}a_{m'}^{(2)}({}_Lk_\alpha') \, {}_L^{(\alpha)}\psi_j^{(2)} \right] \tag{16}$$

with

$$\left.\begin{aligned}
{}_R^{(\alpha)}\psi^{(p)}(\mathbf{r}_o, {}_Rk_\alpha) &= \left[{}^{(\alpha)}D_{m'}(z_o \, ; \, {}_Rk_\alpha)\mathbf{P}_m^{(p)} + {}^{(\alpha)}E_{m'}(z_o \, ; \, {}_Rk_\alpha) \, \mathbf{B}_m^{(p)} \right] e^{im'\phi} \\
{}_L^{(\alpha)}\psi^{(p)}(\mathbf{r}_o, {}_Lk_\alpha) &= {}^{(\alpha)}F_{m'}(z_o \, ; \, {}_Lk_\alpha) \, \mathbf{C}_m^{(p)} \, e^{im'\phi}
\end{aligned}\right\} \tag{17}$$

A similar decomposition applies to the traction $^{(\alpha)}t$.

It is important to note that the eigenfunctions used to expand the Green's functions in equations (2) - (7) are appropriate for the horizontally layered zone in V_α and are themselves normalized such that:

$$\left< {}_R^{(\alpha)}\psi_j^{(p)}(k_\alpha), \, {}_R^{(\alpha)}\psi_j^{(p)}(k_\alpha') \right> \equiv \int_{V_\alpha} {}_R^{(\alpha)}\psi_j^{(p)}(k_\alpha r) {}_R^{(\alpha)}\overline{\psi}_j^{(p)}(k_\alpha' r) dV = \delta(k_\alpha - k_\alpha') \, \delta_m^{m'}$$

$$\left< {}_L^{(\alpha)}\psi_j^{(p)}(k_\alpha), \, {}_L^{(\alpha)}\psi_j^{(p)} \right> \equiv \int_{V_\alpha} {}_L^{(\alpha)}\psi_j^{(p)}(k_\alpha r) \, {}_L^{(\alpha)}\overline{\psi}_j^{(p)}(k_\alpha' r) dV = \delta(k_\alpha - k_\alpha')\delta_m^{m'} \tag{19}$$

where $^{(\alpha)}\overline{\psi}_j$ denotes the complex conjugate of $^{(\alpha)}\psi_j$ and the right hand side involves the usual

delta functions. Therefore the normalization factors appearing in the Green's function expansions are free parameters that may be chosen so as to appropriately normalize the *zonal* Green's functions in V_α, $\alpha = 1, 2, \cdots M$.

To obtain the appropriate normalization factors for $^{(\alpha)}_R G_j^i$ and $^{(\alpha)}_L G_j^i$ and, in addition, to express these Green's functions in forms that are convenient for use with the expanded form for $^{(\alpha)}u_j$ in (15)-(16), it is useful to adopt an expansion form for the Green's functions that is similar to that for $^{(\alpha)}u_j$ in (15). That is, using both $^{(\alpha)}\psi_j^{(1)}$ and $^{(\alpha)}\psi_j^{(2)}$ in the expansion for $^{(\alpha)}G_j^i$, we express the Green's functions as:

$$\left.\begin{array}{l} ^{(\alpha)}_R G_j^i\,(\mathbf{r}, \mathbf{r}_o; \omega) = {}^{(\alpha)}_R G_{ij}^{(1)} + {}^{(\alpha)}_R G_{ij}^{(2)} \\[6pt] ^{(\alpha)}_L G_j^i\,(\mathbf{r}, \mathbf{r}_o; \omega) = {}^{(\alpha)}_L G_{ij}^{(1)} + {}^{(\alpha)}_L G_{ij}^{(2)} \end{array}\right\} \tag{20}$$

where:

$$\left.\begin{array}{l} ^{(\alpha)}_R G_{ij}^{(p)} = 4\pi \displaystyle\sum_{m,\,_R k_\alpha} \dfrac{^{(\alpha)}_R \overline{\psi}_j^{(p)}(\mathbf{r}_o, {}_R k_\alpha)\,{}^{(\alpha)}_R \psi_i^{(p)}(\mathbf{r}, {}_R k_\alpha)}{_R N_p^{(\alpha)}(k_\alpha,\,\omega)} \\[12pt] ^{(\alpha)}_L G_{ij}^{(p)} = 4\pi \displaystyle\sum_{m,\,k_\alpha} \dfrac{^{(\alpha)}_L \overline{\psi}_j^{(p)}(\mathbf{r}_o, {}_L k_\alpha)\,{}^{(\alpha)}_L \psi_i^{(p)}(\mathbf{r}, {}_L k_\alpha)}{_L N_p^{(\alpha)}(k_\alpha,\,\omega)} \end{array}\right\} \tag{21}$$

and similarly for $^{(\alpha)}_R g_j^i$ and $^{(\alpha)}_L g_j^i$, the Green's tractions.

Orthogonality and Normalization Relations for Zonal Eigenfunctions

We can use (15)-(16) in (1) and also substitute (20)-(21) into this representation integral. Since the representation given by (1) should be of the form of the expansion in (15), we should obtain by proper choice of the normalization factors, $_R N_p^{(\alpha)}$ and $_L N_p^{(\alpha)}$, exactly the expansion given in (15) in terms of forward and backward propagating modes. In particular, from (1) we have:

$$^{(\alpha)}u_j\,(\mathbf{r}, \omega) = {}^{(\alpha)}_R u_j\,(\mathbf{r}, \omega) + {}^{(\alpha)}_L u_j\,(\mathbf{r}, \omega) \tag{22}$$

with

$$
\begin{Bmatrix}
{}^{(\alpha)}_R u_i(\mathbf{r}, \omega) = \int\limits_{\Sigma_\alpha + \Sigma_{\alpha-1}} \left[{}_R t_j \; {}^{(\alpha)}_R G_j^i - {}_R u_j \; {}^{(\alpha)}_R g_j^i \right] da_o \; ; \mathbf{r} \, \varepsilon \, V_\alpha \\[2mm]
{}^{(\alpha)}_L u_i(\mathbf{r}, \omega) = \int\limits_{\Sigma_\alpha + \Sigma_{\alpha-1}} \left[{}_L t_j \; {}^{(\alpha)}_L G_j^i - {}_L u_j \; {}^{(\alpha)}_L g_j^i \right] da_o \; ; \mathbf{r} \, \varepsilon \, V_\alpha
\end{Bmatrix}
\tag{23}
$$

Introducing the explicit eigenfunction expansions from (15)-(16) and (20)-(21), we get:

$$
{}^{(\alpha)}_R u_j(\mathbf{r}, \omega) = \sum_{p=1}^{2} {}^{(\alpha)}_R u_j^{(p)}(\mathbf{r}, \omega)
\tag{24}
$$

$$
{}^{(\alpha)}_R u_i^{(p)}(\mathbf{r}, \omega) = \sum_{m',{}_R k_\alpha'} {}^{(\alpha)}_R a_{m'}^{(P)}({}_R k_\alpha') \sum_{m,{}_R k_\alpha} \left\{ \frac{1}{{}_R N_p^{(\alpha)}(k_\alpha, \omega)} \right\} \Biggl[\Biggl\{ \Bigl< {}^{(\alpha)}_R \Psi_j^{(p)}({}_R k_\alpha'), {}^{(\alpha)}_R \psi_j^{(1)}({}_R k_\alpha) \Bigr>_{\alpha, \alpha-1}
$$

$$
- \Bigl< {}^{(\alpha)}_R \psi_j^{(p)}({}_R k_\alpha'), {}^{(\alpha)}_R \Psi_j^{(1)}({}_R k_\alpha) \Bigr>_{\alpha, \alpha-1} \Biggr\} {}^{(\alpha)}_R \psi_i^{(1)}(\mathbf{r}, {}_R k_\alpha) + \Biggl\{ \Bigl< {}^{(\alpha)}_R \Psi_j^{(p)}({}_R k_\alpha'), {}^{(\alpha)}_R \psi_j^{(2)}({}_R k_\alpha) \Bigr>_{\alpha, \alpha-1}
$$

$$
- \Bigl< {}^{(\alpha)}_R \psi_j^{(p)}({}_R k_\alpha'), {}^{(\alpha)}_R \Psi_j^{(2)}({}_R k_\alpha) \Bigr>_{\alpha, \alpha-1} \Biggr\} {}^{(\alpha)}_R \psi_i^{(2)}(\mathbf{r}, k_\alpha) \Biggr]
\tag{25}
$$

Here terms of the form:

$$
\Bigl< \psi_j(k_\alpha'), \chi_j(k_\alpha) \Bigr>_{\alpha, \alpha-1} \equiv \Bigl< \psi_j(k_\alpha'), \chi_j(k_\alpha) \Bigr>_\alpha + \Bigl< \psi_j(k_\alpha'), \chi_j(k_\alpha) \Bigr>_{\alpha-1}
$$

are introduced, where the inner product is defined over the surface Σ_α (or $\Sigma_{\alpha-1}$) as:

$$
\Bigl< \psi_j(k_\alpha'), \chi_j(k_\alpha) \Bigr>_\alpha \equiv \int\limits_{\Sigma_\alpha} \psi_j(\mathbf{r}_o, k_\alpha') \bar{\chi}_j(\mathbf{r}_o, k_\alpha) da_o
$$

with summation over the repeated coordinate index (j) implied. An exactly analogous result

holds for ${}_L u_j$; with the suffix "R" replaced by "L" in (24) and (25).

Comparing (25) with the equivalent expressions in (15) - (16), it is clear that the inner products appearing in (25) must reduce to delta functions over the angular index m and the mode

eigenvalues k_α. In particular, the following orthogonality conditions apply*:

---

*Where it is obvious from context, the R and L identifying subscripts on the wave numbers ${}_R k_\alpha$ and ${}_L k_\alpha$ will be suppressed in order to reduce clutter in the equations

$$\left\langle {}^{(\alpha)}_{R}\Psi_j^{(p)}(k_\alpha')\, {}^{(\alpha)}_{R}\psi_j^{(p)}(k_\alpha)\right\rangle_\beta - \left\langle {}^{(\alpha)}_{R}\psi_j^{(p)}(k_\alpha'),\, {}^{(\alpha)}_{R}\Psi_j^{(p)}(k_\alpha)\right\rangle_\beta$$

$$= \int_{\Sigma_\beta}\left[{}^{(\alpha)}_{R}\Psi^{(p)}(k_\alpha'\mathbf{r}_0)\cdot {}^{(\alpha)}_{R}\overline{\psi}^{(p)}(k_\alpha\mathbf{r}_0) - {}^{(\alpha)}_{R}\psi^{(p)}(k_\alpha'\mathbf{r}_0)\cdot {}^{(\alpha)}_{R}\overline{\Psi}^{(p)}(k_\alpha\mathbf{r}_0)\right]d a_0 \tag{26}$$

$$= n_\beta\left[\mathbf{P}_m^{(p)}(k_\alpha'\rho_\beta)\cdot \overline{\mathbf{P}}_m^{(p)}(k_\alpha\rho_\beta) + \mathbf{B}_m^{(p)}(k_\alpha'\rho_\beta)\cdot \overline{\mathbf{B}}_m^{(p)}(k_\alpha\rho_\beta)\right]\delta_{k_\alpha}^{k_\alpha'}\,\delta_m^{m'}\;;$$

with $\beta = \alpha,\ \alpha - 1$ and $p = 1,2$ and where $n_\beta = 2\pi\rho_\beta$. (Here ρ_β is the constant value of the radial coordinate on the surface Σ_β.) In addition,

$$\left\langle {}^{(\alpha)}_{R}\Psi_j^{(p)}(k_\alpha'),\, {}^{(\alpha)}_{R}\psi_j^{(q)}(k_\alpha)\right\rangle_\beta - \left\langle {}^{(\alpha)}_{R}\psi_j^{(p)}(k_\alpha'),\, {}^{(\alpha)}_{R}\Psi_j^{(q)}(k_\alpha)\right\rangle_\beta =$$

$$\int_{\Sigma_\beta}\left[{}^{(\alpha)}_{R}\Psi_j^{(p)}(k_\alpha'\mathbf{r}_0)\cdot {}^{(\alpha)}_{R}\overline{\psi}^{(q)}(k_\alpha\mathbf{r}_0) - {}^{(\alpha)}_{R}\psi^{(p)}(k_\alpha'\mathbf{r}_0)\cdot {}^{(\alpha)}_{R}\overline{\Psi}^{(q)}(k_\alpha\mathbf{r}_0)\right]d a_0 = 0 \tag{27}$$

for $\beta = \alpha,\ \alpha - 1$ and $p \neq q$. Formally identical relations hold for the eigenfunctions ${}^{(\alpha)}_{L}\psi^{(p)}$ and are obtained by replacing the suffix "R" by "L" in (26) and (27). Here we observe that the forward and backward propagating modes are completely orthogonal sets. These conditions are equivalent to those obtained by Herrera (1964) and McGarr and Alsop (1967) and were used by Kennett (1983) in his development of a formalism for wave propagation in laterally varying media. In more explicit form, equations (26) and (27) are equivalent to:

$$\int_0^\infty\left[{}^{(\alpha)}R_m(z_0\,;k_\alpha')\,{}^{(\alpha)}\overline{D}_m(z_0\,;k_\alpha) - {}^{(\alpha)}D_m(z_0\,;k_\alpha')\,{}^{(\alpha)}\overline{R}_m(z_0\,;k_\alpha)\right]dz_0 = \delta_{k_\alpha}^{k_\alpha'}$$

$$\int_0^\infty\left[{}^{(\alpha)}S_m(z_0\,;k_\alpha')\,{}^{(\alpha)}\overline{E}_m(z_0\,;k_\alpha) - {}^{(\alpha)}E_m(z_0\,;k_\alpha')\,{}^{(\alpha)}\overline{S}_m(z_0\,;k_\alpha)\right]dz_0 = \delta_{k_\alpha}^{k_\alpha'}$$

where the subscript "R" on the P-SV wave number has also been suppressed in these expressions. For the SH modes the analogous orthogonality relation is easily seen to be:

$$\int_0^\infty\left[{}^{(\alpha)}T_m(z_0\,;k_\alpha')\,{}^{(\alpha)}\overline{F}_m(z_0\,;k_\alpha) - {}^{(\alpha)}F_m(z_0\,;k_\alpha')\,{}^{(\alpha)}\overline{T}_m(z_0\,;k_\alpha)\right]dz_0 = \delta_{k_\alpha}^{k_\alpha'}$$

where the wave numbers and k_α and k'_α now refer to the SH wave number set $_Lk_\alpha$. The "vertical eigenfunctions" in V_α are those defined in (13) and are simple expontials in z_o. (See Harvey, 1981.) Here also we consider the k_α to be discrete infinite sets, so that orthogonality is expressed by the Kronecker delta $\delta_{k_\alpha}^{k'_\alpha}$.

Using these orthogonality relations in (25) gives:

$$
{}^{(\alpha)}_R u_j^{(1)}(\mathbf{r},\,\omega) = \sum_{m',\,k'_\alpha} {}^{(\alpha)}_R a_{m'}^{(1)}(k'_\alpha) \sum_{m,\,k_\alpha} \left[\frac{\delta_{k_\alpha}^{k'_\alpha}\,\delta_m^{m'}}{_R N_1^{(\alpha)}(k_\alpha,\,\omega)}\right]\left[n_\alpha\left\{ \mathbf{P}_{m'}^{(1)}(k'_\alpha\rho_\alpha)\cdot\overline{\mathbf{P}}_m^{(1)}(k_\alpha\rho_\alpha) + \mathbf{B}_{m'}^{(1)}(k'_\alpha\rho_\alpha)\cdot\overline{\mathbf{B}}_m^{(1)}(k_\alpha\rho_\alpha)\right\}\right.
$$

$$
\left. + n_{\alpha-1}\left\{ \mathbf{P}_{m'}^1(k'_\alpha\rho_{\alpha-1})\cdot\overline{\mathbf{P}}_m^{(1)}(k_\alpha\rho_{\alpha-1}) + \mathbf{B}_{m'}^{(1)}(k'_\alpha\rho_{\alpha-1})\cdot\overline{\mathbf{B}}_m^{(1)}(k_\alpha\rho_{\alpha-1})\right\}\right]\, {}^{(\alpha)}_R\psi_j^{(1)}(\mathbf{r},\,k_\alpha)
$$

So

$$
{}^{(\alpha)}_R u_j^{(1)}(\mathbf{r},\,\omega) = \sum_{m,\,k_\alpha} {}^{(\alpha)}_R a_m^{(1)}(k_\alpha)\, {}^{(\alpha)}_R\psi_j^{(1)}(\mathbf{r},\,k_\alpha)
$$

provided we take:

$$
_R N_1^{(\alpha)} = \left[n_\alpha\left\{ \mathbf{P}_m^{(1)}(k_\alpha\rho_\alpha)\cdot\overline{\mathbf{P}}_m^{(1)}(k_\alpha\rho_\alpha) + \mathbf{B}_m^{(1)}(k_\alpha\rho_\alpha)\cdot\overline{\mathbf{B}}_m^{(1)}(k_\alpha\rho_\alpha)\right\}\right.
$$

$$
\left. + n_{\alpha-1}\left\{ \mathbf{P}_m^{(1)}(k_\alpha\rho_{\alpha-1})\cdot\overline{\mathbf{P}}_m^{(1)}(k_\alpha\rho_{\alpha-1}) + \mathbf{B}_m^{(1)}(k_\alpha\rho_{\alpha-1})\overline{\mathbf{B}}_m^{(1)}(k_\alpha\rho_{\alpha-1})\right\}\right] \tag{28}
$$

Similarly,

$$
_R u_j^{(2)}(\mathbf{r},\,\omega) = \sum_{m,\,k_\alpha} {}^{(\alpha)}_R a_m^{(2)}(k_\alpha)\, {}^{(\alpha)}_R\psi_j^{(2)}(\mathbf{r},\,k_\alpha)
$$

provided

$$
_R N_2^{(\alpha)} = \left[n_\alpha\left\{ \mathbf{P}_m^{(2)}(k_\alpha\rho_\alpha)\cdot\overline{\mathbf{P}}_m^{(2)}(k_\alpha\rho_\alpha) + \mathbf{B}_m^{(2)}(k_\alpha\rho_\alpha)\cdot\overline{\mathbf{B}}_m^{(2)}(k_\alpha\rho_\alpha)\right\}\right.
$$

$$
\tag{29}
$$

$$+ n_{\alpha-1}\left\{P_m^{(2)}(k_\alpha\rho_{\alpha-1}) \cdot \overline{P}_m^{(2)}(k_\alpha\rho_{\alpha-1}) + B_m^{(2)}(k_\alpha\rho_{\alpha-1}) \cdot \overline{B}_m^{(2)}(k_\alpha\rho_{\alpha-1})\right\}\bigg]\bigg]$$

The results for $^{(\alpha)}_L\mathbf{u}$ are analogous and the normalization factors are:

$$_LN_1^{(\alpha)} = \left[n_\alpha C_m^{(1)}(k_\alpha\rho_\alpha)\cdot\overline{C}_m^{(1)}(k_\alpha\rho_\alpha) + n_{\alpha-1}C_m^{(1)}(k_\alpha\rho_{\alpha-1})\overline{C}_m^{(1)}(k_\alpha\rho_{\alpha-1})\right] \tag{30}$$

$$_LN_2^{(\alpha)} = \left[n_\alpha C_m^{(2)}(k_\alpha\rho_\alpha) \cdot \overline{C}_m^{(2)}(k_\alpha\rho_\alpha) + n_{\alpha-1}C_m^{(2)}(k_\alpha\rho_{\alpha-1})\overline{C}_m^{(2)}(k_\alpha\rho_{\alpha-1})\right] \tag{31}$$

Thus, the form of the displacement field in any one of the zones V_α is given by

$$^{(\alpha)}u_i(\mathbf{r}, \omega) = \sum_{m,Rk_\alpha}\left[^{(\alpha)}_R a_m^{(1)}(_Rk_\alpha)\,^{(\alpha)}_R\psi_i^{(1)}(\mathbf{r}, {_R}k_\alpha) + ^{(\alpha)}_R a_m^{(2)}(_Rk_\alpha)\,^{(\alpha)}_R\psi_i^{(2)}(\mathbf{r}, {_R}k_\alpha)\right]$$

$$+ \sum_{m,Lk_\alpha}\left[^{(\alpha)}_L a_m^{(1)}(_Lk_\alpha)\,^{(\alpha)}_L\psi_i^{(1)}(\mathbf{r}, {_L}k_\alpha) + ^{(\alpha)}_L a_m^{(2)}(_Lk_\alpha)\,^{(\alpha)}_L\psi_i^{(2)}(\mathbf{r}, {_L}k_\alpha)\right] ; \; \mathbf{r} \,\varepsilon\, V_\alpha \tag{32}$$

which is (merely) a sum of P-SV modes propagating in the forward and backward horizontal directions, plus a similar sum of SH modes. Further, the displacement field in V_α is connected to its values on the boundary surfaces Σ_α and $\Sigma_{\alpha-1}$ by the representations in (23), with the Greens functions given by the eigenfunction expansions of (20) - (21) and with the normalizations specified by (28) - (31). Use of these latter representations provide the means of determining the coefficients $^{(\alpha)}_R a_m^{(p)}$ and $^{(\alpha)}_L a_m^{(p)}$ in (32), and thereby an explicit expression of the displacement field in V_α in terms of the modes of this horizontally layered region. As will be shown, the coefficients between all the zones V_α, $\alpha = 1, 2, \cdots, M$, are linked by a propagator formalism.

Zonal Boundary Conditions, Projections and Lateral Propagators

Continuity conditions expressing conservation of momentum, mass and energy apply throughout the medium, however complex the intrinsic material properties. In particular such conditions apply along the control surfaces Σ_α separating the zones of uniform lateral properties

in Figure 1. In the case of a solid medium, with welded contacts at all layer boundaries, the continuity conditions along the surface Σ_α are:

$$\begin{bmatrix} {}^{(\alpha)}u_j \\ {}^{(\alpha)}t_j \end{bmatrix}_\alpha = \begin{bmatrix} {}^{(\alpha+1)}u_j \\ {}^{(\alpha+1)}t_j \end{bmatrix}_\alpha \quad ; j = 1, 2, 3 \tag{33}$$

where the subscript α on the matrix brackets is used to indicate evaluation on the vertical boundary Σ_α between the zones V_α and $V_{\alpha+1}$.

The displacements and tractions in (33) can be expressed in terms of the eigenfunction expansion of (32). However, since the P-SV and SH modes are decoupled in V_α and $V_{\alpha+1}$, then (33) can also be expressed by the decoupled set of relations:

$$\sum_m \sum_{Rk_\alpha} \sum_{p=1}^{2} \left[{}^{(\alpha)}_R A^{(p)}_m ({}_Rk_\alpha) \begin{bmatrix} {}^{(\alpha)}_R \psi^{(p)}_j ({}_Rk_\alpha) \\ {}^{(\alpha)}_R \Psi^{(p)}_j ({}_Rk_\alpha) \end{bmatrix} \right]_\alpha = \sum_m \sum_{Rk_{\alpha+1}} \sum_{p=1}^{2} \left[{}^{(\alpha+1)}_R A^{(p)}_m ({}_Rk_{\alpha+1}) \begin{bmatrix} {}^{(\alpha+1)}_R \psi^{(p)}_j ({}_Rk_{\alpha+1}) \\ {}^{(\alpha+1)}_R \Psi^{(p)}_j ({}_Rk_{\alpha+1}) \end{bmatrix} \right]_\alpha \quad ; j = 1, 2 \tag{34a}$$

$$\sum_m \sum_{Lk_\alpha} \sum_{p=1}^{2} \left[{}^{(\alpha)}_L A^{(p)}_m ({}_Lk_\alpha) \begin{bmatrix} {}^{(\alpha)}_L \psi^{(p)}_j ({}_Lk_\alpha) \\ {}^{(\alpha)}_L \Psi^{(p)}_j ({}_Lk_\alpha) \end{bmatrix} \right]_\alpha = \sum_m \sum_{Lk_{\alpha+1}} \sum_{p=1}^{2} \left[{}^{(\alpha+1)}_L A^{(p)}_m ({}_Lk_{\alpha+1}) \begin{bmatrix} {}^{(\alpha+1)}_L \psi^{(p)}_j ({}_Lk_{\alpha+1}) \\ {}^{(\alpha+1)}_L \Psi^{(p)}_j ({}_Lk_{\alpha+1}) \end{bmatrix} \right]_\alpha \quad ; j = 3 \tag{34b}$$

where the expansions in P-SV and SH moves have been substituted for u_j and t_j on both sides of (33). A similar set of boundary equations apply to the other vertical boundary of V_α, on the surface $\Sigma_{\alpha-1}$, in Figure 1. (In this case the matrices are evaluated on $\Sigma_{\alpha-1}$ so the matrix indices in (34) change to $(\alpha-1)$ throughout, while on the right side of (34) all the eigenvalue and eigenfunction indices change from $(\alpha+1)$ to $(\alpha-1)$.)

We can extract expressions for individual mode coefficients ${}^{(\alpha)}_R A^{(p)}_m$ and ${}^{(\alpha)}_L A^{(p)}_m$, appropriate to the zone V_α, in terms of the mode coefficients in the zone $V_{\alpha+1}$ by taking integral inner products ("projections") between the displacement and traction eigenfunctions on both sides of

(34). Then we can use the (P-SV) orthogonality relations in (26) - (27), along with comparable orthogonal relations for SH modes. Specifically, using inner product bracket notation as before in equation (25) and taking the inner products between displacement and traction eigenfunctions on both sides of (34), we have:

$$
\sum_{m,\,k_\alpha} \sum_{p=1}^{2} {}^{(\alpha)}A_m^{(p)}(k_\alpha)
\begin{Bmatrix}
<{}^{(\alpha)}\psi_j^{(p)}(k_\alpha)\,,\,{}^{(\alpha)}\Psi_j^{(s)}(k_\alpha^{(n)})>_\alpha \\
<{}^{(\alpha)}\Psi_j^{(p)}(k_\alpha)\,,\,{}^{(\alpha)}\psi_j^{(s)}(k_\alpha^{(n)})>_\alpha
\end{Bmatrix}
= \sum_{m,\,k_\alpha} \sum_{p=1}^{2} {}^{(\alpha+1)}A_m^{(p)}(k_{\alpha+1})
\begin{Bmatrix}
<{}^{(\alpha+1)}\psi_j^{(p)}(k_{\alpha+1})\,,\,{}^{(\alpha)}\Psi_j^{(s)}(k_\alpha^{(n)})>_\alpha \\
<{}^{(\alpha+1)}\Psi_j^{(p)}(k_{\alpha+1})\,,\,{}^{(\alpha)}\psi_j^{(s)}(k_\alpha^{(n)})>_\alpha
\end{Bmatrix}
$$

(35)

where indices R or L have been suppressed but are implied, with appropriate use depending on whether $j = 1, 2$ or $j = 3$, as indicated by (34a) and (34b). (That is, this equation applies to either (34a) or (34b)). For specificity, one uses P-SV eigenfunctions and eigenvalues and a subscript "R" when considering component equations with $j = 1, 2$ and uses SH eigenfunctions and eigenvalues with subscript "L" when considering the $j = 3$ component equation.) Here $k_\alpha^{(n)}$ denotes the specific n^{th} eigenvalue of one particular mode with angular index m'.

Now we can subtract the upper matrix equation in (35) from the lower one and then make use of the orthogonality relations for P-SV modes in (26) - (27), and the obvious similar pair for the SH modes, to obtain:

$$
{}^{(\alpha)}A_m^{(s)}(k_\alpha^{(n)}) = \frac{1}{N_s^{(\alpha)}} \sum_{k_{\alpha+1}} \sum_{p=1}^{2} {}^{(\alpha+1)}A_m^{(p)}(k_{\alpha+1}) \Bigg\{ <{}^{(\alpha+1)}\psi_j^{(p)}(k_{\alpha+1})\,,\,{}^{(\alpha)}\Psi_j^{(s)}(k_\alpha^{(n)})>_\alpha -
$$
$$
<{}^{(\alpha+1)}\Psi_j^{(p)}(k_{\alpha+1})\,,\,{}^{(\alpha)}\psi_j^{(s)}(k_\alpha^{(n)})>_\alpha \Bigg\} \quad ; s = 1, 2
$$

(36)

where we have equated the sums over m, on each side of (35), term by term. This equation again applies to either P-SV or SH modes; however, for P-SV modes $j = 1, 2$ and for SH modes, then $j = 3$. Therefore in (36) the implied summation over the coordinate index is over $j = 1$ and 2, for the P-SV case, and for SH modes only the one term, for which $j = 3$, occurs. The free

index (s) denotes the forward and backward horizontally propagating modes, so that (36) expresses a relationship for both mode types. The factor $N_s^{(\alpha)}$ is the normalization "constant" appropriate for the different mode types. These factors are given in (28) - (29), for the forward and backward propagating P-SV modes, and in (30) - (31) for the SH modes.

It can be seen from (36) that a particular mode in V_α, at a particular eigenvalue (or wave number), will be "excited" by *all* the forward and backward propagating modes in $V_{\alpha+1}$ in the manner described by the expression on the right side in (36). Thus, all the modes in $V_{\alpha+1}$, at *all* wave numbers, will contribute to the excitation of any one mode in V_α (at a *particular* wave number) in proportion to the sum of the mode coefficients, $^{(\alpha+1)}A_m^{(p)}(k_{\alpha+1})$, weighted by the inner product factors given by the bracket term on the right side of (36). Thus the weight factors in (36) will be called *coupling coefficients*.

Considering the $k_{\alpha+1}$ eigenvalues as a discrete (infinite) set $\{k_{\alpha+1}^{(l)}\}$, as was implied for k_α by the use of $k_\alpha^{(n)}$, then we can define the discrete coupling coefficients as

$$C_{ln}^{(p,s)}(\alpha+1\,;\alpha) \equiv \frac{1}{N_s^{(\alpha)}} \left[\left< {}^{(\alpha+1)}\psi_j^{(p)}(k_{\alpha+1}^{(l)})\,,\,{}^{(\alpha)}\Psi_j^{(s)}(k_\alpha^{(n)}) \right>_\alpha - \left< {}^{(\alpha+1)}\Psi_j^{(p)}(k_{\alpha+1}^{(l)})\,,\,{}^{(\alpha)}\psi_j^{(s)}(k_\alpha^{(n)}) \right>_\alpha \right]$$

(37)

and (36) becomes:

$$^{(\alpha)}a_m^{(s)}(k_\alpha^{(n)}) = \sum_1 \sum_{p=1}^2 C_{ln}^{(p,s)}(\alpha+1\,;\alpha)\,{}^{(\alpha+1)}a_m^{(p)}(k_{\alpha+1}^{(l)})\;;\;s=1,2 \qquad (38)$$

The coupling coefficients can be expressed in more detail when the specific functional forms of the eigenfunctions appearing in the inner products are used in (37). In this case we can use the orthogonality of the vector cylinderical harmonics to reduce the coupling factors to simple integrals over the vertical (z) coordinate on the boundaries of each zone V_α. Specifically, from (37) for the P-SV case, using the eigenfunction expressions given earlier in (13) - (14), one

has:

$$
_RC_{lh}^{(p,s)}(\alpha+1\,;\alpha) = \frac{n_\alpha}{_RN_s^{(\alpha)}}\left[\left\{<{}^{(\alpha+1)}D_l\,,\,{}^{(\alpha)}R_n> - <{}^{(\alpha+1)}R_l\,,\,{}^{(\alpha)}D_n>\right\}P_m^{(p)}(k_{\alpha+1}^{(l)}\rho_\alpha)\cdot\bar{P}_m^{(s)}(k_\alpha^{(n)}\rho_\alpha)\right.
$$

$$
\left. + \left\{<{}^{(\alpha+1)}E_l\,,\,{}^{(\alpha)}S_n> - <{}^{(\alpha+1)}S_l\,,\,{}^{(\alpha)}E_n>\right\}B_m^{(p)}(k_{\alpha+1}^{(l)}\rho_\alpha)\cdot\bar{B}_m^{(s)}(k_\alpha^{(n)}\rho_\alpha)\right] \tag{39}
$$

where $n_\alpha = 2\pi\rho_\alpha$, with ρ_α denoting the value of the radial coordinate on the surface Σ_α. Further the various inner products involve the "vertical eigenfunctions" defined in (13) and (17); where these inner products have explicit forms of the type:

$$
<{}^{(\alpha+1)}D_l\,,\,{}^{(\alpha)}R_n> \equiv \int_0^\infty {}^{(\alpha+1)}D_m(z_o\,;\,k_{\alpha+1}^{(l)})^{(\alpha)}\bar{R}_m(z_o\,;\,k_\alpha^{(n)})dz_o \tag{39a}
$$

with similar expressions for the other products in (39). If these products are compared to those in (26) and (27) - or more directly to the orthogonality relations involving the vertical eigenfunctions given by the equations following equation (27) - it can be seen that the inner products in (39) reduce to delta functions *if* the eigenfunctions in the zones V_α and $V_{\alpha+1}$ are the same; that is, if ${}^{(\alpha+1)}D_m = {}^{(\alpha)}D_m$, ${}^{(\alpha+1)}R_m = {}^{(\alpha)}R_m$, etc. This, of course, is as it must be, since only when the physical properties in the two zones are identical will the eigenfunctions be the same and it then follows that the coupling matrix must be diagonal - that is that the boundary between the two zones produces no cross mode excitation and is transparent. We see, therefore, that the analytical expression in (39) for the coupling does indeed have this required property.

The normalization factor for $C_{lh}^{(p,s)}$ is the ratio $_RN_s^{(\alpha)}\,/\,n_\alpha$ which can be redefined as $_R\tilde{N}_s^{(\alpha)}$, where from the previous expressions for $_RN_s^{(\alpha)}$, in (28) and (29), this constant has the form:

$$
_RN_s^{(\alpha)} = \left[\left\{P_m^{(s)}(k_\alpha^{(n)}\rho_\alpha)\cdot\bar{P}_m^{(s)}(k_\alpha^{(n)}\rho_\alpha) + B_m^{(s)}(k_\alpha^{(n)}\rho_\alpha)\cdot\bar{B}_m^{(s)}(k_\alpha^{(n)}\rho_\alpha)\right.\right.
$$

$$
\left.\left. + \left[\frac{\rho_{\alpha-1}}{\rho_\alpha}\right]\left\{P_m^{(s)}(k_\alpha^{(n)}\rho_{\alpha-1})\cdot\bar{P}_m^{(s)}(k_\alpha^{(n)}\rho_{\alpha-1}) + B_m^{(s)}(k_\alpha^{(n)}\rho_{\alpha-1})\cdot\bar{B}_m^{(s)}(k_\alpha^{(n)}\rho_{\alpha-1})\right\}\right]\right] \tag{40}
$$

In an exactly analogous fashion the coupling coefficients for the SH modes are found to be:

$$_LC_{\text{lh}}^{(p,s)}(\alpha+1 \, ; \, \alpha) = \frac{n_\alpha}{_LN_s^{(\alpha)}} \left[<^{(\alpha+1)}F_l \, , \, ^{(\alpha)}T_n> - <^{(\alpha+1)}T_l \, , \, ^{(\alpha)}F_n> \right] C_m^{(p)}(k_{\alpha+1}^{(l)}\rho_\alpha) \cdot \bar{C}_m^{(s)}(k_\alpha^{(n)}\rho_\alpha)$$

(41)

where the inner products are again of the simple form:

$$<^{(\alpha+1)}F_l \, , \, ^{(\alpha)}T_n> \equiv \int_0^\infty {}^{(\alpha+1)}F_m(z_o \, ; \, k_{\alpha+1}^{(l)}) {}^{(\alpha)}\bar{T}_m(z_o \, ; \, k_\alpha^{(n)}) \, dz_o$$

(41a)

Further, we can again define a new normalization factor $_L\tilde{N}_s^{(\alpha)} \equiv {}_LN_s^{(\alpha)} / n_\alpha$ which has the form:

$$_L\tilde{N}_s^{(\alpha)} = \left[C_m^{(s)}(k_\alpha^{(n)}\rho_\alpha) \cdot \bar{C}_m^{(s)}(k_\alpha^{(n)}\rho_\alpha) + \left(\frac{\rho_{\alpha-1}}{\rho_\alpha} \right) C_m^{(s)}(k_\alpha^{(n)}\rho_{\alpha-1}) \cdot \bar{C}_m^{(s)}(k_\alpha^{(n)}\rho_{\alpha-1}) \right]$$

(42)

The computations involved in determining these coefficients are straightforward, since the cylinderical harmonics are tabulated and the integrals over the vertical coordinate z_o involve simple integrals of exponentials that can be evaluated analytically, in closed form, for the general case.

Since (38) constitutes a set of two equations for s = 1 and s = 2, corresponding to forward and backward propagating modes and since the sums on the right can clearly be expressed as a product of matrices, it is natural to write the results in matrix form. Therefore we define:

$$\left[{}^{(\alpha)}a_n^{(s)} \right] \equiv \begin{bmatrix} {}^{(\alpha)}a_m^{(s)} \, (k_\alpha^{(1)}) \\ {}^{(\alpha)}a_m^{(s)} \, (k_\alpha^{(2)}) \\ . \\ . \\ . \\ {}^{(\alpha)}a_m^{(s)} \, (k_\alpha^{(N)}) \end{bmatrix} \, ; \, \text{for s = 1 and 2}$$

(43a)

and a similar column matrix of length (L) denoted $[{}^{(\alpha+1)}a_l^{(p)}]$, where the angular index m has been suppressed in writing the mode excitation matrices. Further, we can define coupling

matrices by:

$$
\left[C_{ln}^{(p,s)} \right] = \begin{bmatrix} C_{11}^{(p,s)} C_{21}^{(p,s)} & C_{L1}^{(p,s)} \\ C_{12}^{(p,s)} & C_{22}^{(p,s)} & C_{L2}^{(p,s)} \\ \cdot & & \cdot \\ \cdot & & \cdot \\ \cdot & & \cdot \\ C_{1N}^{(p,s)} & \cdots & C_{LN}^{(p,s)} \end{bmatrix}
\tag{43b}
$$

for each s and p value, where s = 1,2 and p = 1,2. With these definitions one can write the system of equations implied by (38) in the form:

$$
\begin{bmatrix} [^{(\alpha)}a_n^{(1)}] \\ [^{(\alpha)}a_n^{(2)}] \end{bmatrix} = \begin{bmatrix} [C_{ln}^{(1,1)}][C_{ln}^{(2,1)}] \\ [C_{ln}^{(1,2)}] & [C_{ln}^{(2,2)}] \end{bmatrix} \begin{bmatrix} [^{(\alpha+1)}a_l^{(1)}] \\ [^{(\alpha+1)}a_l^{(2)}] \end{bmatrix}
\tag{44}
$$

where the forward and backward propagating mode excitation coefficients are displayed explicitly. In defining the $[C_{ln}^{(p,s)}]$ matrices, and in writing the matrix result in (44), the "α indices" have been suppressed. However, when confusion can arise they should be written as $[C_{ln}^{(p,s)} (\alpha + 1 \; ; \alpha)]$, etc., since the α indices change when the matrix refers to a boundary other than Σ_α. (eg. Between the zones $V_{\alpha-1}$ and V_α, on the surface $\Sigma_{\alpha-1}$, the coupling matrix is expressed as $[C_{ln}^{(p,s)} (\alpha \; ; \alpha-1)]$).

Obviously the coupling matrices are square only if L = N, that is if we use as many modes in V_α as in $V_{\alpha+1}$ to represent the propagating waves. This choice will be adhered to, from this point forward, although it is not a necessary condition.

It is evident that the partitioned matrices can be written in unpartitioned form as well, where, with L = N, the mode coefficient matrices are of dimension (2N × 1) and the coupling matrix is square and of dimension (2N × 2N). Thus, we can also define mode coefficient matrices consisting of the (ordered) mode coefficients for the forward and backward propagating modes in the zones V_α and $V_{\alpha+1}$ as (say):

$$\left[^{(\alpha)}m_n \right] \equiv \begin{bmatrix} \left[^{(\alpha)}a_n^{(1)} \right] \\ \left[^{(\alpha)}a_n^{(2)} \right] \end{bmatrix}$$

(45a)

$$\left[^{(\alpha+1)}m_l \right] \equiv \begin{bmatrix} \left[^{(\alpha+1)}a_l^{(1)} \right] \\ \left[^{(\alpha+1)}a_l^{(2)} \right] \end{bmatrix}$$

and, similarly, we can define what can appropriately be called a horizontal propagator matrix:

$$\left[H_{ln}(\alpha+1 \; ; \; \alpha) \right] \equiv \begin{bmatrix} \left[C_{ln}^{(1,1)} \right] & \left[C_{ln}^{(2,1)} \right] \\ \left[C_{ln}^{(1,2)} \right] & \left[C_{ln}^{(2,2)} \right] \end{bmatrix}$$

(45b)

Now the equation (44) can be written in the more compact form:

$$\left[^{(\alpha)}m_n \right] = \left[H_{ln}(\alpha+1 \; ; \; \alpha) \right] \left[^{(\alpha+1)}m_l \right]$$

(46)

and expresses the required conditions between the mode coefficients in neighboring zones.

If we take successive values of α, with α ranging from 1 to M-1 say, then we get

$$[^{(1)}m_n] = [H_{ln}(2 \; ; \; 1)][^{(2)}m_l]$$
$$[^{(2)}m_n] = [H_{ln}(3 \; ; \; 2)][^{(3)}m_l]$$

$$[^{(M-1)}m_n] = [H_{ln}(M \; ; \; M{-}1)][^{(M)}m_l]$$

Clearly, by noting in these equations that the indices l and n are just dummy indices providing a numbering system for the eigenvalues, then

$$\left[^{(1)}m_n \right] = \left[H_{ln}(2 \; ; \; 1) \right] \left[H_{ln}(3 \; ; \; 2) \right] \cdots \left[H_{ln}(M \; ; \; M{-}1) \right] \left[^{(M)}m_l \right]$$

by successive substitutions. Consequently, we can write, for any $\beta \geq \alpha + 1$:

$$\left[^{(\alpha)}m_n \right] = \left\{ \prod_{q=\alpha+1}^{\beta} \left[H_{ln}(q \; ; \; q{-}1) \right] \right\} \left[^{(\beta)}m_l \right]$$

(47)

This is a propagator equation that connects the mode coefficients in any zone V_β with those in any other zone V_α. In case $\beta = \alpha + 1$ the equation (47) reduces to equation (46), which connects the coefficients in any two neighboring zones. Since the coupling coefficients composing $\left[H_{ln}\right]$ can be computed from the simple eigenfunction inner products at the zone interfaces, this equation provides the means of computing mode coefficients that produce displacements and tractions satisfying all the boundary conditions along the vertical boundaries of the medium. Since the eigenfunctions used already satisfy the boundary conditions along the horizontal boundaries in each zone, then by use of the horizontal propagator relation all the boundary conditions in the laterally and vertically "layered" medium being considered can be satisfied.

Summary and Conclusions

The basic method described here makes use of normal mode expansions of the wave field in each partitioned sub-region of the medium within which the medium is uniform in the lateral directions. Thus the medium is partitioned into laterally uniform zones and complete normal mode solutions are obtained fro each horizontally layered zone. In the analytical development the "zonal eigenvalues and eigenfunctions" are generated by treating each zone as a layered half space or radially layered sphere, as ia appropriate for the medium geometry. The resulting set of modes are then used as bases for expansions of the wave fields in the layered subregions. The mode expansions defined on the zones are then "connected" by matching (equating) the exact Green's function representations of the wave fields in each zone at the common boundaries between the zones where continuity of displacement and traction is required. This results in the definition of a "lateral propagator" of the wave field when applied to all the zones making up the entire medium and is, in application, very similar to the classical "vertical propagator" method.

The method is exact when the lateral variations are actually discontinuous step changes in properties. When the actual changes can be approximated as a sequence of step the method should be superior in computational accuracy and speed to numerical methods.

In implementations of this method it is only necessary to compute the "zonal" normal modes once, and subsequently these zonal mode solutions can be combined in a variety of ways, using the lateral propagator equation, to produce theoretically predicted wave fields in many different laterally varying structures wintout the necessity of a complete recomputation of wave fields in each new structure. Further, the propagators are analytically defined so that manipulations related to inversion and perturbation calculations can be considered. For these reasons, and because of its inherent high accuracy, this method should prove useful in modeling seismic wave fields in complex media and in inversion studies. In the present study the method is developed in detail for two dimensionally variable media, using cylindrical coordinates and wave functions. However, analogous results in rectangular and spherical coordinates may be obtained using the same procudure and are appropriate for media with variability in all three spatial dimensions.

References

Ben Menahem, A. and S.J. Singh, Computation of Models of Elastic Dislocations in the Earth, Methods in Computational Physics, Vol. 12, Academic Press, 1972.

Harkrider, D.G., Surface Waves in Multilayered Media, I. Rayleigh and Love Waves from Sources in a Multilayered Half Space, *Bull. Seism. Soc. of Am., 54*, 1964.

Harvey, D.J., Seismogram Synthesis using normal mode Superposition: the Locked Mode Approximation, *Geophys. J. Roy. Astron. Soc., 66*, 1981.

Herrera, D.J., Contribution to the linearized theory of surface wave transmission, *J. Geophys. Res., 69, 1964.*

Kenneth, B.L.N., Guided wave Propagation in laterally varying media - I. Theoretical development, *Geophys. Res., 69, 1964.*

Mc Garr, A. and L.E. Alsop, Transmission and reflection of Rayleigh waves at vertical boundaries, *J. Geophys. Res., 72,* 1967.

Morse, P.M. and H. Feshbach, Methods of Theoretical Physics, McGraw-Hill, 1953.

Stratton, J.A., Electromagnetic Theory, McGraw-Hill, 1941.